REVEALING THE HYDROLOGICAL HISTORY OF MARS

By

CHAOJUN FAN

A dissertation submitted in partial fulfilment of

the requirements for the degree of

DOCTOR OF PHILOSOPHY IN GEOLOGY

WASHINGTON STATE UNIVERSITY

School of Earth and Environmental Sciences

May 2008

To the faculty of Washington State University:

The members of the committee appointed to examine the dissertation of CHAOJUN FAN find it satisfactory and recommend that it be accepted.

Chair _____

_____

_____

_____

ACKNOWLEGEMENTS

I am indebted to all members of my committee for the completion of my dissertation. First of all, to my chair, Dr. Dirk Schulze-Makuch, for his guidance, advice and inspiration, as well as for providing me the chance of getting into the field of Mars exploration. Second, to Dr. John A. Wolff, Dr. Joan Wu and Dr. Hongjie Xie, for their advice, inspiration and support. Thanks also for their editing advices.

I would like to express my gratefulness to the faculty members at Washington State University (WSU) who taught me and the staff and graduate fellows in the School of Earth and Environmental Science at WSU who helped me in my doctoral research. I especially would like to thank Dr. Kent C. Keller who served on my committee in the first two years of my study at WSU.

My thanks go to the faculty and staff in the Department of Geological Sciences at the University of Texas at El Paso (UTEP) who offered me the opportunity in pursing my advanced degree in the U.S.A. and who taught me during my study there. I especially would like to mention Dr. Philip C. Goodell who served as my advisor when I was at UTEP. Many thanks also go to the Laboratory for Remote Sensing and Geoinformatics at the University of Texas at San Antonio (UTSA) and Dr. Hongjie Xie who welcomed me and partially funded me to study remote sensing in the Lab during the winter break 2005 and summer break 2006.

I am also indebted to Dr. Alberto Fairen who reviewed a part of my dissertation, Dr. Mingqian Zhu who helped me in the operation of the remote sensing software, Ms. Evan

Strand who gave me access to the Remote Sensing and GIS Research Lab at the University of Idaho, and all those who helped me regardless the work was used in the dissertation or not.

Thanks also go to my former employer, Guizhou University of Technology (Guizhou University today) for the financial support I received during the period of my study in the USA.

At last, I thank my parents who passed away during my stay in the USA for their understanding of my study in the USA. Thanks also go to my sister and brothers for their financial and emotional support. Especially, I thank my wife, Dongjie Shen and my son, Junjie Fan, for their companionship during my study in the USA, for their sharing of my stress and depression, and for their understanding of my carelessness of housework and enjoyment together. Sorry, my son! I didn't help you much in your course work because I was really very, very busy!

Philosophy

Simplicity and humbleness to my life

Obligation and responsibility to family members

Integrity and honesty to friends

Contribution to the society

REVEALING THE HYDROLOGICAL HISTORY OF MARS

Abstract

By Chaojun Fan, PhD

Washington State University

May 2008

Chair: Dirk Schulze-Makuch

The study of the history and present availability of water on Mars is critical to understanding geological processes and life on Mars, and to preparing for human exploration of Mars. NASA set forth the theme of "Following the Water" for the Mars exploration program. Following the theme, I presents this dissertation on 1) the origin of sulfates in the equatorial region of western Mars, 2) the water signature of gully-exposed sites on Mars, and 3) a characterization of the Phoenix landing site in an attempt to better understand the hydrologic history of early Mars, and the availability of water on Mars in recent geologic time and the present day. A new hypothesis for the origin and redistribution of sulfates in the equatorial region of western Mars was proposed in terms of the observed distribution occurrence of sulfates and the physiographic processes (volcanic, tectonic and sedimentary) affecting the Martian surface. This hypothesis integrates logically 1) the fate of sulfates in Valles Marineris and the source of sulfates in Meridiani Planum, and 2) the formation of sulfates in the equatorial region of western Mars, the Tharsis rise and Valles Marineris. This research implies that there was a dynamic Martian surface in early Martian history and liquid water was active at least until the Hesperian epoch. Investigation of water signatures at gully-exposed sites on Mars by hyperspectral image analysis finds that the depths of the water-related absorption

bands are greater at the four selected gully-exposed sites than in surrounding areas. The stronger signature of water at the gully-exposed sites than their surrounding areas indicates more water (water-ice, isolated water molecules and hydroxyl) is likely contained in the surface materials at the gully-exposed sites and implies that the formation of gullies on Mars might have involved processes associated with liquid water. One interpretation might be that liquid water has been active in recent geological time, even to the present. Characterization of the Phoenix landing site indicates that it is in a plain composed of the soils or regolith of weathered basaltic andesite on the surface and water-ice or icy soil (permafrost) within centimetres or tens of centimetres below the surface. The landing site is an ideal site for investigating water and water-ice, and its potential as a habitat for life on Mars.

TABLE OF CONTENTS

Page

LIST OF FIGURES

LIST OF TABLE

CHAPTER 1

INTRODUCTION

Mars, the fourth planet in the solar system, orbits the Sun at an average distance of 228 million kilometres. It is 6786 km in diameter and has a similar internal structure to Earth. Its average surface temperature is – 63 ºC and its average pressure is 6.4 millibars on the surface (Appendix 1). Mars, a planet close to Earth, has attracted human wonder since at least 400 BC. However, whether life on Mars exists or not is still an open question, though many exploration missions have studied the planet (see Appendix 2).

Some scientists proposed that life might have emerged in early Mars history and retreated into the subsurface when the Martian surface environment became hostile to life (e. g. Schulze-Makuch, 2005). A combination of energy, appropriate chemical elements and water may allow the emergence and survival of life as we know it. The Mars had similar energy sources and chemical composition as the Earth does, thus water likely played a critical role as well. Understanding the existence and activity of water on Mars also would help us to understand Martian surficial geology and climate, and prepare for human exploration of Mars. NASA set forth "Following the Water" as the theme for Mars exploration programs (http://www.jpl.nasa.gov/science/). This research follows the theme and attempts to make a contribution to the ongoing missions.

The geological history of Mars is generally split into three epochs, Noachian (4.5 to 3.5 Gyr), Hesperian (3.5 to 1.8 Gyr) and Amazonian (1.8 Gyr to present). But the hydrological history of water on Mars is one of the most debatable topics in all sciences (Baker, 2004). The Martian surface is cold and dry today, but might have been wet and warm in its early history and water might have been active in recent geologic time, and even to the present (e.g. Malin et al., 2006). Some workers proposed a water-rich

Noachian period with an ancient ocean or several paleolakes (e.g. Parker et al., 1989; Baker et al., 1991; Cabrol and Grin, 1999; Moore and Wilhelms 2001; Irwin et al., 2002) and wet and warm conditions associated with a thick ancient CO_2 atmosphere (Pollack et al., 1987; Schaefer, 1990) although dissent exists (e.g. Kasting, 1991; Malin and Edgett, 1999). Starting from the early Hesperian, the surface of Mars became cold and dry with water frozen in permafrost, glaciers and both polar ice caps, but local wet and warm environments likely occurred sporadically due to volcanism (e.g. Baker et al., 1991; Schulze-Makuch et al., 2007). The voluminous outflows of water from subsurface sources created cataclysmic flood flows and subsequently continued to produce channels and valley networks (Carr, 1979; Gulick and Baker, 1989, 1990; Clifford and Parker, 2001). Volcano-ice-water interaction and associated formation of channels and valleys likely lasted to the Amazonian period and perhaps to the present (e.g. Dohm et al., 2001; Fairen et al., 2003; Schulze-Makuch et al., 2007). The gully features detected by the Mars Global Surveyor (MGS)/Mars Obiter Camera (MOC) also indicate very recent liquid water action on Mars (Malin and Edgett, 2000a; Malin et al., 2006).

Indicators of a hydrodynamic Mars include, but were not limited to 1) geomorphology, such as shorelines, gullies, channels, valleys and valley networks, and alluvial fans in mid-latitude areas (e.g. Parker et al., 1989; Baker et al., 1991; Malin and Edgett, 2000a, 2003; Fairén, et al., 2003; Mangold et al., 2004; Solomon et al., 2005); 2) sedimentological textures such as layered deposits, cross bedding, and layered evaporites in the Martian northern lowlands (e.g. Malin and Edgett, 2000b; Paige, 2005; Gendrin et al., 2005; Bibring et al., 2005); 3) mineralogy such as hydrated phyllosilicates, hydrated sulphates and other hydroxide minerals near the equatorial areas (e.g. Arvidson et al., 2005; Poulet et al., 2005; Langevin et al., 2005a; Bibring et al., 2006); 4) anomalies of volatile element concentrations such as Br and Cl at several locations on Mars (e.g. Dreibus and Waenke, 1987, 2000; Squyres et al., 2004; Haskin et al., 2005); 5) water-ice

caps in both polar areas and permafrost in the high latitude areas (e.g. Farmer et al., 1976; Kieffer et al., 1976; Jakosky, 1999; Titus et al., 2003; Langevin et al., 2005b); 6) putative sites of hydrothermal activity around the globe (e.g. Schulze-Makuch et al., 2007); and 7) possible volcanic cones in the north circumpolar area (Neukum and Gasselt, 2006).

In this study, I will delve into selected topics related to water on Mars. I investigated the hydrologic history of early Mars, activity of liquid water in recent geologic time and the up-to-date exploration of water on Mars in terms of the origin of Martian sulfates, the water signatures at gully-exposed sites and the Phoenix Landing Site on Mars. The three topics constitute three chapters of the dissertation, Chapter 2: a new hypothesis for the origin and redistribution of sulfates in the equatorial region of western Mars; Chapter 3: investigation of water signatures at gully-exposed sites on Mars by hyperspectral image analysis; and Chapter 4: characterization of the Phoenix landing site.

Reference:

Arvidson, R. E., F. Poulet, J.-P. Bibring, M. Wolff, A. Gendrin, R.V. Morris, J.J. Freeman, Y. Langevin, N. Mangold and G. Bellucci, 2005. Spectral reflectance and morphologic correlations in eastern Terra Meridiani, Mars. *Science* 307, 1591–1594.

Baker, V.R., R.G. Strom, V.C. Gulick, J.S. Kargel, G. Komatsu and V.S. Kale, 1991. Ancient oceans, ice sheets and the hydrological cycle on Mars. *Nature* 352, 589–594.

Baker, V.R., 2004. J. Seckbach (ed.), Origin, Kluwer Academic Publisher, pp. 621–631.

Bibring, J-P., Y. Langevin, A. Gendrin, B. Gondet, F. Poulet, M. Berthé, A. Soufflot, R. Arvidson, N. Mangold, J. Mustard, P. Drossart and the OMEGA team, 2005. Mars surface diversity as revealed by the OMEGA/Mars express observations. *Science* 307, 1576–1581.

Bibring J-P., Y. Langevin, J.F. Mustard, F. Poulet, R. Arvidson, A. Gendrin, B. Gondet, N. Mangold, P. Pinet, F. Forget and the OMEGA team, 2006. Global mineralogical and aqueous Mars history derived from OMEGA/Mars Express data. *Science* 312, 400–404.

Cabrol, N.A. and E.A. Grin, 1999. Distribution, classification, and ages of Martian impact crater lakes. *Icarus* 142, 160–172.

Carr, M.J., 1979. Formation of Martian flood features by release of water from confined aquifers. *J. Geophys. Res.* 84, 2995–3007.

Clifford, S.M. and T.J. Parker, 2001. The evolution of the Martian hydrosphere: implications for the fate of a primordial ocean and the current state of the northern plains. *Icarus* 154, 40–79.

Dohm, J. M., R.R. Casavant, R.G. Strom, J.R. Zimbelman and D.H. Scott, 2001. Latent outflow activity for western Tharsis, Mars: Significant flood record exposed. *J. Geophys. Res.*106, 12301–12314.

Dreibus, G. and H. Waenke, 1987. Volatiles on Earth and Mars: A comparison. *Icarus* 71, 225–240.

Dreibus, G. and H. Waenke, 2000. The volatile inventory of Earth and Mars. *AGU 2000 Spring Meeting,* Washington, DC.

Fairén, A.G., J.M. Dohm, V.R. Baker, M.A. de Pablo, J. Ruiz, J. Ferris and R. Anderson, 2003. Episodic flood inundations of the northern plains of Mars, *Icarus, 165*, 53–67.

Farmer, C.B., D.W. Davies and D.D. Laporte, 1976. Mars: Northern Summer Ice Cap Water Vapor Observations from Viking 2. *Science* 194, 1339–1341.

Gendrin, A. N. Mangold, J-P. Bibring, Y. Langevin, B. Gondet, F. Poulet, G. Bonello, C. Quantin, J. Mustard, R. Arvidson and S. LeMouélic, 2005. Sulphates in Martian layered terrains: The OMEGA/Mars Express View. *Science* 307, 1587–1591.

Gulick, V.C. and V.R. Baker, 1989. Fluvial valleys and Martian paleoclimates. *Nature* 341, 514–516.

Gulick, V.C. and V.R. Baker, 1990. Origin and evolution of valleys on Martian volcanoes. *J. Geophys. Res.* 95, 14325–14344.

Haskin, L.A., A. Wang, B.L. Jolliff, H.Y. McSween, B.C. Clark, D.J. Des Marais, S.M. McLennan, N.J. Tosca, J.A. Hurowitz, J.D. Farmer, A. Yen, S.W. Squyres, R.E. Arvidson, G. Klingelhöfer, C. Schröder, Jr, P.A. de Souza, D.W. Ming, R. Gellert, J. Zipfel, J. Brückner, J.F. Bell, III, K. Herkenhoff, P.R. Christensen, S. Ruff, D. Blaney, S. Gorevan, N.A. Cabrol, L. Crumpler, J. Grant and L. Soderblom, 2005. Water alteration of rocks and soils on Mars at the Spirit rover site in Gusev crater. *Nature* 436, 66–69.

Irwin, R.P., III, T.A. Maxwell, A.D. Howard, R.A. Craddock and D.W. Leverington, 2002. A large paloelake basin at the head of Ma'adim Vallis, Mars. *Science* 296, 2209–2212.

Jakosky, B.M., 1999. Water, Climate, and Life, *Science* 283, 648–649.

Kasting, J.F., 1991. CO2 condensation and the climate of early Mars. *Icarus* 94, 1–13.

Kieffer, H.H., S.C. Chase, Jr, T.Z. Martin, E.D. Miner and F.D. Palluconi, 1976. Martian North Pole Summer Temperatures: Dirty Water Ice. *Science* 194, 1341-1344.

Langevin, Y., F. Poulet, J.-P. Bibring and B. Gondet, 2005a. Sulphates in the north polar region of Mars detected by OMEGA/Mars express. *Science* 307, 1584–1586.

Langevin, Y., F. Poulet, J-P. Bibring, B. Schmitt, S. Douté, and B. Gondet, 2005b, Summer Evolution of the North Polar Cap of Mars as Observed by OMEGA/Mars Express, Science 307, 1581-1584Malin, M.C. and K.S. Edgett, 1999. Oceans or

seas in the Martian northern lowlands: high-resolution imaging tests of proposed coastlines. *Geophys. Res. Lett.* 26, 3049–3052.

Malin, M.C. and K.S. Edgett, 2000a. Evidence for recent groundwater seepage and surface runoff on Mars. *Science* 288, 2330–2335.

Malin, M.C. and K.S.Edgett, 2000b. Sedimentary rocks of early Mars. *Science* 290, 1927–1937.

Malin, M.C. and K.S. Edgett, 2003. Evidence for persistent flow and aqueous sedimentation on early Mars. *Science* 302, 1931–1934.

Malin, M.C., Edgett, K.S., Posiolova, L.V., McColley, S.M. and E.Z.N. Dobrea, 2006. Present-day impact cratering rate and contemporary gully activity on Mars. *Science* 314, 1573–1577.

Mangold, N., C. Quantin, V. Ansan, C. Delacourt, and P. Allemand, 2004. Evidence for precipitation on Mars from dentritic valleys in the Valles Marineris area. *Science* 305, 78–81.

Moor, J.M. and D.E. Wilhelms, 2001. Hellas as a possible site of ancient ice-covered lakes on Mars. *Icarus* 154, 258–276.

Neukum, G., and S.V. Gasselt, 2006. Recent Volcanism at the Martian North Pole. *Geophysical Research Abstracts* 8, 11103.

Paige, D.A., 2005. Ancient Mars: Wet in many places. *Science* 307, 1575–1576.

Parker, T.J., R.S. Saunders and D.M. Schneeberger, 1989. Transitional Morphology in the West Deuteronilus Mensae Region of Mars: Implications for Modification of the Lowland/Upland Boundary. *Icarus* 82, 111–145.

Pollack, J.B., J.F. Kasting, S.M. Richardson and K. Poliakoff, 1987. The case for a wet, warm climate on Mars. *Icarus,* 71, 203–224.

Poulet, F., J-P. Bibring, J.F. Mustard, A. Gendrin, N. Mangold, Y. Langevin, R.E. Arvidson, B. Gondet, and C. Gomez, 2005. Phyllosilicates on Mars and implications for early Martian climate. *Nature* 438, 623–627.

Schaefer, M.W., 1990. Geochemical evolution of the northern plains of Mars: Early hydrosphere, carbonate development, and present morphology. *J. Geophys. Res*. 95, 14291–14300.

Schulze-Makuch, D., L.N. Irwin, J.H. Lipps, D. LeMone, J.M. Dohm and A.G. Fairén, 2005. Scenarios for the evolution of life on Mars. Special Edition on Early Mars of *J. Geophys. Res. – Planets* 110, E12S23, doi:10.1029/2005JE002430.

Schulze-Makuch, D., J.M. Dohm, C. Fan, A.G. Fairén, J.A.P. Rodriguez, V.R. Baker, W. Fink, 2007, Exploration of hydrothermal targets on Mars. *Icarus* 189, 308–324.

Solomon, S.C., O. Aharonson, J.M. Aurnou, W.B. Banerdt, M.H. Carr, A.J. Dombard, H.V. Frey, M.P. Golombek, S.A. Hauck, II, J.W. Head, III, B.M. Jakosky, C.L. Johnson, P.J. McGovern, G.A. Neumann, R.J. Phillips, D.E. Smith and M.T. Zuber, 2005. New perspectives on ancient Mars. *Science* 307, 1214–1220.

Squyres, S.W., J.P. Grotzinger, R.E. Arvidson, J.F. Bell, III, W. Calvin, P.R. Christensen, B.C. Clark, J.A. Crisp, W.H. Farrand, K.E. Herkenhoff, J.R. Johnson, G. Klingelhöfer, A.H. Knoll, S.M. McLennan, H.Y. McSween, Jr., R.V. Morris, J.W. Rice, Jr., R. Rieder and L.A. Soderblom, 2004. In situ evidence for an ancient aqueous environment at Meridiani Planum, Mars. *Science* 306, 1709–1714.

Titus, T.N., H.H. Kieffer and P.R. Christensen, 2003. Exposed Water Ice Discovered near the South Pole of Mars. *Science* 299, 1048–1051.

CHAPTER 2

A New Hypothesis for the Origin and Redistribution of Sulfates in the Equatorial Region of Western Mars

Abstract

The formation of sulfates on Mars has been under debate since they were identified by several Mars missions starting from the 1970s. We propose that sulfates formed as evaporites in enclosed standing bodies of water in the Valles Marineris area following the early alteration of Martian basaltic crust, were then elevated by the Tharsis uplift, and transported together with rock materials to Meridiani Planum by periodic outbursts of water, where they were deposited as sediments. The proposed model comprehensively addresses all forms of sulfate occurrences near the equator in the western Martian hemisphere and relates it to physiographic processes (volcanic, tectonic and sedimentary) affecting the Martian surface.

2.1 Introduction

Sulfates in Martian soil have been identified in situ by the Viking Lander X-Ray Spectrometer experiment (Clark et al., 1982), Mars Pathfinder (Foley et al., 2003), and the two Mars Exploration Rovers (MER) (Herkenhoff et al., 2004; Ming et al., 2006) in surface sands and underlying sulfate-rich sedimentary deposits at their landing sites. The Observatoire pour la Minéralogie, l'Eau, les Glaces et l'Activité (OMEGA)/Mars Express (MEX) hyperspectral imager identified sulfates (Gendrin et al., 2005; Bibring et al.,

2005; Bibring et al., 2006) on outcrops in Valles Marineris, Margaritifer Sinus, and Terra Meridiani in the equatorial region of the western Martian hemisphere.

Here we propose that prior to uplift of the Tharsis rise, sulfates initially formed as sequences of evaporites (Gendrin et al., 2005; Bibring et al., 2005) from enclosed standing bodies of water in the Valles Marineris region. Phyllosilicate weathering of basaltic crust (Bibring et al., 2006; Poulet et al., 2005) provided soluble cations such as K, Na, Ca, Mg (Eggleton et al., 1987), while S was released by volcanic degassing (Schoen and Rye, 1970; Thordarson and Self, 1996) and oxidized in hydrous environments to SO_4^{2-}. Sulfate evaporites were then elevated and mobilized during and after uplift of the Tharsis rise. Beginning in the late Noachian or the early Hesperian (Robinson, 1995), periodic outbursts of water transported sulfates together with fragments of basaltic rocks and pyroclastic materials to Meridiani Planum, where they were deposited as fluvial or alluvial sedimentary deposits (Squyres et al., 2004 a, b).

2.2 Origin of sulfates in the Tharsis area

Sulfate formation by evaporation of standing bodies of acidic and salty water is well-known from Earth (Tucker, 2001), although other processes cannot be ruled out (e.g. acid-fog deposition on a summit of a volcano, Schiffman et al., 2006; hydrothermal alteration and deposition, Heald et al., 1987, Ogawa et al., 2005; oxidation of sulfide, Buckby et al., 2003). Early Mars was probably warmer and wetter than today (e.g. Golombek, 1999), and the major sulfates identified likely formed from similar processes. Formation of sulfate evaporites in Valles Marineris followed phyllosilicate alteration of basaltic crust (Bibring et al., 2006) before uplift of the Tharsis rise (Fig. 2-1a).

Before the Tharsis rise, the area of Valles Marineris was located around the boundary between the southern highlands and the northern lowlands of Mars (Andrews-

Hanna et al., 2007), where basins, lakes, saline pools or lagoons could have been present along the dichotomy boundary. These lower depressions were likely isolated, or partially isolated, from the putative northern lowlands ocean (Baker et al., 1991), which made them ideal sites for the accumulation of soluble elements leaching out from the phyllosilicate altered basaltic crust (Appendix 3). The Tharsis uplift destroyed these depressions, but not before they had become filled with sulfate evaporites.

The composition of the Martian crust is dominated by mafic igneous rocks of basaltic or basaltic andesite composition (e.g. Zuber, 2001). The region lying in and surrounding Valles Marineris was presumably dominated by basaltic rocks, and subjected to long-term intensive alteration by rock-water interactions like other areas of the Martian crust. The recent identification of widely distributed phyllosilicates provides evidence for these processes (Bibring et al., 2006; Poulet et al., 2005). Rock-water interaction would have likely occurred between the atmosphere, the hydrosphere and the crust, or between the crust and circulating hydrothermal fluids (Schulze-Makuch et al., 2007). Less soluble elements like iron, aluminium and silica in basalts remained to form phyllosilicates while soluble ions such as K^+, Na^+, Ca^{2+} and Mg^{2+} were leached out (Eggleton et al., 1987) and dissolved in fluids. These soluble elements were transported elsewhere and accumulated in the enclosed standing bodies of water in the depression areas.

Hydrothermal fluids could additionally release sulfur into the surface environment via hot springs (Schoen and Rye, 1970). Another important source of sulfur is syn-eruptive degassing of basaltic magma (Thordarson and Self, 1996). Martian basaltic magmas had oxygen fugacities similar to or lower than their modern counterparts on Earth that release sulfur dominantly as SO_2, with lesser amounts of H_2S and S_2, all of which are efficiently converted to H_2SO_4 in the humid, O_2-rich modern terrestrial

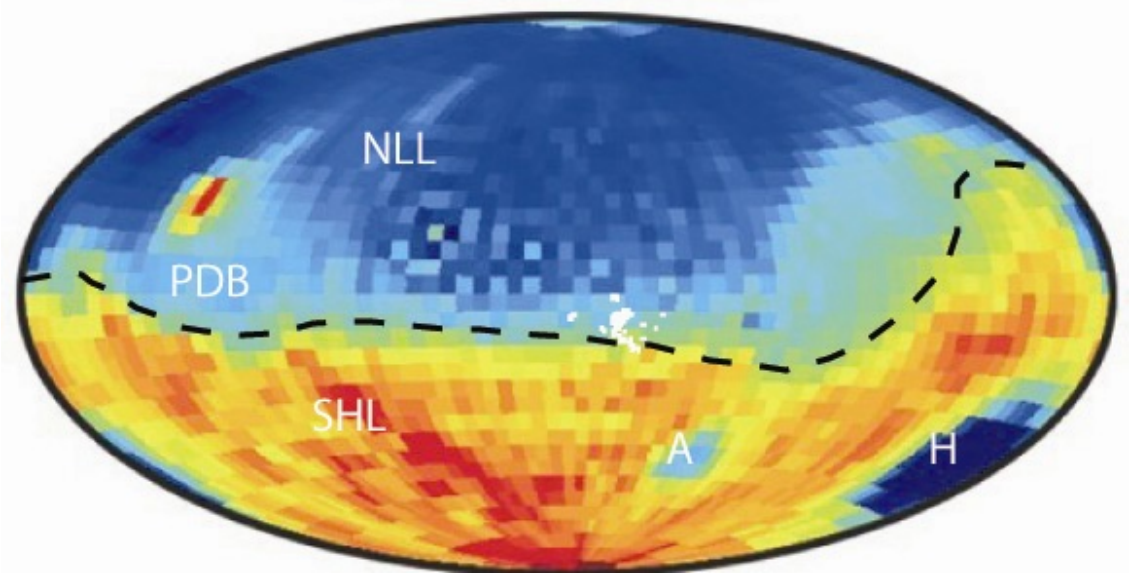

Fig. 2-1a

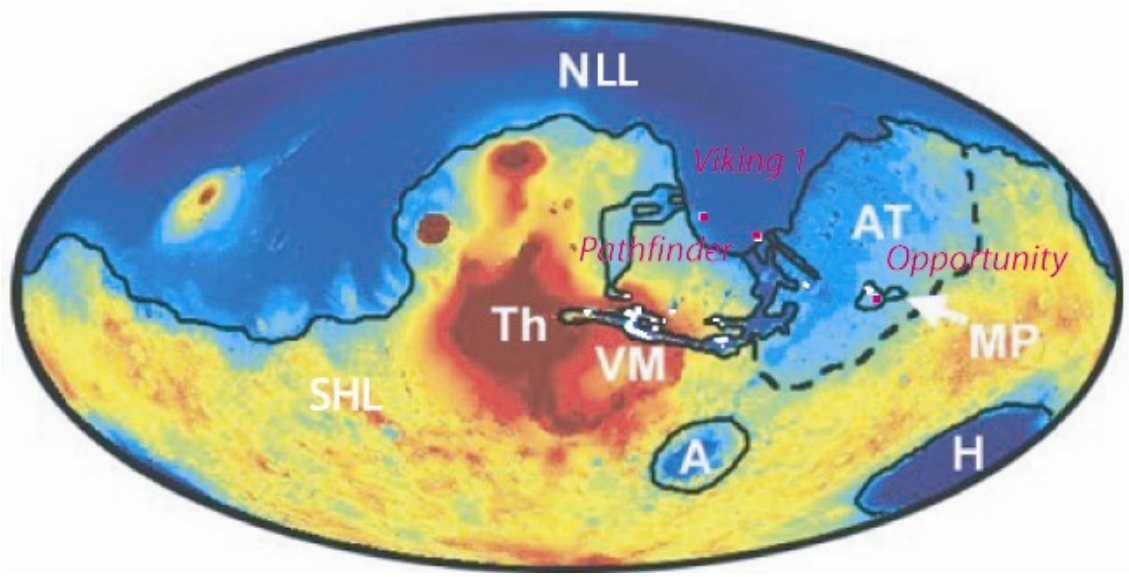

Fig. 2-1b

Fig. 2-1 Topography of Mars and distribution of associated sulfates**.** The panel of figures are modified based on Bibring et al. (2006) and Andrews-Hanna et al. (2007). The color scale (topographic elevation) applies to both panels with identified sulfate deposits denoted in white color. a, Reconstructed pre-Tharsis topography and distribution of sulfates. The dashed black line is the proposed dichotomy boundary (PDB) prior to formation of the Tharsis rise. The labelled major features are: NLL- the northern lowlands, SHL-the southern highlands, H-Hellas basin, A-Argyre basin. b, Present distribution of sulfates detected around the equatorial region of western Mars. Sulfates (in white) were detected by Bibring et al. (2006), and at the Viking 1, Pathfinder and Opportunity landing sites. VM-Valles Marineris canyons, Th-Tharsis rise, AT-Arabia Terra, and MP-Meridiani Planum.

atmosphere. In the absence of a strongly oxidizing atmosphere such as on early Mars, SO_2 and more reduced sulfur species are nonetheless converted to SO_3 via photochemical reactions (Okabe, 1978), and SO_3 in turn converts to H_2SO_4 upon contact with water. Martian meteorites carry S isotopic evidence for the operation of such a photochemical oxidation sequence in the Martian atmosphere (Farquhar et al., 2000).

Evaporation oversaturated the salty water with solutes and led to the precipitation of sulfate salts, which is thought to be the most likely origin of the reported layered occurrences of sulfates, kieserite, gypsum and other as yet unidentified polyhydrated sulfates (Gendrin et al., 2005). Horizontal layers of gypsum surrounded by kieserite layers reach one hundred meters in thickness (Gendrin et al., 2005) and in Juventae Chasma appear to be covered by kieserite (Bibring et al., 2005) indicating that gypsum precipitated earlier than kieserite precursors from a standing body of water. The feature is consistent with $CaSO_4$ being less soluble than $MgSO_4$ (Vinogradova, 1975) although the solubility of their hydrated minerals may vary to some extent. There is a similar occurrence in Aram Chaos, where hydrated minerals are surrounded by kieserite (Gendrin et al., 2005).

An alternation of sulfate evaporites and the deposition of volcanic materials is supported by the systematic correlation of sulfate occurrences with Interior Layered Deposits (ILDs) in West Candor Chasma (Gendrin et al., 2005) and the interbedding of the darker layered units with light-toned deposits as recently observed on High Resolution Imaging Science Experiment (HiRISE) images. Sulfates distributed in the chasmas of Valles Marineris and mainly located on the flanks of massive deposits and on several isolated ILDs (Quantin et al., 2006) were exposed by later erosion. The increasing kieserite on the steeper slopes is thought to represent evidence that kieserite is present in the bedrock and does not derive from surface interactions (Mangold et al., 2006) between

rocks and the atmosphere. These features are also supportive of the mechanism of precipitation of sulfates identified in Valles Marineris.

2.3 Erosion and migration of layered sulfate evaporites

After the formation of sulfate evaporites, Tharsis started to rise. The uplift was probably the result of mantle processes (Janle and Erkul, 1991) during the late Noachian and early Hesperian (Robinson, 1995), and may have continued into the late Hesperian (Schultz, 1991; Dohm et al., 2001). The uplift of Tharsis elevated the layered sulfate evaporites and triggered the formation of Valles Marineris (Peulvast et al., 2001). The light-tone layered sulfates are covered unconformably by dark-tone blocky layers, which are thought to be Hesperian-age lava flows based on Mars Orbiter Camera (MOC) images (Montgomery and Gillespie, 2005).

Uplift of the crust and the growth of volcanoes formed steep slopes and a rift extending from the head of Valles Marineris to Chryse Planitia, subsequently forming a series of chasmas and outflow channels from chaotic terrain. Large amounts of water were sporadically discharged from the subsurface aquifer due to the change in the hydraulic head of groundwater (Andrews-Hanna et al., 2007) and released from the Martian interior due to contemporaneous volcanic activity (Fairén et al., 2003). Repeated catastrophic releases of groundwater discharged towards the east along Valles Marineris. Valles Marineris is considered as a source area for the outflow channels (Luchitta et al., 1992), because its elevation is generally several kilometers higher than the Chryse outflow region.

We propose that sulfate evaporites were eroded and carried away from Valles Marineris to Meridiani Planum and Chryse Planitia along with volcanic debris and fragments of basaltic crust by discharges of water because sulfates are soft and easily re-

dissolved. Exhumation of layered sulfates was accompanied with the formation of chasmas in Valles Marineris. The vertical distribution of sulfates in different chasmas is supportive of the formation of sulfates before the coalescence of the Valles Marineris canyon. Sulfate layers more than 2.5 km thick (Bibring et al., 2005) observed over a wide range of elevations from – 4 km in Ius Chasma to +3 km in Candor Chasma (Gendrin et al., 2005) could be explained by differential elevation and different cutting depths. Sedimentary deposition also likely happened in the remaining water bodies when the flooding was close to ceasing.

2.4 Deposition of sulfates in Meridiani Planum

Sulfate evaporites, together with basaltic debris and pyroclastics in Valles Marineris, were transported to Meridiani Planum and Chryse Planitia, and deposited as alluvial or fluvial sedimentary deposits (Fig. 2-1b) when turbulent flow conditions became reduced. Sulfates in solution and perhaps in tiny granulates such as colloids were deposited as inter-granular cement in siliciclastic material. The environmental conditions in Meridiani Planum involved episodic inundation, evaporation and desiccation (Fairén et al., 2003; Squyres et al., 2004a, b). Each wash-out of sulfates and associated materials from Valles Marineris formed a cross-bedded layer of deposits around Meridiani Planum. The altitude of the cross-bedding indicates flow from west to east (Klingelhöfer et al., 2004), consistent with the flooding from Valles Marineris into Meridiani Planum. The planar laminae are usually on a millimeter scale with single grain thicknesses ranging from 0.3 mm to 1 mm with a maximum stratigraphic thickness exposed at Eagle crater being about 30 to 50 cm (Squyres et al., 2004a).

The sediments in Meridiani Planum are composed of (by weight) ~ 40% sulfate minerals, ~50% siliciclastic fine-grains and ~10% hematite (Squyres et al., 2004a). The

outcrops of finely layered sandstone in the wall of Eagle crater contain nearly 40% by weight sulfate salts, including magnesium sulfate, calcium sulfate, and the iron sulfate jarosite (Bibring et al., 2006). Two types of lithic particles, subangular to irregular at 1.5 to 5.0 mm and rounded at 0.5 to 2.0 mm in diameter (Klingelhöfer et al., 2004), are likely deposits from materials that were transported along Valles Marineris. They are thought to be basalt clasts exhibiting vesicles from two different types of sources of basalt (Soderblom et al., 2004).

Shallow standing bodies of water have been suggested (Squyres et al., 2004a, b) as a possible source of sulfate deposits and weathered siliciclastic components in Meridiani Planum. But sulfate formation by evaporation in shallow water bodies fails to explain 1) extensive sulfate distribution in the absence of a topographic basin (Andrews-Hanna et al., 2007), 2) mixture of sulfates and basaltic particles with sulfates as cement, 3) the wide extent of etched terrains in this region, 4) the observation that the most soluble salts (halides, Mg-sulfate) coexist with the least soluble salts (Ca-sulfate, jarosite) (Knauth et al., 2005), and 5) the 1 km thickness of deposits in Meridiani Planum (Christensen and Ruff, 2004). On the contrary, the fluvial/alluvial transport of significant amounts of sulfates to the Meridiani region adequately explains (1) why sulfates are widely scattered in Meridiani, and the thickness of the deposits, because it is the natural eastern gravitational destination for materials derived from the Tharis uplift; (2) why materials are mixed and cemented with sulfates, including the mixing of salts with very different solubilities (Appendix 4), as a result of a spatially and temporally long transport process resulting in homogenization of materials previously differentiated; and (3) the presence of etched terrains as a consequence of differential deposition processes resulting in uneven topographies, not expected after prolonged sedimentation sequences. Nonetheless, it is certainly possible for shallow water bodies to be present during

intervals of sporadic catastrophic flooding. Formation of thin liquid film evaporites in these water ponds is also possible.

Sulfates in both Valles Marineris and Meridiani Planum have been subjected to later (Amazonian) secondary alteration and aeolian relocation after the earlier (Noachian to Hesperian) processes of erosion and sedimentary deposition ceased.

2.5 Summary

Our hypothesis (Fig. 2-2) links together all forms of sulfates identified near the equator in the western Martian hemisphere based on the evolution of the Martian surface, distribution, textures and compositions of sulfates, and the geomorphology of sulfate occurrences. Sulfates were also identified by MER Spirit in Gusev crater (Squyres et al., 2004c), and by OMEGA/MEX in the dark dunes of the northern polar region of Mars (Langevin et al., 2005). These sulfates occur in subsurface regolith or sand dunes, and their setting may have involved analogous relocation processes to those of sulfates near the equator in the Martian western hemisphere.

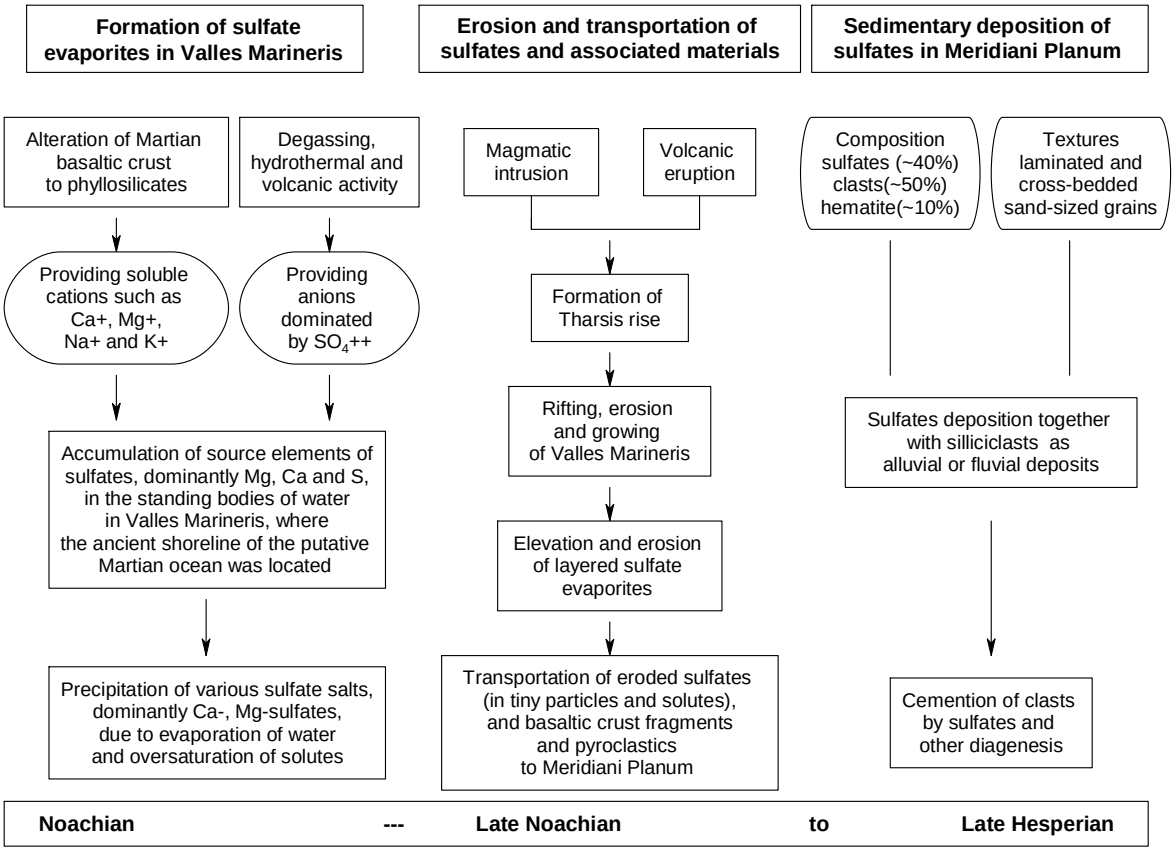

Fig. 2-2 Flow chart of sulfate formation near the equator of the western Martian hemisphere

References:

Andrews-Hanna, J.C., C. Jeffrey, J. P. Roger, and M. T. Zuber, 2007. Meridiani Planum and the global hydrogeology of Mars. *Nature* 446, 163–166.

Baker, V.R., R.G. Strom, V.C. Gulick, J.S. Kargel, G. Komatsu, and V.S. Kale, 1991. Ancient oceans, ice sheets and the hydrological cycle on Mars. *Nature* 352, 589–594.

Bibring, J-P., Y. Langevin, A. Gendrin, B. Gondet, F. Poulet, M. Berthé, A. Soufflot, R. Arvidson, N. Mangold, and J. Mustard, et al. 2005. Mars surface diversity as revealed by the OMEGA/Mars Express observations. *Science* 307, 1576–1581.

Bibring, J-P., Y. Langevin, J.F. Mustard, F. Poulet, R. Arvidson, A. Gendrin, B. Gondet, N. Mangold, P. Pinet, and F. Forget, et al. 2006. Global mineralogical and aqueous Mars history derived from OMEGA/Mars Express data. *Science* 312, 400–404.

Buckby, T., S. Black, M.L. Coleman, and M.E. Hodson, 2003. Fe-sulphate-rich evaporative mineral precipitates from the Río Tinto, southwest Spain. *Mineralogical Magazine* 67, 263–278.

Christensen, P.R., and S.W. Ruff, 2004. Formation of the hematite-bearing unit in Meridiani Planum: Evidence for deposition in standing water. *J. Geophys. Res.* 109, EO8003, doi: 10.1029/2003JE002233.

Clark, B.C., A.K. Baird, R.J. Weldon, D.M. Tsusaki, L. Schnabel, and M.P. Candelaria, 1982. Chemical composition of Martian fines. *J. Geophys. Res.* 87, 10059–10067.

Dohm, J.M., J.C. Ferris, V.R. Baker, R.C. Anderson, T.M. Hare, R.G. Strom, N.G. Barlow, K.L. Tanaka, J.E. Klemaszewski and D.H. Scott, 2001. Ancient drainage basin of the Tharsis region, Mars: Potential source for outflow channel systems and putative oceans or paleolakes. *J. Geophys. Res.* 106, 32943–32958.

Eggleton, R.A., C. Foudoulis, and D. Varkevisser, 1987. Weathering of basalt: Changes in rock chemistry and mineralogy. *Clays & Clay Minerals* 35, 161–169.

Fairén, A.G., J. M. Dohm, V. R. Baker, M. A. de Pablo, J. Ruiz, J. Ferris, and R. Anderson, 2003. Episodic flood inundations of the northern plains of Mars. *Icarus* 165, 53–67.

Farquhar, J., J. Savarino, T.L. Jackson and M.H. Thiemens, 2000. Evidence of atmospheric sulphur in the Martian regolith from sulphur isotopes in meteorites. *Nature* 404, 50-52.

Foley, C.N., T. Economou, and R.N. Clayton, 2003. Final chemical results from the Mars Panthfinder alpha proton X-ray spectrometer. *J. Geophys. Res.* 108, E12, 8096.

Gendrin, A., N. Mangold, J-P. Bibring, Y. Langevin, B. Gondet, F. Poulet, G. Bonello, C. Quantin, J. Mustard, R. Arvidson, and S. LeMouélic, 2005. Sulfates in Martian layered terrains: The OMEGA/Mars Express view. *Science 307*, 1587–1591.

Golombek, M.P., 1999. Martian climate: A message from warmer times. *Science 283*, 1470–1471.

Heald, P., N.K. Foley, and D.O. Hayba, 1987. Comparative anatomy of volcanic-hosted epithermal deposits; acid-sulfate and adularia-sericite types. *Economic Geology* 82, 1–26.

Herkenhoff, K.E., S.W. Squyres, R. Arvidson, D.S. Bass, J.F. Bell, III, P. Bertelsen, B.L. Ehlmann, W. Farrand, L. Gaddis, and R. Greeley, et al. 2004. Evidence from Opportunity's microscopic imager for water on Meridiani Planum. *Science* 306, 1727–1730.

Janle, P., and E. Erkul, 1991. Gravity studies of the Tharsis area on Mars. *Earth, Moon, and Planets* 53, 217–232.

Klingelhöfer, G., R.V. Morris, B. Bernhardt, C. Schröder, D.S. Rodionov, P.A. de Souza, Jr., A. Yen, R. Gellert, E.N. Evlanov, and B. Zubkov, et al. 2004. Jarosite and Hematite at Meridiani Planum from Opportunity's Mössbauer Spectrometer. *Science* 306, 1740–1745.

Knauth, L.P., D.M. Burt, and K.H. Wohletz, 2005. Impact origin of sediments at the Opportunity landing site on Mars. *Nature* 438, 1123–1128.

Langevin, Y., F. Poulet, J-P. Bibring, and B. Gondet, 2005. Sulfates in the North Polar Region of Mars detected by OMEGA/Mars Express. *Science* 307, 1584–1586.

Luchitta, B.K. in D.E. Smith, et al. 1999. The global topography of Mars and implications for surface evolution. *Science* 284, 1495–1503.

Mangold, N., A. Gendrin, C. Quantin, B. Gondet, and J-P. Bibring, 2006. Sulfate deposits and geology of west Candor Chasma: A case study, Martian Sulfates as Recorders of Atmospheric-Fluid-Rock Interactions, LPI, Houston, Texas [7039].

Ming, D.W., D.W. Mittlefehldt, R.V. Morris, D.C. Golden, R. Gellert, A. Yen, B.C. Clark, S.W. Squyres, W.H. Farrand, and S.W. Ruff, et al. 2006. Geochemical and mineralogical indicators for aqueous processes in the Columbia Hills of Gusev crater, Mars. *J. Geophys. Res.,* 111, E02S12.

Montgomery, D.R., and A. Gillespie, 2005. Formation of Martian outflow channels by catastrophic dewatering of evaporite deposits. *Geology* 33, 625–628.

Ogawa, Y., N. Shikazono, D. Ishiyana, H. Sato, and T. Mizuta, 2005. An experimental study on felsic rock-artificial seawater interaction; implications for hydrothermal alteration and sulfate formation in the Kuroko mining area of Japan. *Mineralium Deposita,* 39, 813–821.

Okabe, H., 1978. *Photochemistry of small molecules* (Wiley, New York).

Peulvast, J-P., D. Mège, J. Chiciak, F. Costard, and P. L. Masson, 2001. Morphology, evolution and tectonics of Valles Marineris wallslopes (Mars). *Geomorphology* 37, 329–352.

Poulet, F., J-P. Bibring, J.F. Mustard, A. Gendrin, N. Mangold, Y. Langevin, R.E. Arvidson, B. Gondet, and C. Gomez, 2005. Phyllosilicates on Mars and implications for early Martian climate. *Nature* 438, 623–627.

Quantin, C., A. Gendrin, N. Mangold, J-P. Bibring, and J.P. Hauber, 2006. Geology of Sulfate Deposits in Valles Marineris, Martian Sulfates as Recorders of Atmospheric-Fluid-Rock Interactions, LPI, Houston, Texas [7051].

Robinson, C.A.,1995. The crustal dichotomy of Mars. *Earth, Moon, and Planets* 69, 249–269.

Schiffman, P., R. Zierenberg, N. Marks, J.L. Bishop, and M.D. Dyar, 2006. Acid-fog deposition at Kilauea Volcano; a possible mechanism for the formation of siliceous-sulfate rock coatings on Mars. *Geology (Boulder)* 34, 921–924.

Schoen, R., and R.O. Rye, 1970. Sulfur isotope distribution in Solfataras, Yellowstone National Park. *Science* 170, 1082–1084.

Schultz, R.A., 1991. Structural development of Coprates Chasma and western Ophir Planum, Valles Marineris Rift, Mars. *J. Geophys. Res.* 96, 22,777–22,792.

Schulze-Makuch, D., J.M. Dohm, C. Fan, A.G. Fairén, J.A.P. Rodriguez, V.R. Baker, and W. Fink, 2007. Exploration of hydrothermal targets on Mars. *Icarus* 189, 308–324.

Soderblom, L.A., R. C. Anderson, R. E. Arvidson, J. F. Bell, III, N. A. Cabrol, W. Calvin, P. R. Christensen, B. C. Clark, T. Economou, and B. L. Ehlmann, et al. 2004. Soils of Eagle Crater and Meridiani Planum at the Opportunity Rover landing site. *Science* 306, 1723–1726.

Squyres, S.W., R.E. Arvidson, J.F. Bell, III, J. Brückner, N.A. Cabrol, W. Calvin, M.H. Carr, P.R. Christensen, B.C. Clark, and L. Crumpler, et al. 2004a. The Opportunity

Rover's Athena science investigation at Meridiani Planum, Mars. *Science* 306, 1698–1703.

Squyres, S.W., J.P. Grotzinger, R.E. Arvidson, J.F. Bell, III, W. Calvin, P.R. Christensen, B.C. Clark, J.A. Crisp, W.H. Farrand, and K.E. Herkenhoff,et al. 2004b. In situ evidence for an ancient aqueous environment at Meridiani Planum, Mars. *Science* 306, 1709–1714.

Squyres, S.W., R.E. Arvidson, J.F. Bell, III, J. Brückner, N.A. Cabrol, W. Calvin, M.H. Carr, P.R. Christensen, B.C. Clark, and L. Crumpler, et al. 2004c. The Spirit Rover's Athena Science Investigation at Gusev Crater, Mars. *Science* 305, 794–799.

Thordarson, T, and S. Self, 1996. Sulfur, chlorine and fluorine degassing and atmospheric loading by the Roza eruption, Columbia River Basalt Group, Washington, USA. *J. of Volcanology and Geothermal Research* 74, 49–73.

Tucker, M.E., 2001. *Sedimentary petrology: an introduction to the origin of sedimentary rocks*, Blackwell Scientific Publications, Oxford.

Vinogradova, G.V., 1975. Correlation between the salt content in the hard phase and soil solutions of the Murghab Oasis desert-meadow soils of ancient irrigation. *Probl Osvo Pustyn* 4, 82–84.

Zuber, M.T., 2001. The crust and mantle of Mars**.** *Nature* 412, 220–227.

CHAPTER 3

Investigation of Water Signatures at Gully-Exposed Sites on Mars by Hyperspectral Image Analysis

Abstract

High-resolution images from the Mars Obiter Camera (MOC) onboard the Mars Global Surveyor (MGS) show a variety of gully features on sloped surfaces of Mars. The mechanism of gully formation is still under debate although a majority of studies tend to favor a mechanism related to liquid water flow based on geomorphology and fluid mechanics considerations. In this study, I examined four known gully sites using Visible and Infrared Mineralogical Mapping Spectrometer (OMEGA) imagery. In particular, I analyzed the absorption depths of the water-associated absorption bands and conclude that there is a stronger water signature at the gully-exposed sites than in the surrounding areas. This implies that the water signature, most likely representing water ice, isolated water molecules, and/or hydroxyl molecules incorporated into minerals, is still present in the shallow unconsolidated soil. This study provides additional evidence that water was likely involved in the formation of the gully features and is still locally active on the Martian surface in the present time.

Keywords: Mars; Gully; Water signature; Hyperspectral image; Absorption depth

3.1 Introduction

Mars has experienced wet and possible warm surface conditions in its early history (e.g. Sagan et al., 1973; Pollack et al., 1987; Squyres and Kasting, 1994; Golombek, 1999; Tanaka, 2000; Craddock and Howard, 2002; Kerr, 2003; Paige, 2005; Poulet et al., 2005; Bibring et al., 2006). Localized liquid water activities are thought to have occurred episodically over most of Martian history (Malin and Edgett, 2000a; Christensen, 2003; McCollom and Hynek, 2005; Schulze-Makuch et al., 2007; Soare et al., 2007), up to very recent geologic time (e.g. Malin et al., 2006). The wet and warm conditions of early Mars imply that life might have emerged, and may still be present on Mars (Schulze-Makuch and Irwin, 2004). Thus, any site associated with liquid water may also harbour the potential for life on Mars.

The hydrologic history of Mars has been reconstructed from a variety of indicators, which include 1) geomorphology such as shorelines, gullies, channels, valleys and alluvial fans (e.g. Parker et al., 1989; Malin and Edgett, 2000a, 2003; Fairén, et al., 2003; Mangold et al., 2004; Solomon et al., 2005); 2) sedimentary structures such as layered deposits, cross bedding, and layered evaporites (e.g. Malin and Edgett, 2000b; Paige, 2005; Gendrin et al., 2005; Bibring et al., 2005); 3) mineralogy such as hydrated phyllosilicates, hydrated sulphates and other hydroxide minerals (e.g. Arvidson et al., 2005; Poulet et al., 2005; Langevin et al., 2005; Bibring et al., 2006); and 4) anomalies of volatile element concentrations such as Br and Cl (e.g. Dreibus and Waenke, 1987, 2000; Squyres et al., 2004; Haskin et al., 2005).

Gullies imaged by the Mars Obiter Camera (MOC) (1.5 to 12.0 m/pixel) aboard the Mars Global Surveyor (MGS) were first described by Malin and Edgett (2000a). The gully features have been found on crater walls, valley walls, polar pits, scarp faces, mesas, and fretted terrain mostly in areas of 30º – 72 º latitude in both hemispheres

(Heldmann and Mellon, 2004). A gully-exposed site may consist of a single gully or more commonly a gully system with tens of gullies occurring side by side on the same slope face. A single gully is composed of an alcove, a main V-shape channel, and depositional aprons. This is referred to as the alcove-channel-apron structure, which can be hundreds of meters to a few kilometres in length (Heldmann et al., 2007).

Several mechanisms have been proposed to explain gully formation and can be summarized into two categories: liquid water related and non-liquid water related. The proposed liquid water mechanisms include 1) groundwater seeping out onto the surface i. from a shallow subsurface aquifer (Malin and Edgett, 2000a; Mellon and Phillips, 2001; Heldmann and Mellon, 2004; Heldmann et al., 2005, 2007), ii. from a deep subsurface aquifer (Gaidos, 2001), or iii. via localized geothermal heating of permafrost ice (Hartmann, 2001); 2) water melting from shallow ground ice at high obliquity (Mars' axial tilt) (Costard et al., 2002); and 3) snowmelt from dissipating snow packs at high obliquity (e.g. Christensen, 2003). The non-liquid water mechanisms include 1) liquid CO_2 from a buried reservoir (Musselwhite et al., 2001); 2) liquid hydrocarbon seepage (Direito and Webb, 2007); 3) dry landslides (Treiman, 2003); 4) dust avalanches (Sullivan, 2001); and 5) windy sand dune activity (Bart, 2007).

Heldmann et al. (2007) examined gullies and associated mechanisms in detail and suggested that a liquid water mechanism is most likely. The water source is seepage and surface runoff of groundwater from shallow aquifers due to the melting-freezing cycles of ice-cemented soil plugs between the aquifer and the slope surface. This process would be induced by obliquity changes of Mars or by localized geothermal heating in recent geologic time. Malin et al. (2006) compared MOC images taken in December 2001 and April 2005 for one site and in August 1999 and February 2004 for another site, and

concluded that these sites exhibited evidence for liquid water activity in the past few years.

The formation mechanisms of these features, especially in relation to the fluid agent, have been discussed primarily based on geomorphology and fluid mechanics. Our hypothesis is that if liquid water has been the fluid agent, then we should be able to detect water signatures by using hyperspectral images. Liquid water movement near the subsurface would most likely be associated with 1) fast evaporation of water into the atmosphere; 2) freezing of water in the pore space of loose materials; or 3) incorporation of water into minerals by chemical alteration. If so, the gully-exposed sites are likely to maintain more water than their surrounding areas if the gullies were generated by liquid water, especially for those gullies formed recently. This "wetter" surface (sand, soil, regolith) could then be detected with reflectance spectral images.

Hyperspectral images in visible and infrared wavelengths were obtained from OMEGA on board the ESA/Mars Express. The spacecraft began to take images in 2003 and operates within the wavelength range of 0.35 to 5.2 μm using 352 spectral bands of 7 to 20 nm spectral resolution. OMEGA provides images at a spatial resolution of 1.5 – 5 km globally and 350 m for selected areas (Bibring et al., 2005; Gendrin et al., 2005). Visible and near-infrared reflectance spectra are very sensitive to water and hydrated minerals.

In this paper, four gully-exposed sites at Terra Sirenum (36.5ºS/198.2ºE), the north of Reull Vallis (40.0ºS/108.2ºE), on the northeast wall of Hale Crater (35.5ºS/324.6ºE) and the upper Dao Vallis (33.1ºS/93.2ºE) (Fig. 1) were selected to investigate the presence of water, based on 1) availability of OMEGA images covering gully-exposed sites; 2) quality of the available OMEGA images; 3) compatible scale of the size of gully-


N
5 km
N
500 m
N
30 km
A

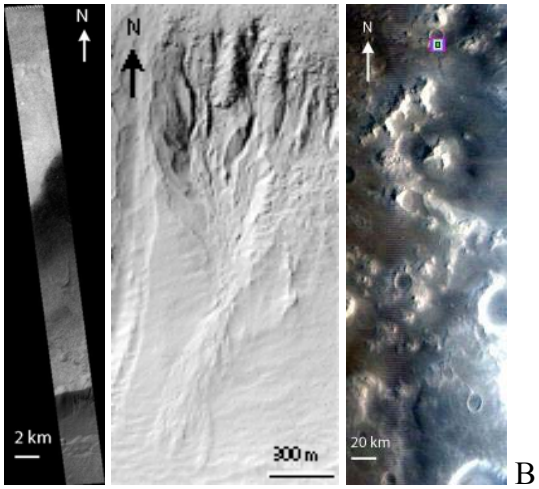
N
2 km
N
300 m
N
20 km
B

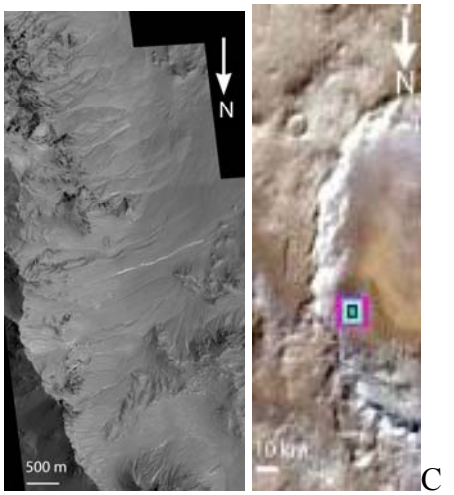
N
500 m
N
10 km
C

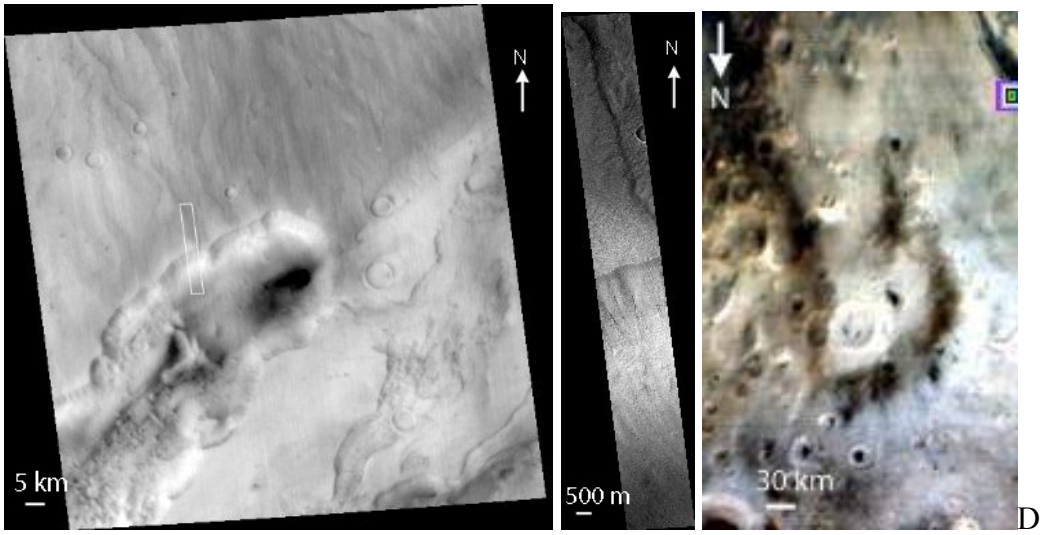
N
5 km
N
500 m
N
30 km
D

Fig. 3-1 MOC and OMEGA images of four investigated gully-exposed sites. The scale and orientation are shown on each image. The square in OMEGA image denotes the gully location. A. MOC wide-angle image S05-01464 (left), narrow-angle image S05-01463 (middle), and OMEGA image orb0140_5 (right) of the gully-exposed site at 36.5ºS/198.2ºE. B. MOC narrow-angle image M04-02479 (left), a subframe of MOC image M04-02479 (middle, from Malin and Edgett, 2000), and the OMEGA image orb1899_2 of the gully-exposed site at 40.0ºS/108.2ºE (right). C. The image of MOC2-1620 (left) released by MGS/MOC, a mosaic of MOC images R07-02277, R13-01791 and S16-01780, and the OMEGA image orb1143_7 (right) of the gully-exposed site at 35.5ºS/324.6ºE. D. MOC wide-angle image M11-01620 (left), narrow-angle image M11-01601 (middle), and the OMEGA image orb1464_4 of the gully-exposed site at 33.1ºS/93.2ºE (right).

exposed sites with the spatial resolution of the corresponding OMEGA image; 4) representation of different types of gully features located at relative lower latitudes for avoiding the effect of CO_2; 5) appropriate Martian season and local time that OMEGA image of gully-exposed site was taken for avoiding the effect of water-frost.

3.2 Methods

We analyzed reflectance spectra of OMEGA images, measured and compared the absorption band depths of water (molecular or hydroxyl) on a pixel scale (statistically), and interpreted the abundances of water components in the surface soils and rocks at the gully-exposed sites (the target site) and its surrounding areas. The absorption depth of the water absorption bands is linearly proportional to the abundance of water-related materials by which the absorption is produced because absorption depth is proportional to the absorption intensity represented by the water absorption band (Clark and Roush, 1984). This is generally true for a small area where the environmental effects (mainly atmospheric abundance and composition, dust, and wind) are invariant and the effect of grain size is limited.

The OMEGA images downloaded from the European Space Agency (ESA) were first transformed to .tiff image format using the IDL code (SOFT03) developed by the ESA/OMEGA team. Atmospheric correction was conducted using the model provided by the ESA/OMEGA team. This model assumes that the Martian atmospheric column is homogeneous and the materials on the summit and at the base of Olympus Mons are identical. Atmospheric absorptions could be removed by dividing the reflectance spectra by a ratio of spectra acquired on Olympus Mons and scaled to the same column density of CO_2 (Langevin et al., 2005).

Reflectance spectra were extracted from a pixel or a group of pixels at the target site and from the surrounding pixel rings (as shown in Fig 2). Reflectance spectra were also extracted pixel by pixel along cross sections through the target site in near E –

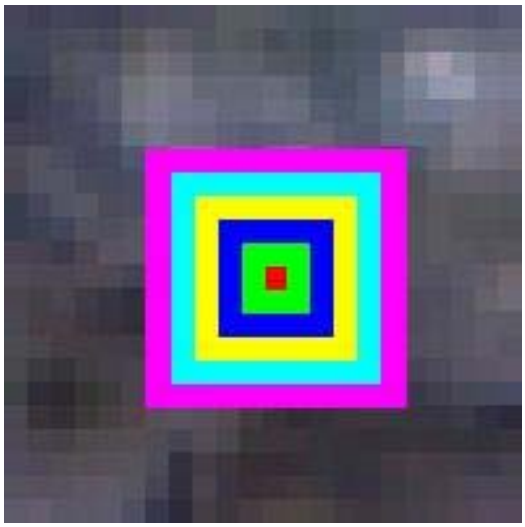

Fig. 3-2 Schematic location of a gully-exposed site as a pixel in the centre (red) and its surrounding areas as pixel rings in an OMEGA image. For example, the 1st ring (green) is a group of 8 pixels, the 2nd ring (blue) is a group of 16 pixels, the 3rd ring (yellow) is a group of 24 pixels, the 4th ring (cyan) is a group of 32 pixels, and the 5th ring (magenta) is a group of 40 pixels.

W and N – S directions. The pixel(s) at the target site and five pixels away from the target site in both directions were investigated. This was assumed to be a reasonable range to observe the variation of the Martian surface materials around gully-exposed areas on the basis of the scale of a gully-exposed site (hundreds meters to a few kilometers) and a pixel in an OMEGA image (0.3 – 5 kilometers). It is reasonable to assume that the center of gully-exposed site might have been subjected to more frequent seepages of groundwater than the surroundings. So more water traces should have been left in the center of gully-exposed site than the surroundings. A correlation coefficient between the absorption depths of water features and the distances from the center outward is thus calculated and analyzed.

A continuum (background absorption) was removed to analyze absorption features as described by Clark (1981a) and Clark and Roush (1984). Continuum removal was employed to eliminate the influence of spectral background, which makes similar spectra distinctive and concentrates on the absorption features. The process can be expressed by:

$$R_c(w) = R_a(w) / C(w) \qquad (1)$$

where R_c is the continuum-removed observed spectrum; R_a is the apparent reflectance spectrum as a function of wavelength, and C is the continuum for the apparent spectrum.

In this paper, we focused our analysis on absorption features of wavelengths ranging from 0.97 to 2.55 μm with a total of 114 channels of OMEGA images. In this wavelength range the presence of H_2O and/or OH can cause a number of absorptions. Water (H_2O) and hydroxyl (OH) in the state of a free molecule, and in minerals or organic matter generates distinct absorptions. The water molecule has three fundamental vibrations; υ_1 (symmetric OH stretch); υ_2 (H-O-H bend); and υ_3 (asymmetric OH stretch). The overtones of water (involving multiples of a single fundamental mode) and

combinations (involving different modes of vibrations) were observed in reflectance spectra of the isolated water and the H_2O-bearing materials (Clark, 1999).

Isolated water molecules have absorption bands at 0.942 μm ($2\upsilon_1+\upsilon_3$, 10615 cm^{-1}), 1.135 μm ($\upsilon_1 + \upsilon_2 + \upsilon_3$, 8810 cm^{-1}), 1.379 μm ($\upsilon_1 + \upsilon_3$, 7251 cm^{-1}), 1.454 μm ($2\upsilon_2 + \upsilon_3$, 6878 cm^{-1}), and ~1.875 μm ($\upsilon_2 + \upsilon_3$, 5333 cm^{-1}) (Hunt and Salisbury, 1970). Water in minerals has combination and overtone bands close to these positions (Clark et al., 1990). OH has only one stretching vibration (υ_{OH}) and its overtones are near 1.40 μm ($2\upsilon_{OH}$, 7143 cm^{-1}) and 0.95 μm ($3\ \upsilon_{OH}$, 10526 cm^{-1}) (e.g., Cloutis et al., 2006). For water ice, the overtones and combination bands are shifted to 1.04 (vs 0.94) μm, 1.25 (vs 1.13) μm, 1.50-1.66 (vs 1.38-1.45) μm, and 1.96-2.05 (vs 1.88) μm (e.g., Clark, 1981, Cloutis et al., 2006). The hydroxyl linked to metals produces a metal-OH bend. Combination vibrations involving the OH stretch and metal-O-H bend cause absorptions in the 2 – 2.5 μm range, such as 2.2 μm for AlOH and 2.29 μm for MgOH and FeOH (Clark et al., 1990).

The depths of absorption features of water vary as a function of water content and structure state (Dalton, 2003). The higher the abundance of a material is, the greater the corresponding absorption band depth. The absorption depth is calculated using two adjacent spectral channels of continuum spectra. The centre band of absorption can be expressed by:

$$D = 1 - R_b / R_c \qquad (2)$$

where D is the depth of absorption band; R_b is the reflectance at the band centre; and R_c is the reflectance of the continuum at the band centre.

A MNF (minimum noise fraction) transformation was used to separate the original bands into MNF bands of noise-free and MNF bands of noise, and then the inverse MNF

was applied to convert the noise-free (less) MNF bands back into the original dimension. Therefore, absorption band depths of water absorption bands were measured using ENVI software for an individual pixel or the mean of a pixel ring from continuum-removed reflectance spectra. Then we compared absorption band depths of the spectra at the target site and its surrounding areas, and pixel by pixel along a cross section through the target site.

3.3 Investigation of selected gully-exposed sites

3.3.1 Gully feature in Terra Sirenum (36.5ºS/198.2ºE)

Gullies were observed on the wall of an unnamed crater of about 3.8 km in diameter at 36.5ºS/198.2ºE as shown in the MOC narrow-angle image S05-01463 with a spatial resolution of 1.56 m/pixel (Fig. 3-1-A). Among these gullies a light-toned flow about 300 meters long was identified by Malin et al. (2006) on the northwest wall of the crater when they compared the MOC image taken in Dec. 2001 (Ls = 290˚) and the image taken in Apr. 2005 (Ls = 193˚). The light-toned flow was interpreted as a fresh deposit with liquid water seeping out onto the surface from a shallow aquifer (Malin et al. 2006).

The OMEGA image Orb1408_5 (Fig. 3-1-A) was downloaded and processed based on the methods described above. The image was taken on Feb. 21, 2005 (Ls =163.5˚). The Mars local time of this site when the OMEGA image was taken was at about 11:05 am (MTC −11, Coordinated Mars Time) in the Martian southern hemisphere later winter. The pixel X: 106/Y: 139 (Lat. –36.477398, Long. 198.218796E) in the image matches with the crater, where gullies were found. One pixel in the OMEGA image at the target site has the areal extent of about 3.9 km×3.2 km on the ground. This is about the same size as the crater itself.

The target pixel and its five surrounding rings of pixels were selected as regions of interest (ROIs). Their reflectance spectra after MNF transformation are shown in Fig. 3-3- A. The spectra of the target site and its surroundings are similar, which indicates that the materials at the target site and in its surrounding areas are similar. Ten absorption bands were observed and examined, among them the water related bands at 1.04, 1.40, 1.50, 1.80, 1.87, 1.91, 2.04, and 2.18 μm. Absorption bands at 1.17 μm related to ferrous materials (coordinated by H_2O, Cloutis et al., 2006) and at 1.97 μm related to CO_2 ice (clathrate, such as CO_2 in water ice, Bernstein et al., 2005) were also examined. The absorption band centres, band ranges, and absorption band depths are shown in Table 3-1. The correlation coefficients between absorption band depths and the locations (distance) of pixel rings relative to the target site were calculated (Table 3-1).

Table 3-1-A indicates that in the target pixel the absorption depths of all water-related bands were larger or equal to those of its adjacent pixel rings except in the atmospheric water vapor band (1.87 μm). The variations from the target pixel to the adjacent pixel rings were 21.4%, 50.0%, 18.8%, 11.2%, 12.5%, and 12.5%, for the 1.04, 1.50, 1.80, 1.91, 2.04 and 2.18 μm bands, respectively. The variations were 16.7% from the target pixel to the second pixel ring and 40% to the forth pixel ring for the 1.40 μm band. At 1.04, 1.40, 1.50 and 2.04 μm the absorption depths decreased as the distances increased from the target site, with a correlation coefficient of 0.83, 0.97, 0.66 and 0.79, respectively (Fig. 3-4-A). In contrast, the absorption depths of the two non-water absorption bands (1.17 and 1.97 μm) and atmospheric water vapour absorption band (1.87 μm) in the target pixel were less than those of the surrounding pixel rings. There was no significant correlation found between the target pixel and adjacent rings for those bands, meaning that the materials in the region are similar, except for the water signatures associated with the gully formation that were indicated at the site.

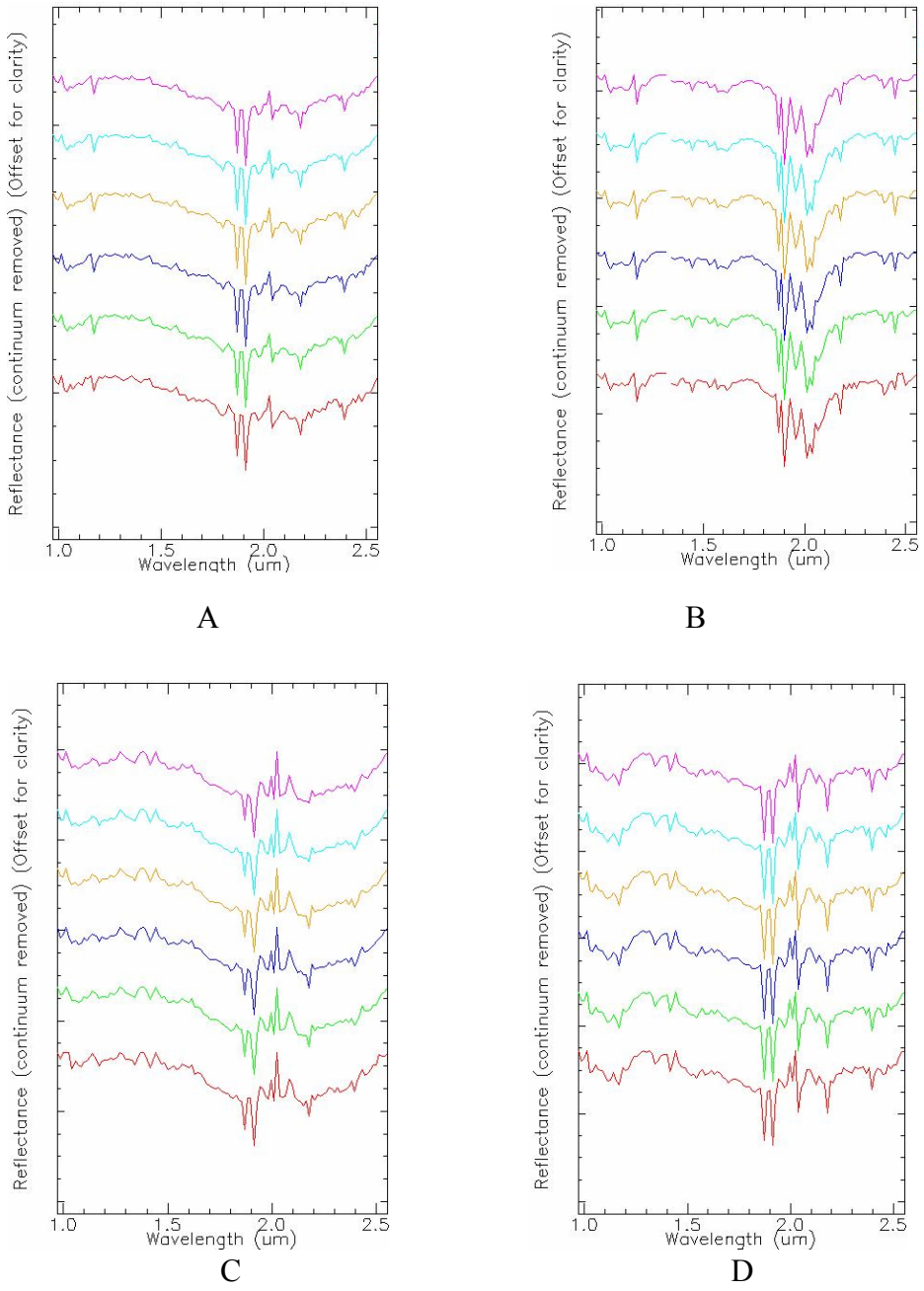

Figure 3-3 Continuum removed reflectance spectra of the target site and its surrounding pixel rings. From the bottom to the top are spectra of the target site (red), 1st pixel ring (green), 2nd pixel ring (blue), 3rd pixel ring (orange), 4th pixel ring (cyan), and 5th pixel ring (magenta). A. at 36.5ºS/198.2ºE, B. at 40.0ºS/108.2ºE, C. at 35.5ºS/324.6ºE, D. at 33.1ºS/93.2ºE.

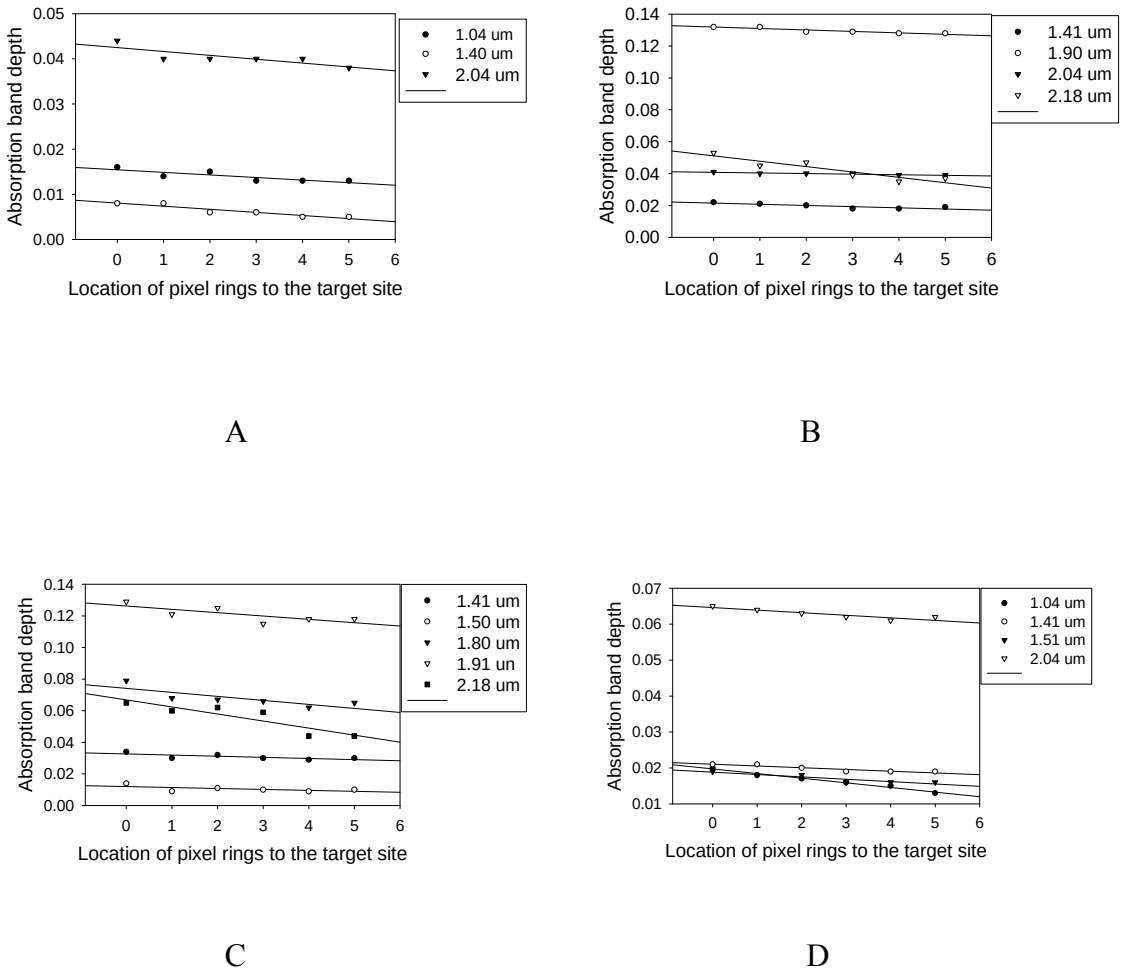

Fig. 3-4 The relationship of the absorption depths related to water and the location of pixel rings. The number 0 in X-axis represents the location of the target site, 1 to 5 correspond to the 1st to 5th ring from the target site. A. at 36.5ºS/198.2ºE, B. at 40.0ºS/108.2ºE, C. at 35.5ºS/324.6ºE, D. at 33.1ºS/93.2ºE.

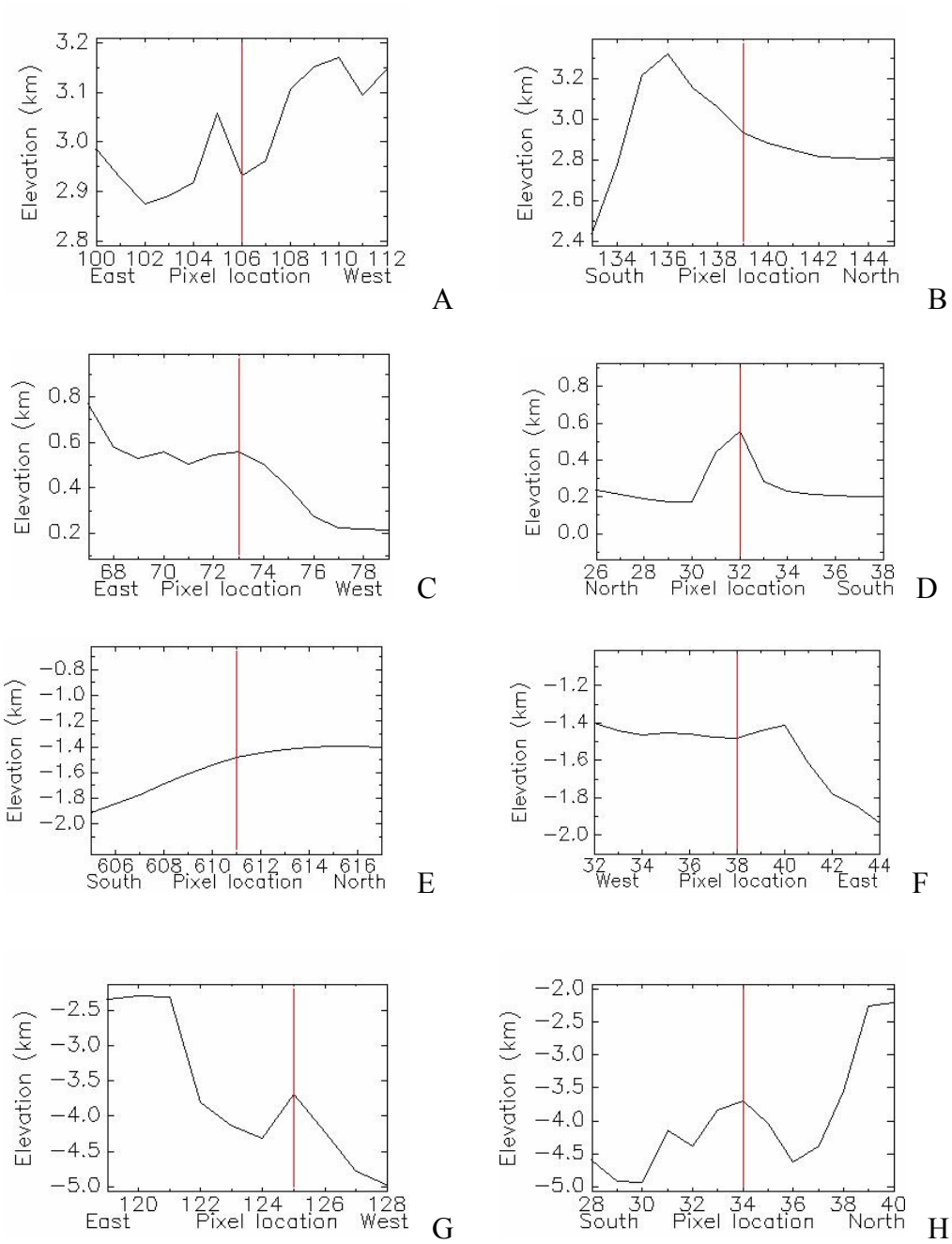

Figure 3-5 Elevation profiles of the investigated sites. The vertical line is the location of the target pixel with each number representing spacing of pixels. A and B is at 36.5ºS/198.2ºE; C and D is at 40.0ºS/108.2ºE ; E and F is at 35.5ºS/324.6ºE ; G and H is at 33.1ºS/93.2ºE.

Table 3-1 (B and C) displays absorption depths of the above band centres along the two cross sections (approximately W-E and S-N) through the target site. Once again, the absorption band depths at the target site were greater than that at the adjacent pixels for most absorption bands associated with water. In contrast, the absorption depths at the target site for 1.17, 1.87 and 1.97 μm bands were lower than or equal to the adjacent pixels. The landforms and elevations may affect absorption band depths, but no relationship between the landform and absorption band depths was recognized when examining the relationship between the elevation of the two cross sections (Fig. 3-5-A, B) and the absorption depths of the water-related bands.

3.3.2 Gully feature to the north of Reull Vallis (40.0ºS/108.2ºE)

An apron with digitate flows was observed to the north of Reull Vallis at 40.0ºS, 108.2ºE (Malin and Edgett, 2000) among a cluster of gullies in the MOC narrow-angle image M04-02479 (Fig. 3-1-B). This MOC image was taken on Aug. 22, 1999 (Ls = 192.5º) with a spatial resolution of 2.79 meter/pixel. About 5 subsidiary channels merge into one downslope forming a gully system of about 1 km in width and 2 km in length.

The OMEGA image orb1887_3 taken on July 05, 2005 (Ls = 243.0º) was downloaded (Fig. 3-1-B). The Mars local time of this site when the OMEGA image was taken was at about 4:49 pm (MTC + 7) in the Martian southern hemisphere late spring. The pixel X:73/Y:32 (Lat. –40.009499, Long. 108.204300E) was assigned to be the gully-exposed site based on their matched coordinates. One pixel in the OMEGA image at the target site has the areal extent of about 1.6 km×2.1 km on the ground. This is about the size of the apron with digitate flows.

The target pixel and its five surrounding pixel rings were selected as the regions of interest (ROIs). Their reflectance spectra after MNF transformation are shown in Fig. 3-

3-B. Seven absorption bands were examined, including the water related bands at 1.04, 1.41, 1.87, 1.90, 2.04, and 2.18 μm and the ferrous materials related one at 1.17 μm. Shown in Table 3-2 are the absorption band centres, band ranges, absorption band depths, and the correlation coefficients between absorption band depths and the locations (distance) of pixel rings relative to the target site.

As indicated in Table 3-2, the absorption depths of the target pixel are greater than or equal to those of the adjacent pixel ring for the water-related bands of 1.04, 1.41, 1.90, 2.04 and 2.18 μm, but reversely for the band of 1.17 μm and the water vapor related bands of 1.87 μm. The decreases of absorption depths from the target site to the adjacent pixel ring were 5.8%, 4.8%, 2.5% and 17.8% for the bands of 1.04, 1.41, 2.04 and 2.18 μm, respectively. Higher correlation coefficients (greater than 0.85) between these absorption depths and reverse distances to the target site were recognized for the bands of 1.41 1.90, 2.04 and 2.18 μm (Fig. 3-4-B). In contrast, the absorption depths of non-water absorption band (1.17 μm) and atmospheric water vapour absorption band (1.87 μm) in the target pixel were less than those of the surrounding pixel rings. The correlation coefficients for the two bands are also very low. The stronger signatures of water were only shown to be associated with the surface material at the gully-exposed site.

The absorption depths of the above bands along the two cross sections (approximately W-E and S-N) through the target site were also investigated. Once again, the absorption band depths at the target site were greater than or equal to that at the adjacent pixels for the absorption bands associated with water on the ground rather than non-water and water vapour related bands. Although no significant correlation between the water related absorption depths and the reverse distance to the target site was found, no relationship between these absorption band depths and the landform (Fig. 3-5-C, D) was also recognized.

Table 3-1 Data of absorption band depths of gully feature in Terra Sirenum **(**36.5ºS/198.2ºE**)**

A. at the target site and its surrounding rings										
Band range	1.0121 /1.0550	1.1555 /1.1986	1.3568 /1.4430	1.4861 /1.5291	1.7291 /1.8285	1.8285 /1.8850	1.8850 /1.9553	1.9553 /2.0253	2.0253 /2.0948	2.0948 /2.2188
Center	1.0407	1.1699	1.3999	1.5004	1.8002	1.8709	1.9132	1.9693	2.0392	2.1776
Target pixel	0.017	0.021	0.007	0.003	0.019	0.07	0.09	0.019	0.045	0.036
1st	0.014	0.027	0.007	0.002	0.016	0.071	0.089	0.02	0.04	0.032
2nd	0.014	0.026	0.006	0.002	0.015	0.07	0.091	0.021	0.041	0.032
3rd	0.013	0.025	0.006	0.002	0.016	0.067	0.092	0.02	0.041	0.032
4th	0.013	0.025	0.005	0.002	0.018	0.068	0.09	0.019	0.039	0.036
5th	0.013	0.026	0.005	0.002	0.016	0.071	0.089	0.02	0.039	0.035
Correlation	0.828	-0.459	0.956	0.655	0.284	0.228	0.046	-0.071	0.791	-0.183
B. in the cross section of East-West direction through the target site										
East	0.015	0.028	0.007	0.003	0.015	0.072	0.088	0.023	0.039	0.029
	0.016	0.024	0.008	0.002	0.02	0.073	0.091	0.018	0.037	0.033
	0.015	0.025	0.006	0.002	0.016	0.068	0.093	0.018	0.042	0.03
	0.017	0.024	0.008	0.003	0.021	0.066	0.097	0.023	0.044	0.03
	0.015	0.026	0.008	0.003	0.016	0.065	0.093	0.02	0.043	0.036
Target	0.017	0.021	0.007	0.003	0.019	0.07	0.09	0.019	0.045	0.036
	0.017	0.029	0.005	0.004	0.017	0.064	0.085	0.023	0.037	0.031
	0.016	0.032	0.008	0.002	0.016	0.081	0.087	0.021	0.04	0.033
	0.018	0.023	0.006	0.002	0.014	0.068	0.08	0.018	0.043	0.03
	0.019	0.025	0.007	0.002	0.014	0.071	0.087	0.021	0.036	0.03
West	0.017	0.028	0.009	0.003	0.015	0.067	0.089	0.027	0.043	0.03
Correlation	-0.029	-0.186	-0.283	0.361	0.403	-0.196	0.140	-0.316	0.369	0.693
C. in the cross section of South-North direction through the target site										
South	0.012	0.022	0.006	0.002	0.02	0.066	0.087	0.018	0.038	0.035
	0.011	0.02	0.005	0.002	0.023	0.071	0.089	0.02	0.043	0.036
	0.016	0.026	0.008	0.002	0.026	0.071	0.093	0.026	0.046	0.036
	0.018	0.023	0.006	0.003	0.021	0.074	0.091	0.024	0.044	0.034
	0.011	0.017	0.007	0.003	0.021	0.076	0.088	0.019	0.041	0.03
Target	0.017	0.021	0.007	0.003	0.019	0.07	0.09	0.019	0.045	0.036
	0.014	0.028	0.01	0.002	0.01	0.073	0.091	0.025	0.041	0.035
	0.016	0.021	0.006	0.002	0.012	0.069	0.093	0.025	0.041	0.022
	0.008	0.022	0.01	0.004	0.02	0.073	0.097	0.02	0.042	0.036
	0.019	0.021	0.004	0.005	0.021	0.076	0.098	0.022	0.039	0.042
North	0.012	0.023	0.008	0.004	0.012	0.082	0.098	0.02	0.038	0.042
Correlation	0.258	-0.011	0.283	-0.213	-0.140	-0.146	-0.331	0.230	0.555	-0.467

Table 3-2 Data of absorption band depths of gully feature to the north of Reull Vallis (40.0ºS/108.2ºE)

A. at the target site and its surrounding rings									
Band range	1.0121 /1.0550	1.1555 /1.2849	1.3999 /1.4717	1.8568 /1.8850	1.8850 /1.9272	1.9272 /1.9834	1.9834 /2.0253	2.0253 /2.0531	2.1501 /2.1914
Center	1.0407	1.1699	1.4130	1.8709	1.8991	1.9553	2.0113	2.0392	2.1776
Target	0.018	0.053	0.022	0.07	0.132	0.065	0.057	0.041	0.053
1st ring	0.017	0.054	0.021	0.079	0.132	0.065	0.053	0.04	0.045
2nd ring	0.018	0.051	0.02	0.074	0.129	0.065	0.053	0.04	0.047
3rd ring	0.019	0.052	0.018	0.077	0.129	0.062	0.052	0.04	0.039
4th ring	0.018	0.053	0.018	0.074	0.128	0.061	0.053	0.039	0.035
5th ring	0.018	0.052	0.019	0.072	0.128	0.063	0.053	0.039	0.037
Correlation	-0.338	0.357	0.851	0.033	0.919	0.759	0.638	0.923	0.919
B. in the cross section of East-West direction through the target site									
East	0.02	0.057	0.017	0.072	0.035	0.068	0.074	0.041	0.044
	0.017	0.059	0.02	0.071	0.128	0.071	0.059	0.04	0.049
	0.018	0.063	0.018	0.068	0.129	0.057	0.055	0.041	0.053
	0.022	0.067	0.018	0.069	0.129	0.06	0.05	0.042	0.04
	0.02	0.059	0.021	0.07	0.132	0.064	0.055	0.04	0.039
Target	0.018	0.053	0.022	0.07	0.132	0.065	0.057	0.041	0.053
	0.02	0.051	0.022	0.072	0.13	0.07	0.043	0.041	0.032
	0.022	0.05	0.021	0.08	0.131	0.069	0.057	0.04	0.039
	0.022	0.049	0.019	0.074	0.13	0.068	0.053	0.04	0.042
	0.018	0.056	0.019	0.073	0.129	0.061	0.056	0.041	0.054
West	0.016	0.06	0.018	0.081	0.127	0.063	0.057	0.04	0.045
Correlation	0.364	-0.245	0.794	-0.355	0.491	0.036	-0.569	0.185	-0.292
C. in the cross section of South-North direction through the target site									
North	0.016	0.055	0.022	0.066	0.132	0.068	0.053	0.034	0.008
	0.022	0.043	0.02	0.071	0.128	0.07	0.05	0.039	0.017
	0.023	0.055	0.019	0.069	0.13	0.066	0.052	0.039	0.009
	0.018	0.053	0.022	0.071	0.121	0.061	0.047	0.039	0.057
	0.015	0.053	0.022	0.075	0.133	0.062	0.054	0.037	0.045
Target	0.018	0.053	0.022	0.07	0.132	0.065	0.057	0.041	0.053
	0.021	0.054	0.023	0.097	0.13	0.071	0.052	0.04	0.04
	0.02	0.051	0.021	0.074	0.131	0.067	0.059	0.04	0.036
	0.019	0.065	0.022	0.078	0.131	0.056	0.044	0.04	0.068
	0.015	0.057	0.018	0.067	0.126	0.061	0.053	0.04	0.046
South	0.019	0.043	0.027	0.07	0.129	0.061	0.05	0.039	0.068
Correlation	0.018	0.217	-0.049	0.478	0.173	0.090	0.344	0.443	0.236

Table 3-3 Data of absorption band depths of gully feature on the northeast wall of Hale Crater (35.5ºS/324.6ºE)

A. at the target site and its surrounding rings										
Band range	1.0121 /1.0550	1.1555 /1.1986	1.3855 /1.4430	1.4861 /1.5291	1.7291 /1.8285	1.8285 /1.8850	1.8850 /1.9413	1.9413 /1.9973	2.0253 /2.0809	2.0948 /2.2188
Center	1.0407	1.1699	1.4143	1.5004	1.8002	1.8709	1.9132	1.9693	2.0531	2.1776
Target pixel	0.026	0.013	0.034	0.014	0.079	0.011	0.129	0.041	0.085	0.065
1st	0.011	0.009	0.03	0.009	0.068	0.019	0.121	0.04	0.08	0.06
2nd	0.015	0.011	0.032	0.011	0.067	0.019	0.125	0.041	0.082	0.062
3rd	0.015	0.012	0.03	0.01	0.066	0.014	0.115	0.04	0.085	0.059
4th	0.015	0.015	0.029	0.009	0.062	0.016	0.118	0.044	0.081	0.044
5th	0.016	0.013	0.03	0.01	0.065	0.015	0.118	0.043	0.086	0.044
Correlation	0.471	-0.498	0.728	0.600	0.814	-0.104	0.764	-0.683	-0.237	0.900
B. in the cross section of East-West direction through the target site										
East	0.022	0.005	0.03	0.011	0.066	0.028	0.116	0.037	0.075	0.073
	0.021	0.029	0.024	0.009	0.061	0.02	0.107	0.049	0.078	0.052
	0.023	0.012	0.029	0.011	0.066	0.01	0.117	0.051	0.091	0.059
	0.034	0.029	0.029	0.011	0.067	0.014	0.12	0.044	0.085	0.057
	0.009	0.003	0.03	0.012	0.072	0.018	0.123	0.042	0.077	0.055
Target	0.026	0.016	0.034	0.014	0.079	0.011	0.129	0.041	0.085	0.056
	0.025	0.006	0.031	0.012	0.071	0.01	0.129	0.035	0.082	0.054
	0.02	0.015	0.032	0.014	0.065	0.016	0.129	0.052	0.085	0.063
	0.014	0.015	0.032	0.011	0.051	0.009	0.113	0.043	0.082	0.063
	0.011	0.017	0.032	0.01	0.061	0.01	0.115	0.044	0.081	0.062
West	0.012	0.011	0.033	0.01	0.057	0.019	0.128	0.048	0.084	0.05
Correlation	0.321	-0.077	0.251	0.757	0.718	-0.505	0.534	-0.246	0.254	-0.273
C. in the cross section of South-North direction through the target site										
South	0.014	0.026	0.031	0.009	0.073	0.022	0.119	0.026	0.097	0.07
	0.018	0.024	0.032	0.015	0.054	0.01	0.116	0.047	0.089	0.093
	0.023	0.025	0.033	0.006	0.074	0.026	0.115	0.025	0.097	0.079
	0.009	0.024	0.042	0.016	0.06	0.034	0.137	0.015	0.096	0.069
	0.016	0.009	0.028	0.005	0.08	0.02	0.109	0.043	0.085	0.075
Target	0.026	0.019	0.034	0.014	0.079	0.011	0.129	0.041	0.085	0.065
	0.019	0.008	0.025	0.009	0.079	0.016	0.138	0.038	0.081	0.052
	0.03	0.008	0.031	0.011	0.074	0.019	0.125	0.045	0.079	0.076
	0.045	0.015	0.028	0.012	0.069	0.014	0.125	0.05	0.084	0.052
	0.013	0.015	0.03	0.01	0.066	0.015	0.136	0.037	0.077	0.078
North	0.026	0.016	0.031	0.011	0.065	0.013	0.115	0.035	0.077	0.054
Correlation	0.064	-0.442	0.012	-0.003	0.585	0.071	0.302	0.164	-0.079	-0.153

Table 3-4 Data of absorption band depths of gully feature in the upper Dao Vallis (33.1ºS/93.2ºE)

A. at the target site and its surrounding rings										
Band range	1.0121 /1.0550	1.01411 /1.1842	1.3136 /1.3855	1.3855 /1.4430	1.4430 /1.6150	1.8586 /1.8850	1.8850 /1.9413	1.9413 /1.9973	2.0253 /2.0948	2.1363 /2.1914
Centre	1.040	1.17	1.342	1.414	1.514	1.871	1.913	1.969	2.039	2.178
Target	0.019	0.018	0.013	0.021	0.019	0.06	0.07	0.020	0.066	0.039
1st ring	0.018	0.020	0.014	0.021	0.018	0.061	0.068	0.022	0.064	0.034
2nd ring	0.017	0.020	0.015	0.02	0.018	0.06	0.07	0.023	0.064	0.038
3rd ring	0.016	0.019	0.015	0.019	0.016	0.061	0.07	0.017	0.064	0.038
4th ring	0.015	0.019	0.014	0.019	0.016	0.061	0.07	0.014	0.062	0.036
5th ring	0.014	0.018	0.014	0.019	0.016	0.061	0.068	0.019	0.062	0.038
Correlation	1.000	0.239	-0.355	0.924	0.925	-0.621	0.207	0.565	0.923	0.262
B. in the cross section of South-West direction through the target site										
South	0.015	0.024	0.024	0.024	0.023	0.064	0.073	0.032	0.068	0.031
	0.021	0.023	0.024	0.022	0.02	0.057	0.073	0.028	0.068	0.033
	0.022	0.022	0.019	0.022	0.021	0.059	0.075	0.024	0.071	0.030
	0.016	0.021	0.017	0.022	0.021	0.062	0.074	0.027	0.07	0.036
	0.016	0.022	0.017	0.024	0.021	0.06	0.067	0.024	0.067	0.034
Target	0.027	0.017	0.015	0.022	0.021	0.059	0.07	0.018	0.067	0.033
Target	0.025	0.019	0.015	0.02	0.019	0.065	0.072	0.021	0.065	0.044
	0.017	0.023	0.014	0.019	0.017	0.062	0.068	0.020	0.061	0.040
	0.015	0.018	0.012	0.019	0.016	0.059	0.07	0.017	0.06	0.045
	0.014	0.020	0.013	0.019	0.016	0.061	0.066	0.020	0.06	0.043
	0.015	0.020	0.013	0.018	0.015	0.06	0.07	0.018	0.057	0.035
North	0.014	0.019	0.012	0.017	0.014	0.061	0.068	0.013	0.061	0.039
Correlation	0.572	-0.373	-0.309	0.154	0.209	0.124	-0.140	-0.171	0.128	0.301
C. in the cross section of East-West direction through the target site										
East	0.018	0.015	0.011	0.017	0.013	0.059	0.068	0.019	0.059	0.043
	0.014	0.014	0.012	0.018	0.014	0.058	0.068	0.018	0.061	0.046
	0.016	0.016	0.012	0.018	0.014	0.06	0.07	0.014	0.061	0.047
	0.018	0.021	0.012	0.018	0.014	0.062	0.069	0.017	0.06	0.048
	0.017	0.017	0.013	0.018	0.015	0.058	0.067	0.020	0.059	0.047
Target	0.025	0.019	0.013	0.019	0.017	0.058	0.069	0.021	0.061	0.044
Target	0.014	0.020	0.015	0.02	0.019	0.065	0.072	0.019	0.065	0.042
	0.020	0.021	0.016	0.021	0.02	0.063	0.072	0.023	0.068	0.041
	0.019	0.023	0.02	0.021	0.02	0.061	0.075	0.027	0.068	0.030
Correlation	0.364	0.631	0.410	0.600	0.666	0.403	0.311	0.312	0.380	-0.105

3.3.3 Gully feature on the northeast wall of Hale Crater (35.5ºS/324.6ºE)

Several gullies with light-toned material on their floors and deposited in their aprons were observed on the northeast wall of Hale Crater (35.5ºS/324.6ºE) by the MOC team at Malin Space Science System (Fig. 3-1-C). The light-toned deposits (about 1.5 km in length) may be produced by water flow during the past few years (http://www.msss.com/mars_ images/moc/2006/12/06/gullies/).

The matched OMEGA image orb1143_7 (Fig. 3-1-C) was taken on Dec. 8, 2004 (Ls = 126.2). The Mars local time when the OMEGA image was taken was at about 2:15 pm (MTC –2). An individual pixel in the image at the site covers about 1.1 km × 1.2 km area. The pixel X:38/Y:611 (Lat. –35.498600, Long. 324.592285) in the OMEGA image was assigned to be the target site due to their best match.

The reflectance spectra of the target site and five surrounding rings after the process of MNF transformation are shown in Fig. 3-3-C. The absorptions of ten bands were examined, among them the water-related being 1.04, 1.41, 1.50, 1.80, 1.87, 1.91, 2.05 and 2.18 μm. As Table 3-3 indicated, the absorption depths of all water-related bands at the target site were greater than the adjacent pixel ring except the absorption of water vapor at 1.87 μm. The variations of absorption depths from the target site to the adjacent pixel ring is by 145.5%, 13.3%, 55.6%, 6.7%, 6.3% and 8.3% for the bands of 1.04, 1.41, 1.50, 1.91, 2.05 and 2.18 μm. These variations are significantly greater than the variations of absorption depths from one pixel ring to another pixel ring for each absorption band above.

Some absorption bands show higher correlation between the absorption depths and the reverse distance to the target site but some do not. The absorption bands with the

higher correlation coefficients are 1.41 μm (0.73), 1.50 μm (0.60), 1.80 μm (0.81), 1.91 μm (0.76) and 2.18 μm (0.90) (Fig. 3-4-C). In contrast, non water-related absorption bands at 1.17 and 1.97 μm displays negative correlation between the absorption depths and the reverse distance to the target site.

Through examination of the two cross sections passing through the gully-exposed site in the W-E direction and the N-S direction (Table 3-3), the absorption depths at the target site are higher or equal to that of the adjacent pixels for most water-related bands. But most of these bands don't show a significant correlation between the absorption depths and the distance to the target site. No relationship was recognized between the variations of these absorption depths and the profiles of in-situ landforms in both W-E and N-S directions (Fig. 3-5-E and F).

3.3.4 Gully feature in the upper Dao Vallis (33.1ºS/93.2ºE)

Alcoves filled or partially filled with deposit materials at the site at 33.1ºS/93.2ºE were interpreted to be the result of sapping due to groundwater seeping out from subsurface layers (Malin and Edgett, 2000a). The features are common throughout the wall of Dao Vallis. The specific site is shown in the MOC narrow-angle image M11-01601 with spatial resolution of 2.78 m/pixel (Fig. 3-1-D), which is 2.85 km in width and 21.71 km in length.

The OMEGA image orb1464_4 (Fig. 3-1-D) processed was taken on March 3, 2005 (Ls = 168.9). The Mars local time at the OMEGA image acquisition was taken was at about 10:26 am (MTC +6) in the Martian southern hemisphere later winter. One pixel at the site was about 3.9 km x 3.3 km. The ROI of four pixels X: 125-126/Y:33-34 (Lat. –

33.068600 to –33.120399, Long. 93.183800 to 93.257896E) was selected to match up with the site exposing alcoves and associated deposits.

The absorptions of ten bands after MNF transformation were examined (Fig. 3-3-D). The absorption depths of water-related bands (1.04, 1.41, 1.51, 1.91, 2.04, and 2.18 μm) at the target site were greater than or equal to those in the adjacent pixel ring (Table 3-4-A). The variations from the target site to the adjacent pixel ring are 5.6%, 5.6%, 2.9%, 3.1% and 14.7% for the absorption bands of 1.04, 1.41, 1.51, 1.91, 2.04 and 2.18 μm. In contrast, the absorption depths of non water-related bands (1.17, 1.34 and 1.97 μm) and water vapour related band (1.87 μm) are smaller at the target site than the adjacent pixel ring.

The absorption depths of the 1.04, 1.41, 1.51, and 2.04 μm bands showed spatial variations with high correlation coefficients (above 0.92) (Fig. 3-4-D). In contrast, the 1.87 μm band (atmospheric H_2O) showed a reverse trend and the 1.17 and 1.34 μm (non-water absorption bands) remained fairly stable. The inconsistency of absorption depths of these bands might indicate that the stronger absorptions of 1.04, 1.41, 1.54 and 2.04 μm at the target site compared to the surrounding areas have to be attributed to the influences of water components in the rocks and soil, but not the atmosphere or systematic errors of instruments and analysis.

Along the cross sections (Table 3-4-B and C), the absorption depths related to water essentially showed an increasing trend towards the south in the N-S direction and towards the west in the E-W direction. The trends are likely attributed to the profile of landforms at the site (Fig. 3-5-G and F), because the differences of elevation were about 2.8 km between both ends of the N-S cross section and 2.7 km between both ends of the E-W cross section. The significant difference of elevation led to accumulation of water in

the lowland areas. Nevertheless, the absorption depths at the target site were still larger than their adjacent pixels for most of the water absorption bands.

3.4 Discussion

Investigation of the four sites in this study showed greater absorption depths of water-related bands at the gully-exposed sites than those at the adjacent pixel rings, and smaller absorption depths of water-related bands in the surrounding pixel rings. The decrease trend of some absorption depths when moving further away from the site were also observed at the investigated gully-exposed sites. This likely indicates higher abundance of water ice, OH-bearing or hydrated materials in surface soil at the gully-exposed site.

Absorptions of the investigated sites commonly occurred at all or part of bands, ~1.04, ~1.17, ~1.34, ~1.40, ~1.50, ~1.80 ~1.87, ~1.91, ~1.97, ~2.04, and ~2.18 μm, although a few other weak absorptions were recognized occasionally. Recognizable were the shifts of band positions, and the variation of absorption shapes, width (full width at half maximum) and depth of band centre from pixel to pixel in most cases. Analyzing absorption features of reflectance spectra and measuring their depths are vital to studying subtle differences of composition and structure of materials.

The overtones and combinations of vibrations of water at ~1.40 and ~1.91 μm, the lower frequencies of water ice at ~1.50 and ~2.04 μm, and the combination of metal-OH bend and OH stretch at 2.18 etc. were evident for most reflectance spectra of OMEGA images at the gully-exposed sites on Mars. In addition, the following were observed: a weak absorption of water ice at 1.04 μm; absorption at 1.80 μm attributed to a combination of H-O-H and O-H stretching and bending (Cloutis et al., 2006); and absorption of atmospheric water at 1.87 μm. If the investigated site is close to the polar

areas, the absorptions of CO_2 ice might dominate reflectance spectra and severely affect the measurement of subtle variation of water-related absorptions.

The absorption band at 1.91 μm was the most obvious among the absorptions of water-related bands and its depth was 3% or more greater at the target sites than the adjacent areas for four investigated sites. The absorption depths at 1.80 μm were about 16% greater at the target site than the adjacent area at two sites (36.5ºS/198.2ºE and 35.5ºS/324.6ºE) and showed a higher correlation (0.814) with respect to the target site at the gully-exposed site of 35.5ºS/324.6ºE. Absorption at 1.80 um is not significantly overlapped by bands from other common minerals (Cloutis et al., 2006). The absorptions at the 1.41 μm band were not significant in regard to absolute depths, but they were the largest at the target sites. Higher correlation (greater than 0.83) between the absorption depth of 1.41 μm and the distance to the target site was shown at two gully-exposed sites (36.5ºS/198.2ºE and 33.1ºS/93.2ºE).

The absorption depths of water ice at the 1.04, 1.50 and 2.04 μm bands were all greater at the target sites than those at adjacent pixel ring. The largest variations of absorption depths from the target site to the adjacent ring was 136% for 1.04 μm and 56% for 1.50 μm at the site of 35.5ºS/324.6ºE, and 13% for 2.04 μm at the site of 36.5ºS/198.2ºE. Higher correlation coefficients between the absorption depths of these bands and the distance to the target site were recognized at two sites (36.5ºS/198.2ºE and 33.1ºS/93.2ºE). The absorption of 1.50 μm is thought to be the best band to monitor water ice on the Martian surface with OMEGA (Langevin et al., 2007).

The absorption depths at 2.18 μm were all the greatest at the target sites and about 8.3 – 17.8% greater than those at adjacent pixel ring for four investigated sites. High correlation coefficients (> 0.9) between the absorption depths and the distance to the

target site were recognized at two gully-exposed sites (40.0ºS/108.2ºE and 35.5ºS/324.6ºE). The absorption is likely associated with metal-OH bonds, but other factors such as S-O bonding (2.2 – 2.4 μm when associated with H_2O) may play a role. The absorption depths of water-related bands had a maximum at the target sites, even given that their variations were affected by extreme changes of the landforms. In some cross sections, the variations of absorption depths were consistent with the extensions of the gully-exposed sites.

In contrast, non-water associated absorption bands such as those less than 1.20 μm, of 1.97 μm, and water vapour absorption (1.87 μm) usually did not show the same characteristics as water-related absorption bands. The absorption depths of these bands were less at the target site than the adjacent pixel ring at all the investigated sites except for the site at 35.5ºS/324.6ºE. Some of them even showed a reverse relation to water–related bands, that is, the absorption depths increased with distance from the target site. Absorptions at a wavelength of less than the 1.20 μm band are usually associated with transition elements, most commonly ferric and ferrous minerals. They may be caused by iron atoms linking through shared oxygen or hydroxyl ions (Rossman, 1975), and ferrous crystal field transition or coordination with H_2O and SO_4^{2-} (Cloutis et al., 2006). The absorption at 1.97μm is the contribution of CO_2 ice (e.g. Bernstein et al., 2005), which is detected at four investigated sites. Atmospheric water vapor at 1.87 μm did not follow the trend of absorption depths as other forms of water in the surface soil.

For a small local area in the same OMEGA image, the environmental and instrumental conditions should be the same when these pixels were imaged. They were also subject to the same image processing procedure including atmospheric correction. Thus, the greater absorption band depths indicated the content of water in the surface materials at the target sites than their surrounding areas.

The stronger signature of water at the gully-exposed sites may be caused by water-ice, isolated water molecules or hydroxyl groups in the soils, or seasonal water frost on the surface (Svitek and Murray, 1990; Reiss and Jaumann, 2003; Schorghofer and Edgett, 2006; Bellucci et al., 2007). Water frost was not likely the main cause because the images we investigated were taken in the Martian late spring, in the Martian late winter, or at about 2:15 pm of Mars local time in the early winter. The observed frost appears during the period of early to mid southern hemisphere winter but not in later winter and spring times (Schorghofer and Edgett, 2006). So at least three of the four investigated OMEGA images were taken in later winter and spring time. Even for the image taken in the early winter, the local surface temperature could be higher than 200° K (the sublime point of water frost) at about 2:15 pm of the Martian day. But the effect of water frost on the absorption depths of water-related bands at gully-exposed sites deserves further discussion, especially for the image taken in the early winter time.

The pressure - temperature conditions on the surface of Mars are very close to the triple point of water, thus some water will likely freeze very fast in the loose materials. Alternatively, it may stay attached to the mineral surface or evaporate into the atmosphere after it has seeped out from the subsurface. Alteration could take place if hydrothermal fluids were involved and remained there for a fairly long period of time. So the accumulation of water at the gully-exposed sites implies that liquid water was once likely more active at the site than in its surrounding regions. Subsequently, liquid water was involved in the formation of the gully features and associated deposits.

The extension of about 5 pixels away from the target site was considered to be a reasonable range for the investigation, because the size of gully-exposed sites is about the size of an individual pixel (2-5 x 2-5 km^2) in the OMEGA image. The influence of the residual of atmospheric correction or the systematic errors of the imaging spectrometer

on the absorptions of reflectance spectra should be limited because 1) all absorption band depths at a specific site were calculated in the same OMEGA image, so all pixels were subject to the same processes; 2) the analysis of absorption variations were restricted in the scope of a few pixels, which were imaged almost at the same time, with the same atmospheric conditions and under the same solar radiation; 3) the trace content (0.03%) of water vapour in the Martian atmosphere does not make much difference in regard to absorption band depths (a few to tens percent as shown here) within the elevation change of the landform in hundreds of meters.

There are a variety of factors that may limit the conclusions drawn from this study. They include 1) limited knowledge of grain size that might have affected the absorption depth; 2) the influence of seasonal changes of temperature on imaged materials; 3) strong CO_2 absorption features at wavelengths around 2 μm both in the solid state and in the atmosphere (Langevin et al. 2007), especially for the gully-exposed site close to the polar areas; and 4) the limitation of the spatial resolution of OMEGA hyperspectral images in the case study, 5) errors in registering gully-exposed sites found from from MOC images to OMEGA images due to the possible inaccuracy of two geo-referencing systems (this is likely the reason why not all assumed gully-exposed sites we investigated indicate stronger water signatures at the target site than the surrounding areas).

No hydrated mineral was detected at the gully-exposed site in the Centauri Montes region in the hyperspectral image taken by the Compact Reconnaissance Imaging Spectrometer for Mars (CRISM) (McEwen et al., 2007), where a light toned deposits was thought to be the fresh deposits created by liquid water (Malin et al., 2006). Numerical flow modelling shows that the deposits of dry granular flow are more consistent with the observed morphology of the deposits (Pelletier et al., 2008). These suggest that the gullies formed by mechanisms rather than liquid water agents could not be ruled out.

However, a stronger water signature at the gully-exposed sites than the adjacent pixel ring and a clear trend of variation of water related absorption depths between gullies and their surrounding areas at some gully-exposed sites have been observed in this study. More analysis of hyperspectra at higher spatial and spectral resolution such as CRISM, covering wavelength from 0.362 to 3.92 μm at 6.55 nm/channel and 15.7 to 19.7 m/pixel (http://crism.jhuapl.edu/), should provide detailed evidence about it.

3.5 Conclusions

The depth of the water related absorption bands was observed to be greater at the gully-exposed site than in its surrounding areas, thus supporting the conclusion that the formation of gullies has involved processes associated with liquid water. Subtle variations of absorption band depths, especially their trends provide insights in identifying small differences of materials with very similar reflectance spectra due to the sensitivity of imaging spectroscopy to material composition and structure. Further study of hyperspectral images is desirable with higher spatial and spectral resolutions (e.g. CRISM) for better understanding of the water occurrence at gully sites.

Acknowledgement: We are indebted to the ESA/OMEGA team for making available OMEGA hyperspectral images to us and providing algorithm of atmospheric correction. We also like to thank the MGS/MOC team for making available MOC high resolution images. We especially want to thank two anonymous reviewers for their critical and insightful comments which help to improve the paper significantly.

References:

Arvidson, R.E., F. Poulet, J-P. Bibring, M. Wolff, A. Gendrin, R.V. Morris, J.J. Freeman, Y. Langevin, N. Mangold and G. Bellucci, 2005. Spectral reflectance and morphologic correlations in eastern Terra Meridiani, Mars. *Science* 307, 1591–1594.

Bart, G.D., 2007. Comparison of small lunar landslides and Martian gullies. *Icarus* 187, 417–421.

Bellucci, G., J. Helbert, F. Altieri, D. Reiss, J.P. Bibring, S. van Gasselt, H. Hoffmann, Y. Langevin, G. Neukum and F. Poulet, 2007. Evidence for enhanced hydration on the northern flank of Olympus Mons, Mars. *Icarus* 192, 361-377.

Bernstein, M.P., D.P. Cruikshank and S.A. Sandford, 2005. Near-infrared laboratory spectra of solid H_2O/CO_2 and CH_3OH/CO_2 ice mixtures. *Icarus* 179, 527–534.

Bibring, J-P., Y. Langevin, A. Gendrin, B. Gondet, F. Poulet, M. Berthé, A. Soufflot, R. Arvidson, N. Mangold, J. Mustard, P. Drossart and the OMEGA team, 2005. Mars surface diversity as revealed by the OMEGA/Mars express observations. *Science* 307, 1576–1581.

Bibring J-P., Y. Langevin, J.F. Mustard, F. Poulet, R. Arvidson, A. Gendrin, B. Gondet, N. Mangold, P. Pinet, F. Forget and the OMEGA team, 2006. Global mineralogical and aqueous Mars history derived from OMEGA/Mars Express data. *Science* 312, 400–404.

Christensen, P.R., 2003. Formation of recent Martian gullies through melting of extensive water-rich snow deposits. *Nature* 422, 45–48.

Clark, R.N., 1981a. Water frost and ice: the near-infrared special reflectance 0.65-2.5 um. *J. Geophys. Res.* 86, 3087–3096.

Clark, R.N., 1981b. The spectral reflectance of water-mineral mixtures at low temperatures. *J. Geophys. Res.* 86, 3074–3086.

Clark, R.N. and T.L. Roush, 1984. Reflectance spectroscopy: quantitative analysis techniques for remote sensing application. *J. Geophys. Res.* 89, 6329–6340.

Clark, R.N., T.V.V. King, M. Klejwa, G.A. Swayze and N. Vergo, 1990. High spectral resolution reflectance spectroscopy of minerals. *J. Geophys. Res.* 95, 12653–12680.

Clark, R.N., 1999. Spectroscopy of rocks and minerals and principles of spectroscopy. In: Rencz, A.N. (Ed.), Manual of Remote Sensing, John Wiley and Sons, New York.

Cloutis, E.A., F.C. Hawthorne, S.A. Mertzman, K. Krenn, M.A. Craig, D. Marcino, M. Methot, J. Strong, J.F. Mustard, D.L. Blaney, J.F. Bell III and F. Vilas, 2006. Detection and discrimination of sulfate minerals using reflectance spectroscopy. *Icarus* 184, 121–157.

Costard, F., F. Forget, N. Mangold and J.P. Peulvast, 2002. Formation of recent Martian debris flows by melting of near-surface ground ice at high obliquity. *Science* 295, 110–113.

Craddock, R.A. and A.D. Howard, 2002. The case for rainfall on a warm, wet early Mars. *J. Geophys. Res.* 107, 5111, doi: 10.1029/2001JE001505.

Dalton, J.B., 2003. Spectral behaviour of hydrated sulphate salts: Implications for Europa mission spectrometer design. *Astrobiology* 3, 771–784.

Direito, M.S. and M.E. Webb, 2007. Search for oil reservoirs on Mars. *International J. of Astrobiology* 6, 62–63.

Dreibus, G. and H. Waenke, 1987. Volatiles on Earth and Mars: A comparison. *Icarus* 71, 225–240.

Dreibus, G. And H. Waenke, 2000. The volatile inventory of Earth and Mars. *AGU 2000 Spring Meeting*, Washington, DC.

Fairén, A.G., J.M. Dohm, V.R. Baker, M.A. de Pablo, J. Ruiz, J. Ferris and R. Anderson, 2003. Episodic flood inundations of the northern plains of Mars. *Icarus* 165, 53–67.

Gaidos, E.J., 2001. Cryovolcanism and the recent flow of liquid water on Mars. *Icarus* 153, 218–223.

Gendrin, A. N. Mangold, J-P. Bibring, Y. Langevin, B. Gondet, F. Poulet, G. Bonello, C. Quantin, J. Mustard, R. Arvidson and S. LeMouélic, 2005. Sulphates in Martian layered terrains: The OMEGA/Mars Express View. *Science* 307, 1587–1591.

Golombek, M.P., 1999. Martian climate: A message from warmer times. *Science* 283, 1470–1471.

Grundy, W.M. and B. Schmitt, 1998. The temperature-dependent near-infrared absorption spectrum of hexagonal H_2O ice. *J. Geophys. Res.* 103**,** 25809–25822.

Hamilton, C.J., Views of the solar system, http://www.solarviews.com/cap/mgs/PIA01040.htm.

Hartmann, W.K., 2001. Martian seeps and their relation to youthful geothermal activity. *Space Sci. Rev.* 96, 405–410.

Haskin, L.A., A. Wang, B.L. Jolliff, H.Y. McSween, B.C. Clark, D.J. Des Marais, S.M. McLennan, N.J. Tosca, J.A. Hurowitz, J.D. Farmer, A. Yen, S.W. Squyres, R.E. Arvidson, G. Klingelhöfer, C. Schröder, P.A. de Souza, Jr, D.W. Ming, R. Gellert, J. Zipfel, J. Brückner, J.F. Bell, III, K. Herkenhoff, P.R. Christensen, S. Ruff, D. Blaney, S. Gorevan, N.A. Cabrol, L. Crumpler, J. Grant and L. Soderblom, 2005. Water alteration of rocks and soils on Mars at the Spirit rover site in Gusev crater. *Nature* 436, 66–69.

Heldmann, J.L. and M.T. Mellon, 2004. Observations of Martian gullies and constraints on potential formation mechanisms. *Icarus* 168, 285–304.

Heldmann, J.L., O.B. Toon, W.H. Pollard, M.T. Mellon , J. Pitlick, C.P. McKay and D.T. Anderson, 2005. Formation of Martian gullies by the action of liquid water flowing under current Martian environmental conditions. *J. Geophys. Res.* 110, E05004, 110, E05004, doi: 10.1029/2004JE002261.

Heldmann, J.L., E. Carlsson, H. Johansson, M.T. Mellon and O.B. Toon, 2007. Observations of Martian gullies and constraints on potential formation mechanisms: II. The northern hemisphere. *Icarus* 188, 324–344.

Hunt, G.R. and J.W. Salisbury, 1970. Visible and near infrared spectra of minerals and rocks, I, silicate minerals. *Mod. Geol.* 2, 283–300.

Kerr, R.A., 2003. Running water eroded a frigid early Mars. *Science* 300, 1496–1497.

Langevin, Y., F. Poulet, J-P. Bibring and B.Gondet, 2005. Sulphates in the north polar region of Mars detected by OMEGA/Mars express. *Science* 307, 1584–1586.

Langevin, Y., J-P., Bibring, F. Montmessin, F. Forget, M. Vincendon, S. Doute, F. Poulet and B. Gondet, 2007. Observations of the south seasonal cap of Mars during recession in 2004–2006 by the OMEGA visible/near-infrared imaging spectrometer on board Mars express. *J. Geophys. Res.* 112, E08S12, doi: 10.1029/2006JE002841.

Malin, M.C. and K.S. Edgett, 2000a. Evidence for recent groundwater seepage and surface runoff on Mars. *Science* 288, 2330–2335.

Malin, M.C. and K.S. Edgett, 2000b. Sedimentary rocks of early Mars. *Science* 290, 1927–1937.

Malin, M.C. and K.S. Edgett, 2003. Evidence for persistent flow and aqueous sedimentation on early Mars. *Science* 302, 1931–1934.

Malin, M.C., K.S. Edgett, L.V. Posiolova, S.M. McColley and E.Z.N. Dobrea, 2006. Present-day impact cratering rate and contemporary gully activity on Mars. *Science* 314, 1573–1577.

Malin Space Science Systems, 2000. Mars Global Surveyor Mars Orbiter Camera Image Gallery. http://www.msss.com/moc_gallery/.

Mangold, N., C. Quantin, V. Ansan, C. Delacourt and P. Allemand, 2004. Evidence for precipitation on Mars from dentritic valleys in the Valles Marineris area. *Science* 305, 78–81.

McCollom, T.M. and B.M. Hynek, 2005. A volcanic environment for bedrock diagenesis at Meridiani Planum on Mars. *Nature* 438, 1129–1131.

Mellon, M.T. and R.J. Phillips, 2001. Recent gullies on Mars and the source of liquid water. *J. Geophys. Res.* 106, 23165–23179.

Musselwhite, D.S., T.D. Swindle and J.I. Lunine, 2001. Liquid CO_2 breakout and the formation of recent small gullies on Mars. *Geophys. Res. Lett.* 28, 1283–1286.

Paige, D.A., 2005. Ancient Mars: Wet in many places. *Science* 307, 1575–1576.

Parker, T.J., R.S. Saunders and D.M. Schneeberger, 1989. Transitional morphology in west Deuteronilus Mensae, Mars: Implications for modifications of the lowland/ upland boundary. *Icarus* 82, 111–145.

Pollack, J.B., J.F. Kasting, S.M. Richardson and K. Poliakoff, 1987. The case for a wet, warm climate on early Mars. *Icarus* 71, 203–224.

Poulet, F., J-P. Bibring, J.F. Mustard, A. Gendrin, N. Mangold, Y. Langevin, R.E. Arvidson, B. Gondet and C. Gomez, 2005. Phyllosilicates on Mars and implications for early Martian climate. *Nature* 438, 623–627.

Reiss, D. and R. Jaumann, 2003. Recent debris flows on Mars: Seasonal observations of the Russell Crater dune field. *Geophys. Res. Lett.* 30, DOI 10.1029/2002GL016704.

Rossman, G.R., 1975. Spectroscopic and magnetic studies of ferric iron hydroxyl sulphates: Intensification of colour in ferric iron clusters bridged by a single hydroxide ion. *Am. Mineral.* 60, 698–704.

Sagan, C., O.B. Toon and P.J. Gierasch, 1973. Climatic change on Mars. *Science* 181, 1045–1049.

Schorghofer, N. and K. S. Edgett, 2006. Seasonal surface frost at low latitudes on Mars. *Icarus* 180, 321–334.

Schulze-Makuch, D., J.M. Dohm, C. Fan, A.G. Fairén, J.A.P. Rodriguez, V.R. Baker and W. Fink, 2007. Exploration of hydrothermal targets on Mars. *Icarus* 189, 308–324.

Schulze-Makuch, D. and L.N. Irwin, 2004. Life in the universe: Expectations and constraints. Springer, Berlin.

Soare, R.J., J.S. Kargel, G.R. Osinski and F. Costard, 2007. Thermokarst processes and the origin of crater-rim gullies in Utopia and western Elysium Planitia. *Icarus* 191, 95–112.

Solomon, S.C., O. Aharonson, J.M. Aurnou, W.B. Banerdt, M.H. Carr, A.J. Dombard, H.V. Frey, M.P. Golombek, S.A. Hauck, II, J.W. Head, III, B.M. Jakosky, C.L. Johnson, P.J. McGovern, G.A. Neumann, R.J. Phillips, D.E. Smith and M.T. Zuber, 2005. New perspectives on ancient Mars. *Science* 307, 1214–1220.

Squyres, S.W. and J.F. Kasting, 1994. Early Mars: How warm and how wet? *Science* 265, 744–749.

Squyres, S.W., J.P. Grotzinger, R.E. Arvidson, J.F. Bell, III, W. Calvin, P.R. Christensen, B.C. Clark, J.A. Crisp, W.H. Farrand, K.E. Herkenhoff, J.R. Johnson, G. Klingelhöfer, A.H. Knoll, S.M. McLennan, H.Y. McSween, Jr., R.V. Morris, J.W.

Rice, Jr., R. Rieder and L.A. Soderblom, 2004. In situ evidence for an ancient aqueous environment at Meridiani Planum, Mars. *Science* 306, 1709–1714.

Sullivan, R., P. Thomas, J. Veverka, M. Malin and K.S. Edgett, 2001. Mass movement slope streaks imaged by the Mars Orbiter Camera. *J. Geophys. Res.* 106, 23607–23634.

Svitek, T and B. Murray, 1990. Winter Frost at the Viking Lander 2 site. *J. Geophys. Res.* 95, 1495–1510.

Tanaka, K.L., 2000. Fountains of youth. *Science* 288, 2325.

Treiman, A.H., 2003. Geologic settings of Martian gullies: Implications for their origins. *J. Geophys. Res.* 108(E4), doi: 10.1029/2002JE001900.

CHAPTER 4

CHARACTERIZATION OF THE PHOENIX LANDING SITE

Abstract

The Phoenix spacecraft is scheduled to land on Mars in May 2008. Its mission is to focus on subsurface water-ice, climate and the habitability of Mars. The landing site has been determined to be in a region centered at 68.35N, 233.0E based on the considerations of both science and safe landing constraints. In this study, I characterized the Phoenix Landing Site (PLS) from the surrounding environment, the topography, the composition of surface and sub-surface materials at the landing site, and the atmosphere above the landing site based on OMEGA (Visible and Infrared Mineralogical Mapping Spectrometer) hyperspectral images. The results show that the PLS is quite flat with the gradient of the land being less than 1% and featureless at the kilometer scale. The surface materials are likely soils or regolith of basaltic andesite composition. The sub-surficial water-ice table at the PLS is several centimetres below the surface and water signatures on the ground and in the atmosphere are stable at the scale of tens of kilometers. The site is concluded to be an ideal site for landing the Phoenix spacecraft safely and conducting its investigations to reveal clues about the habitability of Mars.

Keywords: Phoenix Landing Site, Topography, Soil and Regolith, Water-ice Table.

4.1 Introduction

The Phoenix spacecraft was launched on Aug. 4, 2007 and is scheduled to land on Mars on May 25, 2008. Phoenix is the first mission targeting the sub-polar region of Mars and its robotic arm may dig into an icy layer just beneath the surface. The mission follows NASA's theme of "Following the Water", and will 1) study the history of the water in the ice or icy soil, 2) study the climate and weather of the northern sub-polar region, and 3) search for evidence of habitable zones and investigate the biologic potential of the ice-soil boundary (Smith et al., 2006).

On board the Phoenix spacecraft are a suite of science instruments representing state of the art technology. These instruments include 1) a Microscopy, Electrochemistry and Conductivity Analyzer (MECA), an instrument package consisting of a wet chemistry laboratory, optical and atomic force microscopes and a thermal and electrical conductivity probe; 2) a Thermal and Evolved Gas Analyzer (TEGA), which is a high temperature furnace and mass spectrometer; 3) a Robotic Arm (RA); 4) a Robotic Arm Camera (RAC); 5) a Surface Stereo Imager (SSI); 6) a Mars Descent Imager (MARDI) and 7) a Meteorological Station (MET).

Samples of soil and ice collected by the Phoenix Lander's robotic arm will be analyzed by MECA and TEGA. RA is designed to dig trenches, scoop up soil and water-ice samples, and deliver these samples to the MECA and TEGA instruments. TEGA will analyze water and carbon-containing compounds by heating soil samples in tiny (about 30 microliters) ovens and examine the vapors that are given off. MECA will test soil samples by adding water and analyzing the dissolution products. Cameras and microscopes will provide information on scales spanning 10^{10} orders of spatial magnitude. A weather station will provide information about daily weather and seasonal changes in the northern sub-polar region by using temperature and pressure sensors plus a

laser-reflection instrument (Phoenix Mars Mission, http://phoenix.lpl.arizona.edu/ mission. php).

The selection of the PLS is critical for conducting the mission successfully, which should meet both science goals and engineering safety requirements. The down selection (reducing candidates) process was used to make a final decision of the PLS. The primary criterion was the depth of ice at the landing site for science (Arvdison et al. 2006). Site altitude, slope, atmospheric dynamics, surface reflectivity, thermal inertia and albedo were also considered for science and engineering safety (Guinn et al., 2006). In this research, I attempt to characterize the PLS and its surrounding environment, the topography, the composition of surface materials at the landing site, and the water or water-ice in the subsurface and in the atmosphere above the landing site based on OMEGA (Visible and Infrared Mineralogical Mapping Spectrometer) hyperspectral images and research conducted previously.

4.2 Location and Topography of the Phoenix Landing Site

4.2.1 Location of the Phoenix Landing Site

Research on the landing site selection of the Phoenix Lander has been conducted for years. The region centered at 68.35N, 233.0E, spanning 7º latitude in the N-S direction and 20º longitude in the W-E direction, has been finalized as the PLS (communication with Peter H. Smith, PI of the Phoenix mission) from four regions within a zone from 65 to 72 degrees north latitude (Smith et al. 2007) by the down-selection process (Fig. 4-1). This zone was chosen based mainly on initial estimates of subsurface ice abundance (Kirk et al., 2006). As shown in Fig. 4-1, the PLS is located at a region called “Kansas flat” within the arctic plains of Vastitas Borealis and close to the west circumpolar area of the Martian northern pole. The west Martian circumpolar area is

considered to be more active than its opposite side due to the occurrences of sulfates and volcanic cones.

To the north of the landing site, there is an extended region at 240°E, 85°N of 60 × 200 km^2 identified as calcium-rich sulfates, most likely gypsum, by Langevin et al. (2005) through OMEGA hyperspectral images. The signature of sulfates is strongest in the red region with 1.94 μm absorption greater than 25% and decreases as the color changes from red (absorption depth >25%) to purple (6%) based on the absorption strength of band 1.927 μm (Langevin et al., 2005). The origin of the sulfates is debatable, but likely related to volcanic processes. Among proposed mechanisms are the interaction of acidic snow with basalt during periods of volcanic activity (Bibring *et al.,* 2005; Gendrin *et al.,* 2005) and outflows from the ice cap during a warm climate followed by evaporation of salt-rich water (Langevin et al., 2005).

More than two dozen volcanic cones or domes were identified by the European Space Agency (ESA)/High Resolution Stereo Camera (HRSC) team in the northern circumpolar regions of Mars. Listed in Table 4-1 are the coordinates of six volcanic cones (courtesy of Dr. Ganna Portyankina, Max-Planck Institute). These volcanic cones are mainly located in the dark polar dune fields at longitude from 240º to 300º and latitude from 75º to 85º. They are several tens of meters to 600 meters in size and have been proposed to be as young as ~10^4 – 10^5 years, and have potentially still active (Neukum and Gasselt, 2006).

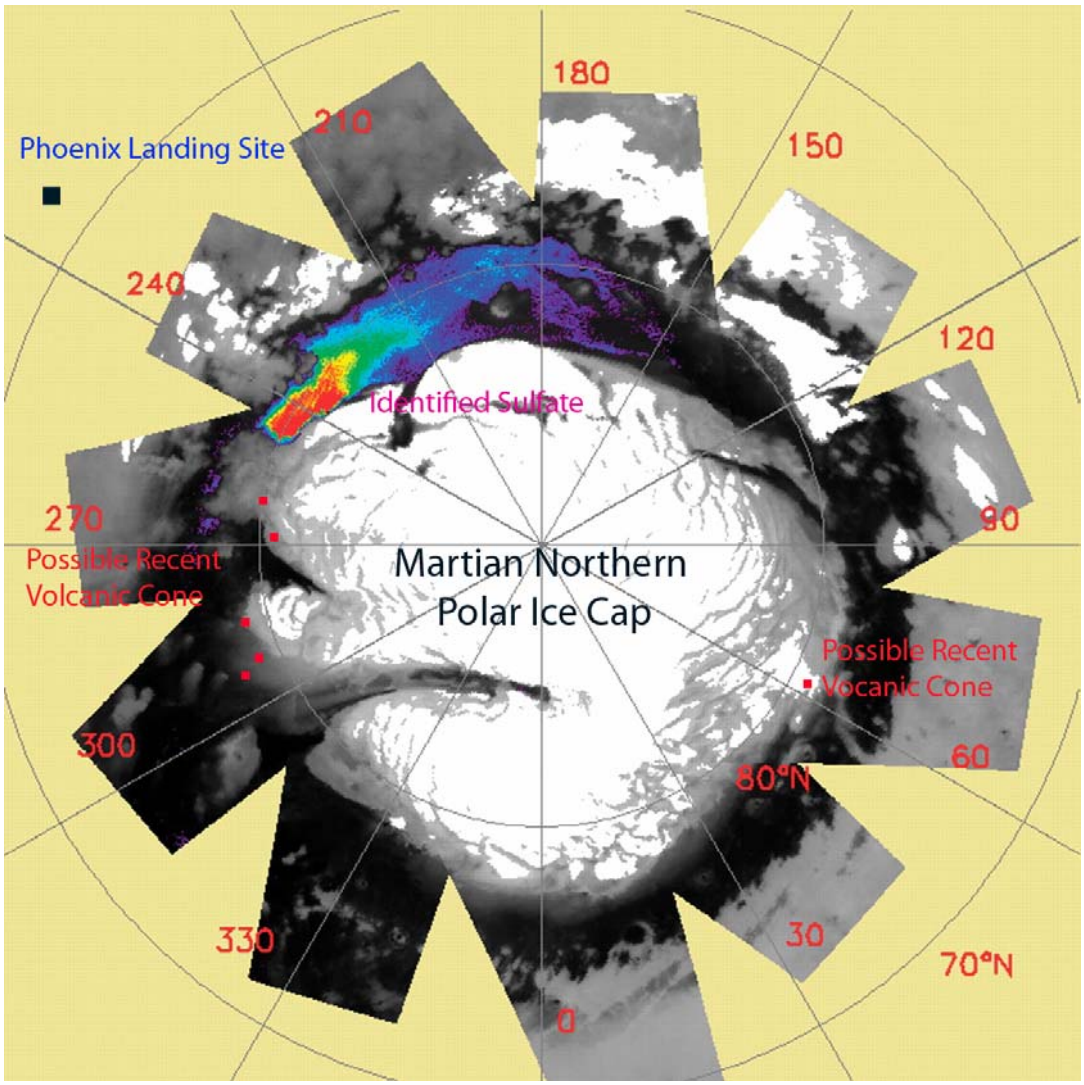

Fig. 4-1 Location of the Phoenix Landing Site modified based on Langevin et al. (2005). The dark blue square is the Phoenix Landing Site at a region called "Kansas flat" within the arctic plains of Vastitas Borealis. Red squares are the proposed recent volcanic cones. White patches are the northern polar ice cap or ice slabs in the circumpolar areas based on water ice band strength at 1.5 μm (>20%). The colorful patch is sulfates identified by OMEGA team, with colors from purple (6%) to red (>25%) based on band strength (Langevin et al., 2005).

Table 4-1 Location of the proposed recent volcanic cones in the northern polar area and the available images for these areas (from Portyankinna, 2007).

Number	Coordinate	HRSC or MOC image	OMEGA image
1	80.5ºN 269.0ºE	HRSC image 1169	Unavailable
2	79.0ºN 289.2ºE	HRSC image 1264	Orb0955-0
3	80.1ºN 260.0ºE		Orb0964-2
4	79.2ºN 285.5ºE		Orb1054-2
5	78.2ºN 293.5ºE		Orb1026-3
6	78.9ºN 60.4ºE	MOC image R1602017	Unavailable

The relationship between the PLS, the identified sulfate distribution and the proposed recent volcanic cones is not clear. This may be an interesting topic when more detailed information from the PLS is available.

4.2.2 Topography of the Phoenix Landing Site

The topography of the PLS candidate sites has been studied by numerous workers (e.g. Kirk et al., 2006, Beyer, 2006). Kirk et al. (2006) analyzed MOC (Mars Orbiter Camera) narrow-angle image sets of the PLS candidate sites using the USGS (United States Geological Survey) in-house digital cartographic software ISIS (Intelligent Searching of Images and Signals) based on steroanalysis and photoclinometry. These images have a high resolution ranging from 1.8 to 8.4 m/pixel. Based on his research on the stereo digital elevation models (DEMs) of the PLS candidate sites, the relief is generally less than 100m, consistent with the Mars Orbiter Laser Altimeter (MOLA) data. The range of RMS (root mean square) slopes over shortest baseline is 0.8º to 4.5º, much less than 16º, the requirement for safe entry, descent and landing (EDL) of the Phoenix spacecraft. Beyer (2006) analyzed meter-scale slopes of the PLS candidate sites from the MOC narrow-angle images using the point photoclinometry technique. Based on the analysis, the images are very similar with low roughness characteristics and their RMS slopes are less than 10°.

Topographic mapping by MGS's (Mars Global Surveyor) laser altimeter shows a specific target ellipse of a broad, shallow valley about 50 km in width and 250 meters in depth at the finalized PLS (Fig. 4-2) (Phoenix Launch: Mission to the Martian polar north, www.nasa.gov). The finalized PLS appears flat and featureless, so it is likely safe enough for the Phoenix Lander to touch down.

Here, we identify the topography of the finalized PLS based on the OMEGA image orb1034_3 (Fig. 4-3) downloaded from ESA/Planetary Science Archive (PSA) website. Extracted are the profiles of the W-E traverse through the PLS at different scales (Fig. 4-4) and the profiles of the N-S traverse through the PLS at different scales (Fig. 4-5).

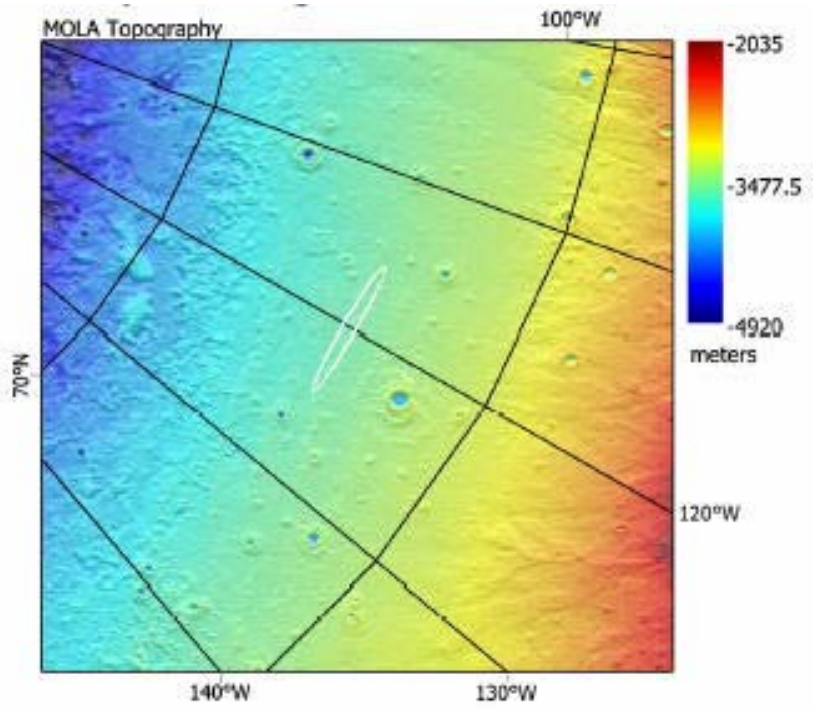

Fig. 4-2 The target ellipse of the Phoenix Landing Site outlined in white (http://planetary.chem.tufts.edu/Phoenix/landing_site_selection.htm)

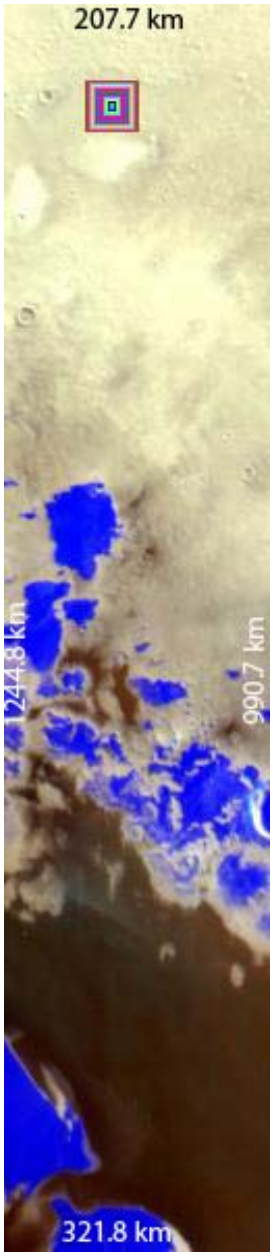

A

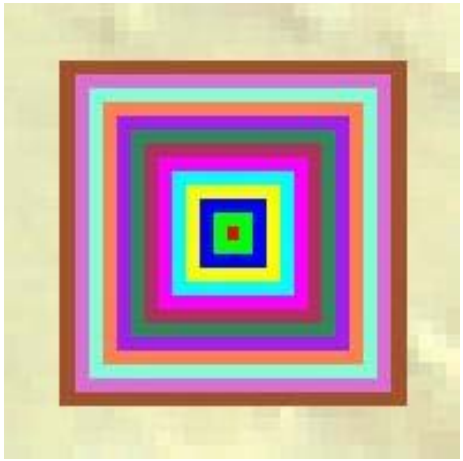

B

Fig. 4-3 OMEGA image orb1034_3 (A) and the schematic square box of the Phoenix Landing Site in OMEGA image (B). A. The scale of OMEGA image orb1034_3 (real distance on Mars) is shown on each edge. B. The center of the square is the PLS (one pixel) and each ring of the square is made up of a line of pixels.

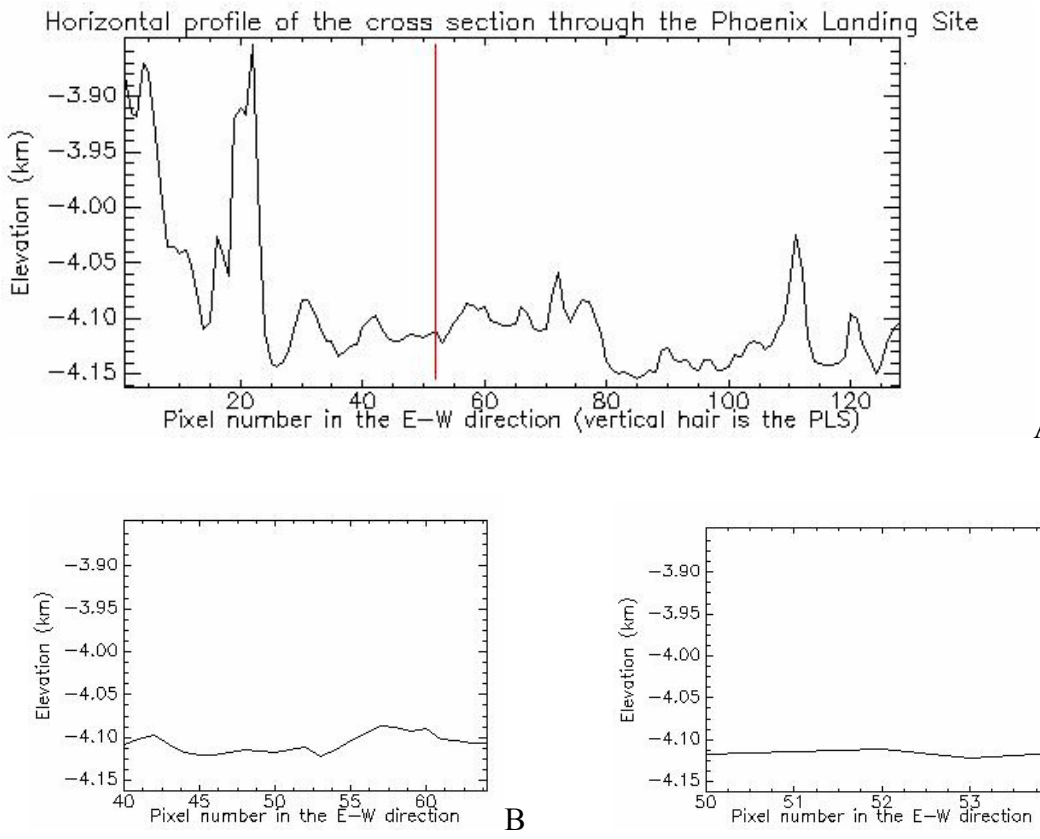

Fig. 4-4 Profiles of the W-E traverse through the Phoenix Landing Site at different scales. Pixel number 52 is the PLS. The traverse A is across of the entire OMEGA image orb1034_3. Traverse B is about 50 km and traverse C is about 5 km.

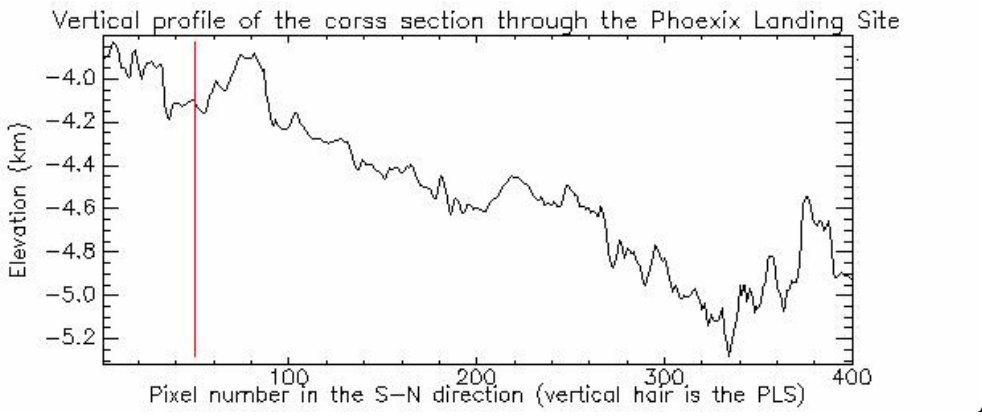

A

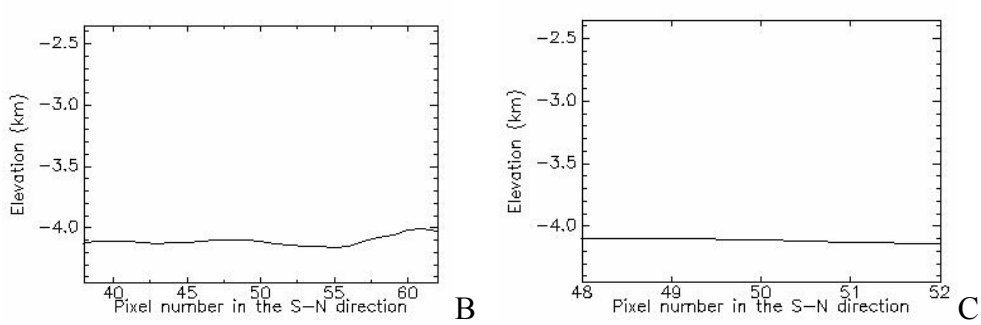

B C

Fig. 4-5 Profiles of the N-S traverse through the Phoenix Landing Site at different scales. Pixel number 50 is the PLS. The traverse A is across the entire OMEGA image orb1034_3. Traverse B is about 50 km and traverse C about 5 km.

In order to estimate individual pixel size at the specific OMEGA image, the Haversine formula was used assuming a smooth spherical surface for Mars. The great-circle distance of two points on the Martian surface is given by:

$$D = R \times 2 \times a \tan 2\left(\sqrt{\alpha}, \sqrt{(1-\alpha)}\right) \quad (1)$$

Where D is the distance of two points on the Martian surface; $\alpha = \sin^2\left((lat2 - lat1)/2\right) + \cos(lat1) \times \cos(lat2) \times \sin^2\left((long2 - long1)/2\right)$; R is Mars's radius; *lat*1 and *lat*2 are the latitudes of two points; *long*1 and *long*2 are longitudes of the two points.

One pixel at the PLS in this OMEGA image covers about 1.57 × 1.81 km^2 based on the coordinates of two adjacent pixels. Gradients and the degrees of surface slopes at the PLS at scales of kilometers to tens of kilometers are calculated based on the relief of pixels of W-E and N-S traverses through the PLS (Table 4-2). As Table 4-2 indicates, this region is a very flat plain with gradients of slope less than 0.97% (0.56 degrees) within 5 km and less than 0.39% (0.22 degrees) within 50 km from the PLS in all four major directions. This region is an ideal site for the Phoenix spacecraft to land based on landforms on the scale of kilometres. However, this scale may not be large enough to know the meter and sub-meter scale variation of the PLS landform required for safe landing. A comprehensive analysis including MOC, HRSC, HiRISE (High Resolution Imaging Science Experiment), THEMIS (Thermal Emission Imaging System) images is needed for more compelling insights.

Table 4-2 The elevation of pixels and the gradient and degree of ground surface slope along W-E and N-S traverses through the Phoenix Landing Site.

N-S profile	Pixel location	38	48	49	PLS pixel	51	52	62
	Elevation (km)	–4.121	–4.096	–4.096	–4.112	–4.130	–4.137	–4.025
	Distance (km)	22.256	3.722	1.861		1.861	3.716	22.318
	Gradient to PLS	0.04%	0.43%	0.86%		0.97%	0.67%	0.39%
	Degree of slope	0.02	0.25	0.49		0.56	0.38	0.22
W-E profile	Pixel location	40	50	51	PLS pixel	53	54	64
	Elevation (km)	–4.108	–4.118	–4.115	–4.112	–4.122	–4.115	–4.107
	Distance (km)	20.250	3.149	1.572		1.801	3.375	19.793
	Gradient to PLS	0.02%	0.19%	0.19%		0.56%	0.09%	0.03%
	Degree of slope	0.01	0.11	0.11		0.32	0.05	0.02

4.3 Composition of surface materials at the Phoenix landing site

Mineral distribution at the PLS candidate sites was investigated by Poulet et al. (2006) through the OMEGA hyperspectral images. Their investigation indicated that the spectral properties are quite homogenous for all PLS candidate sites and no mafic, sulphate or phyllosilicate minerals are evident. In this study, we used reflectance spectra of wavelengths between 0.97 and 2.55 μm of OMEGA image orb1034_3 to investigate the composition of surface materials, because spectra in this wavelength range are very sensitive to water and hydrated minerals.

The OMEGA image used was obtained between 0.35 and 5.2 μm wavelengths using 352 spectral bands of 7 to 20 nm spectral resolution (Bibring et al., 2005). The image orb1034_3 was downloaded from the ESA/PSA website and transformed to .tiff image format using IDL software. Atmospheric correction was made using the model provided by the ESA/OMEGA team. This model assumes that the Martian atmospheric column is homogeneous and the materials on the summit and at the bottom of Olympus Mons are identical. Atmospheric absorptions could be removed by dividing the

reflectance spectra by a ratio of spectra acquired on Olympus Mons and scaled to the same column density of CO_2 (Langevin et al., 2005).

4.3.1 General composition identified by hyperspectra of the OMEGA image

The pixel X:52/Y:50 of the OMEGA image orb1034_3 is assigned to be the PLS because their coordinates are the most closely matched. Reflectance spectra for the PLS were extracted from the pixel X52/Y50 and compared with sample spectra of ign_fn_sli (igneous function sample library) and sed_fn_sli (sedimentary function sample library) data sets of Johns Hopkins University. Giving equal weights to three matching methods, spectral angle mapper (SAM), spectral feature fitting (SFF) and binary encoding (BE), the best matched igneous rock was basaltic andesite (Fig. 4-6-A) with a total score of 0.846 (the probability of two spectra matching each other; SAM 0.960, SFF 0.781, BE 0.798). The probability is higher than the second best matched rock, basalt (0.795) (Fig. 4-6-B). The sedimentary rock with the highest match was arkosic sandstone (Fig. 4-6-C) with a total score of 0.782 (SAM 0.947, SFF 0.819, BE 0.579), which is higher than the second best matched rock, arenaceous shale (0.721). The spectrum at the PLS match best with the mixing spectrum of 80% basaltic andesite and 20% arkosic sandstone (Fig. 4-7).

The spectra of the PLS were also tested to match with spectra of individual mineral samples and analyzed based on the absorption features of chemical bond vibrations of stretching and bending. No specific minerals matched up with the spectra with significant confidence. Mafic minerals and their alteration products have relatively high matching scores. Thus, regolith or "soil" deposits of weathered basaltic andesite are likely to be present. The top "soil" may be loose sand-sized deposits at the three sites with similar latitude, where the overlying soil layer has a thermal inertia of ~200, consistent with

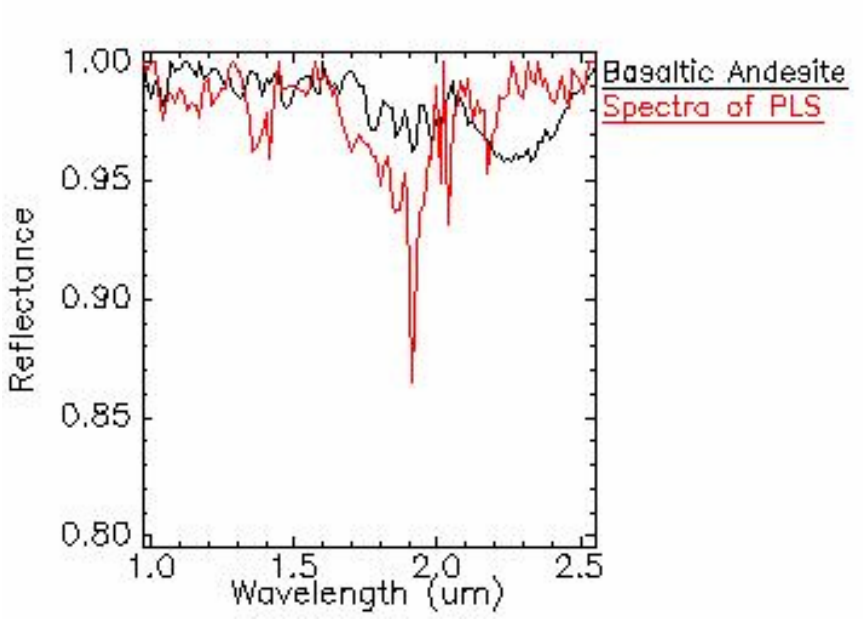
1.00
0.95
0.90
0.85
0.80
Reflectance
1.0
1.5
2.0
2.5
Wavelength (um)
Basaltic Andesite
Spectra of PLS

A

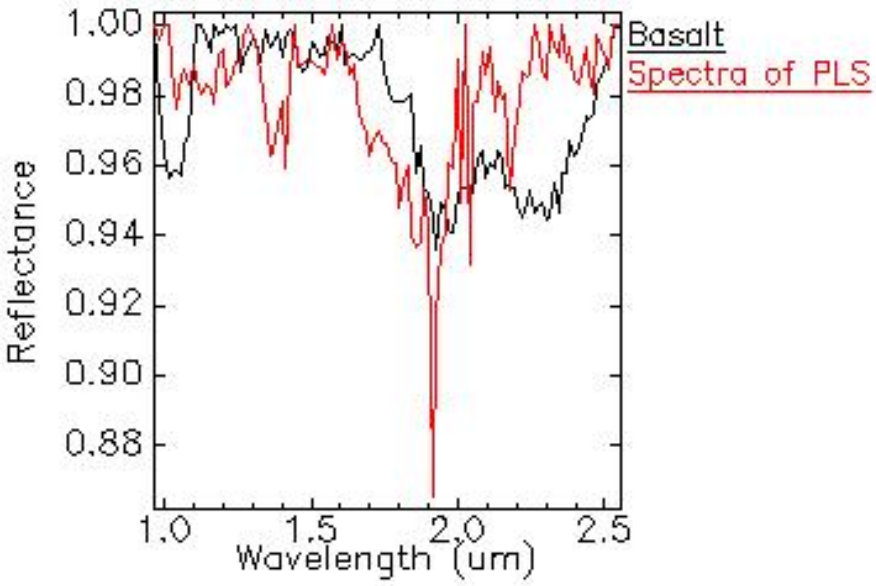
1.00
0.98
0.96
0.94
0.92
0.90
0.88
Reflectance
1.0
1.5
2.0
2.5
Wavelength (um)
Basalt
Spectra of PLS

B

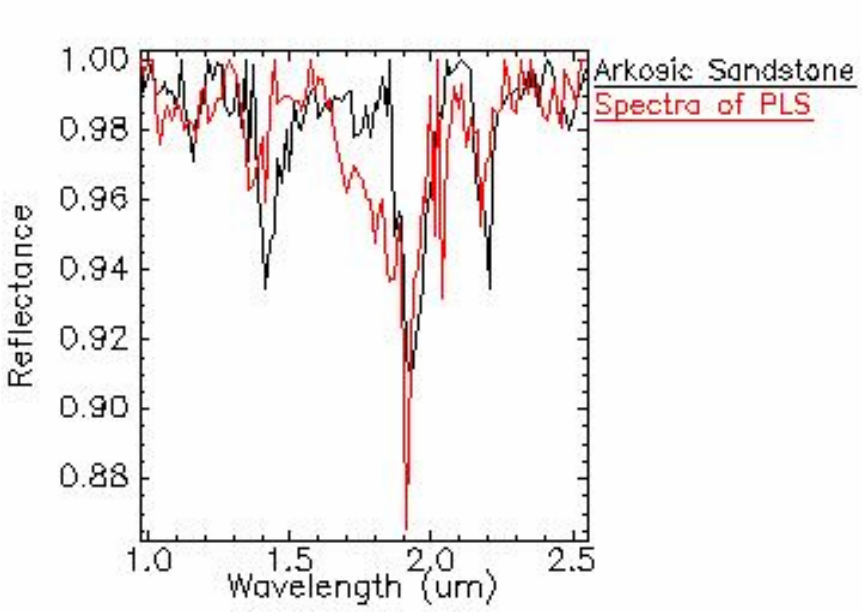

C

Fig. 4-6 Comparison of reflectance spectra at the Phoenix Landing Site and library spectra. A is basaltic andesite; B basalt; and C arkosic sandstone.

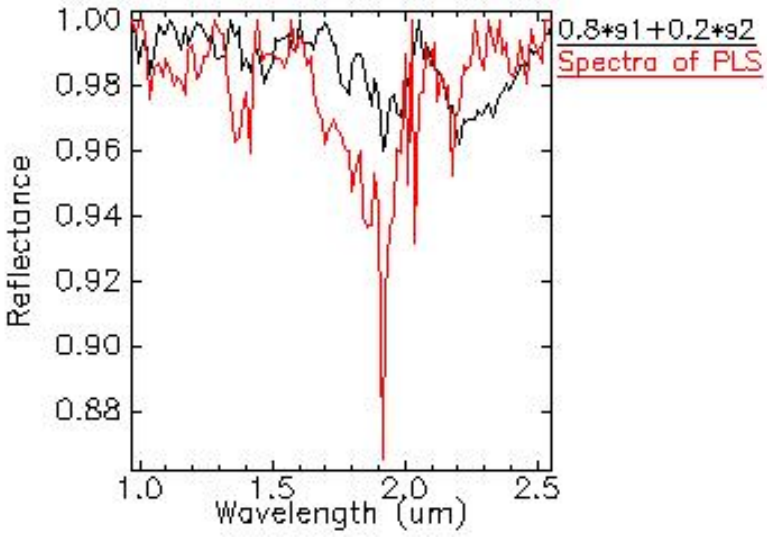

A

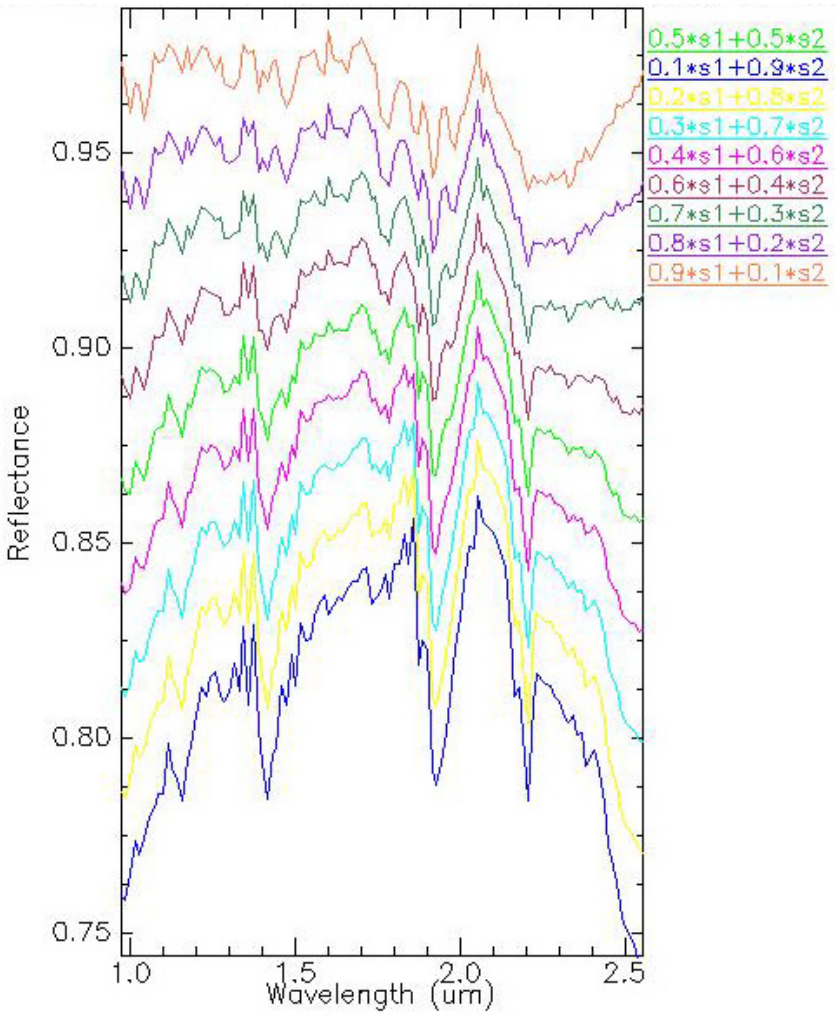

B

Fig. 4-7 Comparison of reflectance spectra at the Phoenix Landing Site and the mixing spectra of basaltic andesite (s1) and arkosic sandstone (s2). A is the spectra of 80% basaltic andesite and 20% arkosic sandstone, and at the Phoenix Landing Site; B is the spectra of basaltic andesite from 10% to 90% and arkosic sandstone from 90% to 10% from the bottom to the top of the spectra profile.

non-cemented sand-sized particles (Titus et al., 2006).

4.3.2 Composition variation of the surface materials at the Phoenix Landing Site

The reflectance spectra of the PLS and its surrounding rings (Fig. 4-3) were extracted (Fig. 4-8). As shown in Fig. 4-8, these spectra are very similar with their absorption bands and very close absorption intensities. The similar spectra indicate that the surface materials at the PLS (about 1.6 × 1.8 km^2 in extent) and within the scope of at least 50 × 50 km^2 exibit no significant change.

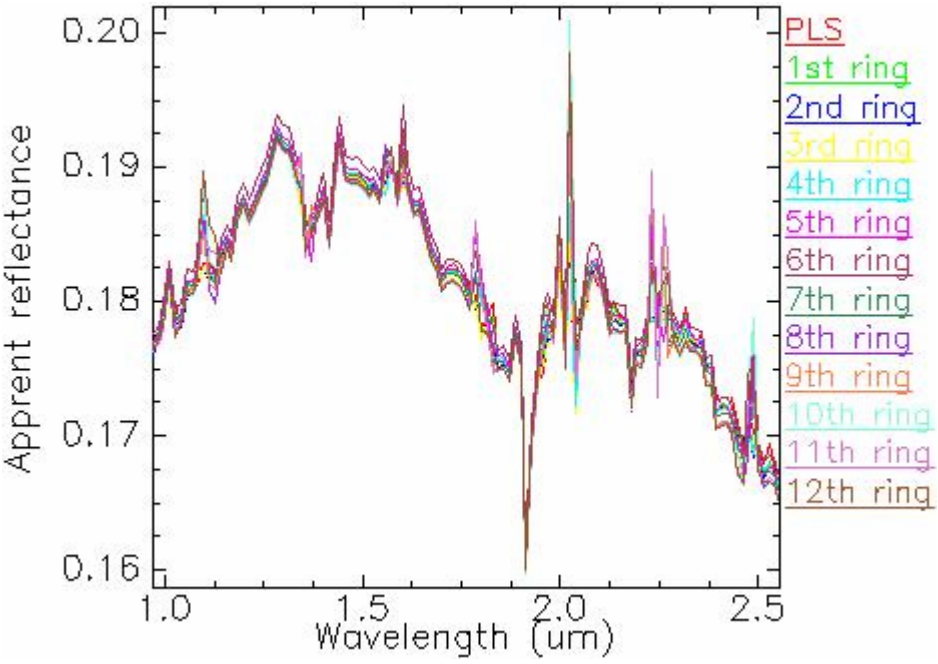

Fig. 4-8 Reflectance spectra of the Phoenix Landing Site and its 12 surrounding rings. PLS is the Phoenix landing site, 1st ring is closest to the PLS and 12th ring is the furthest away from the PLS.

4.3.3 Classification and geologic mapping of OMEGA image orb1034_3

Advanced hyperspectral analysis was conducted to classify and map geologic units of OMEGA image orb1034_3 to better understand the distribution of surface materials at the PLS and its surrounding areas. The methodology included a correction of radiance to apparent reflectance, use of a linear transformation to minimize noise fraction (MNF) and determine data dimensionality, location of the most spectrally pure pixels (PPI), extraction and automated identification of endmember spectra, and spatial mapping and abundance estimates for specific image endmembers (Kruse, http://www.hgimaging.com/PDF/Kruse).

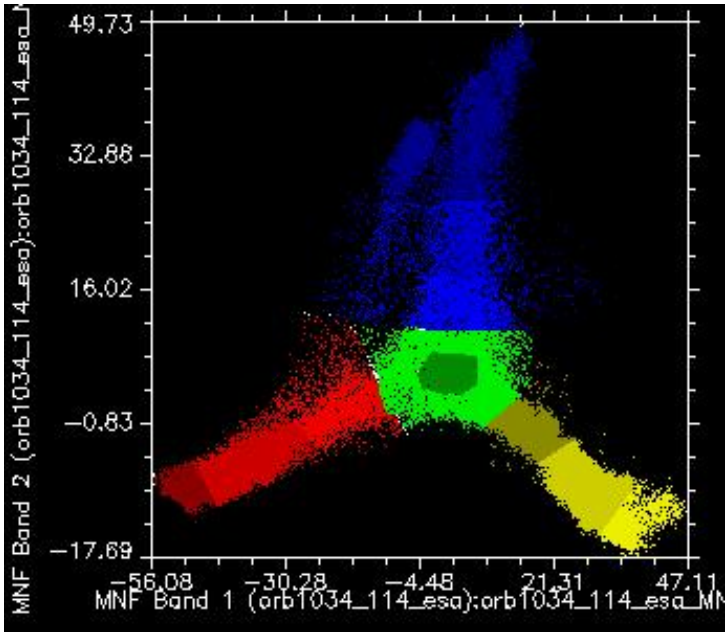

Fig. 4-9 Scatter plot of band 1 and band 2 of MNF transformation. Three arms denote three groups of distinctive components of surface materials in OMEGA image orb1034-3 (see Fig. 4-10).

As indicated by the 2D scatter plot of MNF band 1 and band 2 (Fig. 4-9), there are three distinctive groups of materials shown in the three arms. The mixture is located in the center and the pixels closest to the tips of the arms are the areas made up of purest materials. We sub-classified each group into two or three types of materials. The mean spectrum of each type of material was extracted and compared (Fig. 4-10).

Figure 4-10 indicates that each group of spectra has its own reflectance and unique absorption bands. Generally, the spectra of ROI1, ROI2 and ROI4 (ROI = Region of Interest) have more similarity with each other than ROI3. This is likely because the three groups of ROIs are mainly made up of rock materials while ROI3 is mainly made up of water-ice. The Albedo (NIR reflectance here) decreases from ROI1 to ROI3 by 0.18,

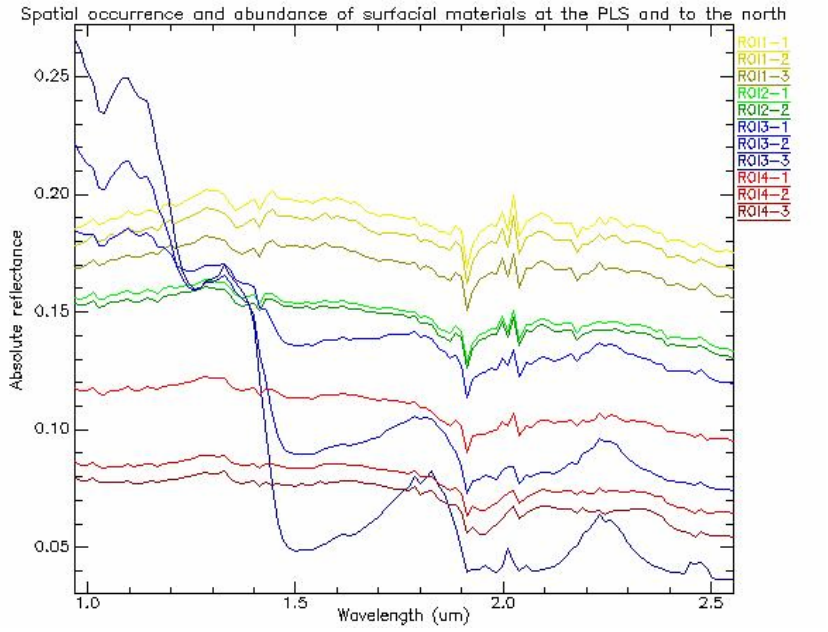

Fig. 4-10 Spectra of classified materials at the Poenix Landing Site and its surrounding areas. ROI is Region of Interest and classified as four regions, ROI1 (yellow), ROI2 (green), ROI3 (blue) and ROI4 (red).

0.16 to 0.11 (at 1.012 μm). The mean spectra of ROIs were compared with sample spectra of usgs_min_lib based on the SFF method. For ROI1, the mineral with the highest match was monticellite (0.835), followed by other mafic rock-forming minerals, such as hypersthene and enstatite. Based on the change of IR (Infrared) reflectance and topography, ROI1-1 is likely a rock outcrop or sand dunes (higher albedo and elevation), whereas Martian soils or regoliths likely make up ROI1-2 and ROI1-3 (lower albedo and

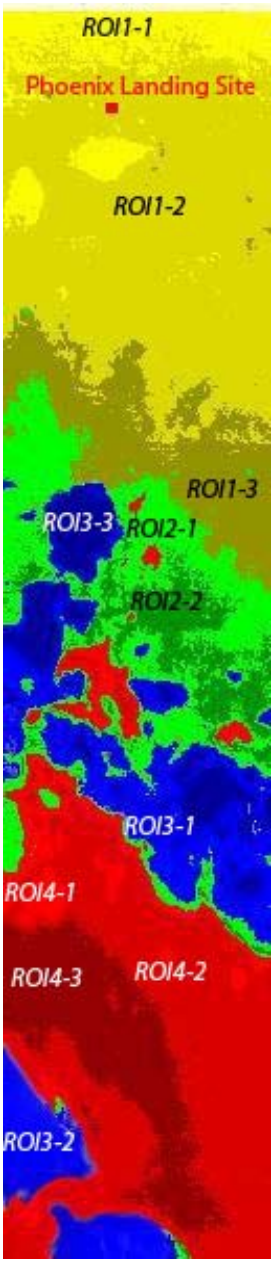

Fig. 4-11 Geologic map of the OMEGA image orb1034_3. Yellow is the Martian soils or regolith, green is the mixture of Martian soils and sulfates, blue is water-ice, and red is sulfates.

elevation). For ROI2, the mineral with the highest match was tincalconite (0.826), which is unlikely the main composition of this area. The following rock-forming minerals, such as hypersthene (0.811), anorthite (0.807) and monticellite (0.807) are likely the composition of surficial materials in the area. Sulfate minerals were also among the top ten most matched minerals. ROI2 has characteristics of both ROI1 and ROI4. For ROI3, the reflectance spectra displayed obvious features of water-ice with three significant unique absorption bands of water-ice, 1.04, 1.50 and ~2.00 μm. The three water-ice-related absorption bands become more and more distinctive from ROI3-1 to ROI3-3. This is also reflected by the comparison of each spectrum with the spectra library using the SAM method. ROI3-1 may be the mixture of soil and water-ice. ROI3-2 shows more signals of water-ice but containing dust. ROI3-3 is likely dominated by water-ice based on its best match to spectra of H2O-ice (0.841). ROI4 indicates a stronger correlation to sulphate minerals based on its match to eugsterite (ROI4-3, 0.942) using the SAM method. The content of sulfates increases from ROI4-1 to ROI4-3.

The distributions of ROIs were mapped on the OMEGA image orb1034_3 (Fig. 4-11). The PLS is located in ROI1-2 within the Martian soil or regolith.

4.4 Study of the Phoenix Landing Site related to water

Water is the most important parameter when searching life on Mars. It is also important in regard to climate change and geological processes. The water or water-ice on the ground and in the sub-surface, and the water vapour in the atmosphere at the PLS candidates or in the north polar area were investigated by some workers (Mellon and Jakosky, 1995; Boynton et al., 2002; Titus et al., 2006; Tamppari et al., 2006; Bandfield, 2007). Here, we study the water or water-ice on the ground, in the subsurface and in the atmosphere based on OMEGA hyperspectral image orb1034_3.

4.4.1 Surfacial water signatures at the Phoenix Landing Site

OMEGA image 1034_3 was imaged at 6:14 to 6:22 on Nov. 8, 2004, which is during the early summer on Mars (Ls, Martian solar longitude, is 111.98) and. From the image, it can clearly be observed that the water-ice slabs in the north circumpolar area and an isolated water-ice patch (about 4 pixels) to the north of the PLS (Fig. 4-12). It is

Fig. 4-12 The occurrence of surface water-ice in OMEGA image orb1034_3. Marked in red are the Phoenix Landing Site or the borders of surface water-ice occurrences.

about 322.0 km from the PLS to the closest point of the circumpolar water-ice slabs (73.804695ºN, 231.508896ºE) and merely about 123.7 km to the isolated water-ice patch (70.136795ºN, 236.278687ºE). The occurrence of surfacial water-ice close to the PLS may indicate that the water ice table of the PLS is close to the surface.

In order to determine the variation of water (water ice, isolated water molecules and hydroxyl) at the PLS and its surrounding areas, continuums of reflectance were removed (Fig. 4-13) and absorption band depths related to water were calculated (Table 4-3) within 12 pixel rings (about 50 km). These absorption bands were related to water-ice (1.04, 1.50 and 2.04 μm), isolated water molecules (1.91 μm), hydroxyls (1.35, 1.80 and 2.18 μm) and atmospheric water (1.87 μm). These absorption depths vary without a clear trend as it was observed at gully-exposed sites (in chapter 3). The correlations between the values of absorption depths and the reverse distance to the PLS were low, -0.12 for the absorption band of 1.41 μm and from -0.6 to -0.77 for 1.04, 1.35, 1.50, 1.91, 2.04 and 2.18 μm.

Absorption at 1.80 μm is observed at the target site and the first three rings between two continuum bands, 1.786 and 1.814 μm. The absorption depths decreased from the PLS pixel (0.013) to the 3rd ring (0.010). Starting from the 4th ring, no absorption at 1.80 μm is observed. From the 5th ring to the 12th ring, there is a significant absorption at the range of 2.260 to 2.488 μm with several sub-absorptions at 2.273, 2.395 and 2.461 μm. The absorption depths were 0.051, 0.033, 0.058, 0.042, 0.069, 0.042, 0.074 and 0.043 from the closest to rings further away from the PLS. In contrast, the target site and the rings within the 4th ring show much smaller absorption intensity in this range of wavelength. A weak absorption with two sub-absorptions at 2.395 and 2.448 μm could be observed. The absorption depths were 0.022 to 0.014 μm from the PLS pixel to the 4th ring.

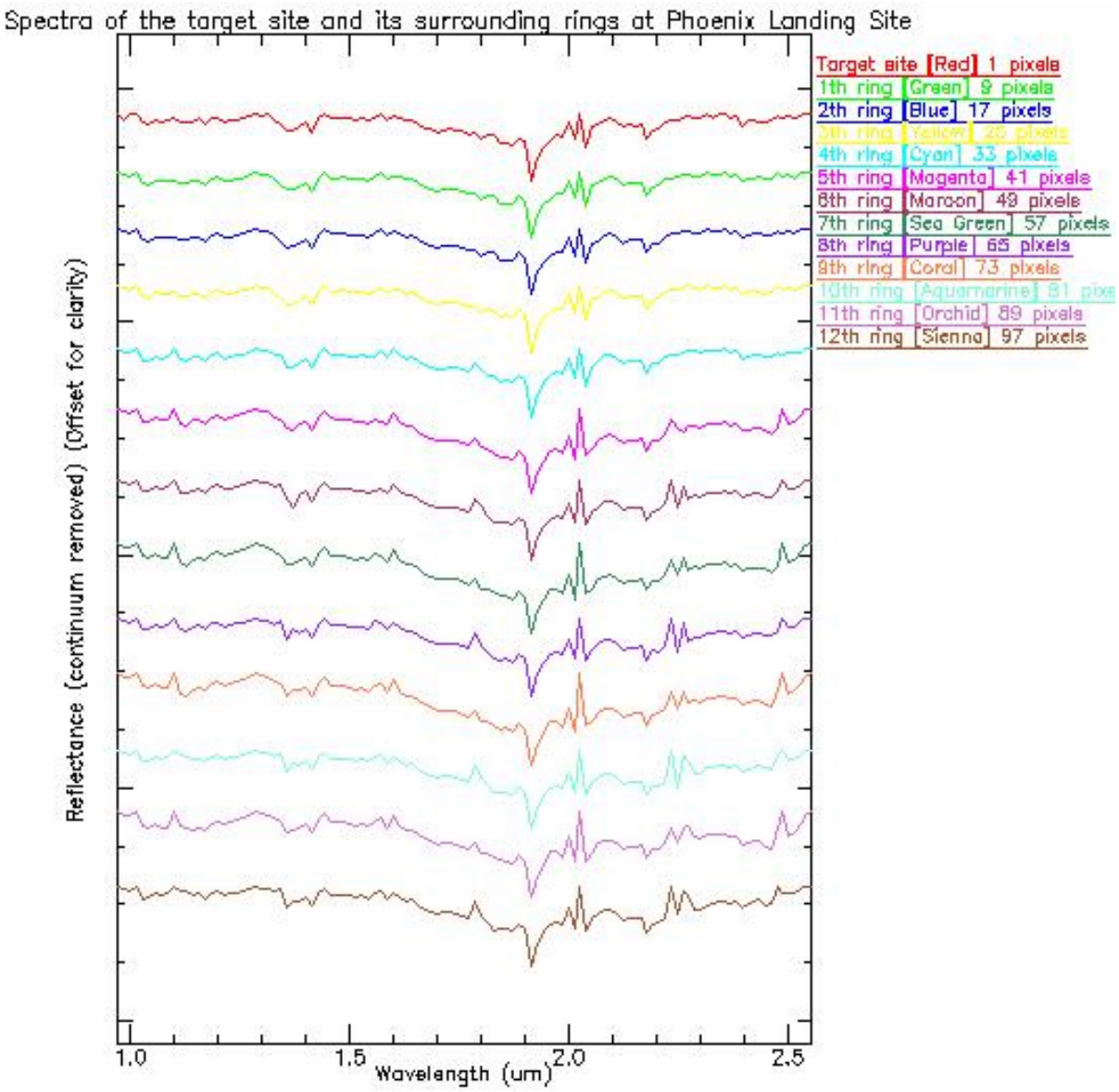

Fig. 4-13 Continuum removed reflectance spectra of the PLS pixel and its 12 surrounding rings. The spectra go from the top one (red, PLS) to the bottom (sienna, 12th ring).

Table 4-3 Data of absorption band depths at the Phoenix Landing Site and its surrounding rings

Band rang	1.0121 1.0550	1.3136 1.3999	1.3999 1.4430	1.4430 1.5721	1.7860 1.8850	1.8850 1.9973	1.9973 2.0253	2.0253 2.0948	2.0948 2.2324
Center	1.0407	1.3568	1.4143	1.5004	1.8709	1.9132	2.0113	2.0392	2.1776
Target	0.015	0.026	0.026	0.013	0.018	0.102	0.046	0.069	0.04
1st ring	0.016	0.024	0.026	0.014	0.019	0.104	0.046	0.068	0.037
2nd ring	0.018	0.026	0.026	0.014	0.019	0.101	0.048	0.07	0.04
3rd ring	0.018	0.025	0.026	0.013	0.019	0.103	0.047	0.069	0.04
4th ring	0.02	0.026	0.026	0.014	0.026	0.104	0.051	0.075	0.041
5th ring	0.019	0.027	0.026	0.013	0.026	0.107	0.079	0.091	0.058
6th ring	0.018	0.044	0.026	0.011	0.034	0.105	0.069	0.084	0.068
7th ring	0.018	0.028	0.027	0.018	0.025	0.108	0.086	0.095	0.056
8th ring	0.021	0.033	0.026	0.018	0.039	0.105	0.068	0.084	0.074
9th ring	0.018	0.03	0.027	0.02	0.025	0.108	0.093	0.098	0.058
10th ring	0.019	0.035	0.026	0.018	0.04	0.105	0.069	0.085	0.076
11th ring	0.022	0.03	0.027	0.022	0.024	0.109	0.083	0.093	0.058
12th ring	0.021	0.037	0.025	0.018	0.033	0.106	0.069	0.083	0.058
correlation	-0.770	-0.600	-0.116	-0.774	-0.712	-0.737	-0.753	-0.757	-0.752

Reflectance spectra of the traverse in the N-S direction through the PLS was also extracted pixel by pixel (Fig. 4-14). The absorption band depths related to water were calculated (Table 4-4). The correlation between the absorption depths and the reverse distance to the PLS were very low for all absorption bands related to water. These indicated that the water contents at the PLS and its surrounding areas has no significant change. CRISM (Compact Reconnaissance Imaging Spectrometer for Mars), covering wavelength from 0.362 to 3.92 μm at 6.55 nm/channel and 15.7 to 19.7 m/pixel (http://crism.jhuapl.edu/), may provide better images to analyze the variation of water signatures on the Martian surface.

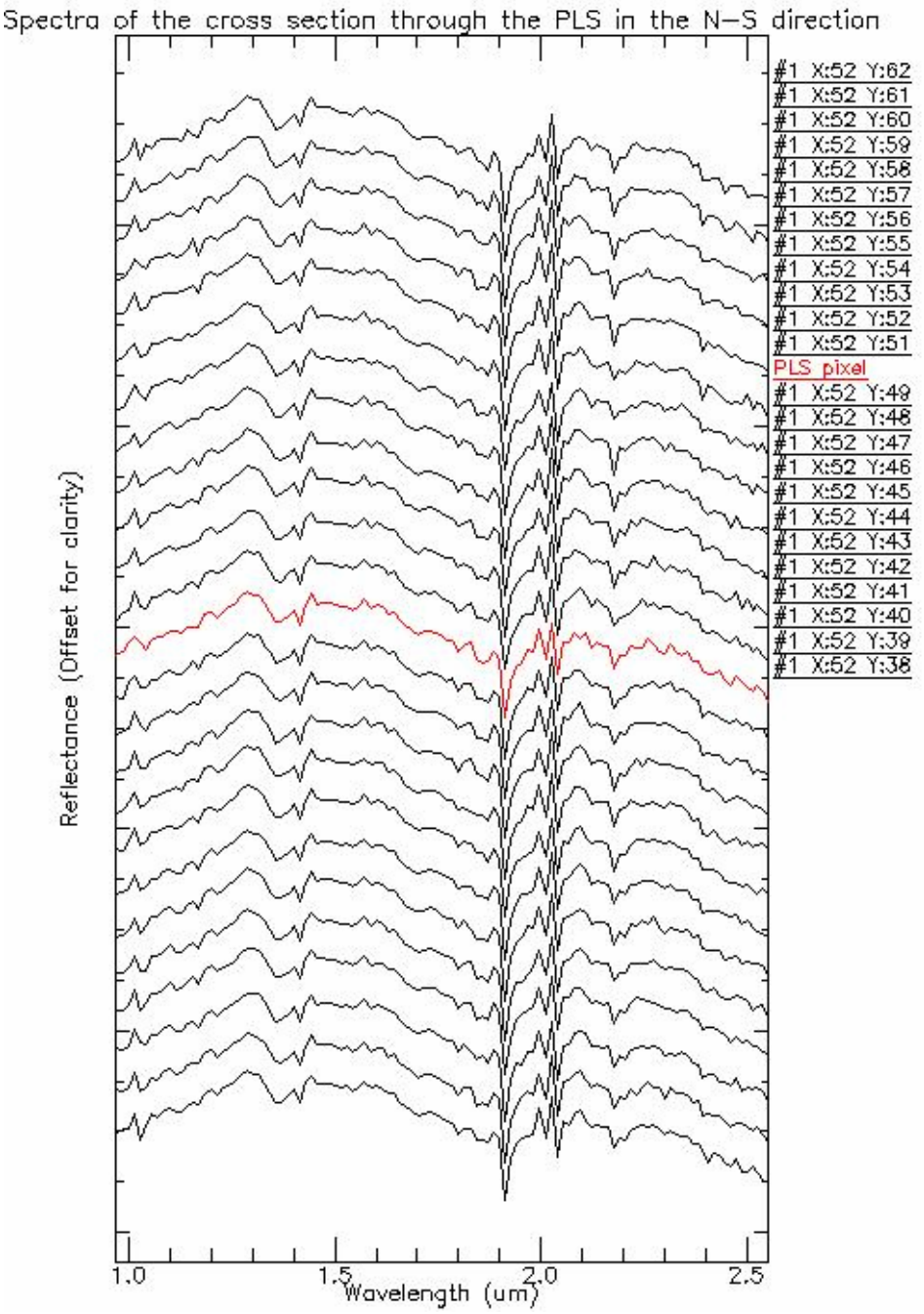

Fig. 4-14 Reflectance spectra of pixels in the traverse of N-S direction through the Phoenix Landing Site. The spectrum in red is the reflectance spectrum of the PLS. The spectra going up represent the reflectance spectrum of each pixel to the north of the PLS in the image. The spectra going down represent the reflectance spectrum of each pixel to the south of the PLS in the image.

Table 4-4 Data of absorption band depths at the Phoenix Landing Site and pixels in the traverse of N-S direction

Band rang	1.0121/ 1.0550	1.0981/ 1.1986	1.3999/ 1.4430	1.4430/ 1.5721	1.8143/ 1.8850	1.8850/ 1.9973	1.9973/ 2.0253	2.0253/ 2.0948	2.0948/ 2.2461
Center	1.0407	1.1268	1.4143	1.5004	1.8709	1.9132	2.0113	2.392	2.1776
12th ring	0.024	0.017	0.041	0.014	0.025	0.099	0.049	0.078	0.044
11th ring	0.016	0.014	0.036	0.013	0.024	0.1	0.05	0.074	0.043
10th ring	0.019	0.015	0.038	0.015	0.017	0.109	0.049	0.068	0.047
9th ring	0.012	0.023	0.037	0.016	0.025	0.107	0.047	0.068	0.043
8th ring	0.022	0.02	0.037	0.01	0.023	0.105	0.046	0.072	0.047
7th ring	0.02	0.01	0.037	0.013	0.022	0.105	0.051	0.072	0.033
6th ring	0.018	0.012	0.037	0.01	0.019	0.095	0.038	0.077	0.031
5th ring	0.017	0.01	0.04	0.015	0.016	0.1	0.044	0.076	0.056
4th ring	0.019	0.016	0.039	0.013	0.02	0.103	0.05	0.075	0.05
3rd ring	0.025	0.018	0.038	0.015	0.023	0.103	0.044	0.073	0.044
2nd ring	0.02	0.011	0.036	0.014	0.021	0.105	0.041	0.067	0.041
1st ring	0.02	0.015	0.039	0.014	0.018	0.087	0.043	0.068	0.043
Target	0.014	0.014	0.041	0.014	0.021	0.101	0.046	0.067	0.038
1st ring	0.015	0.014	0.039	0.013	0.018	0.101	0.046	0.067	0.04
2nd ring	0.019	0.012	0.04	0.014	0.023	0.107	0.044	0.069	0.042
3rd ring	0.02	0.013	0.041	0.014	0.026	0.106	0.049	0.073	0.049
4th ring	0.018	0.012	0.041	0.01	0.016	0.104	0.049	0.071	0.041
5th ring	0.022	0.014	0.04	0.014	0.02	0.101	0.044	0.071	0.051
6th ring	0.018	0.019	0.036	0.012	0.019	0.107	0.046	0.074	0.041
7th ring	0.022	0.021	0.041	0.016	0.02	0.108	0.047	0.071	0.041
8th ring	0.019	0.018	0.037	0.014	0.024	0.107	0.042	0.07	0.034
9th ring	0.026	0.018	0.038	0.013	0.024	0.105	0.043	0.069	0.041
10th ring	0.016	0.017	0.036	0.013	0.02	0.106	0.043	0.077	0.039
11th ring	0.023	0.01	0.04	0.014	0.023	0.103	0.044	0.075	0.038
12th ring	0.037	0.012	0.038	0.015	0.014	0.104	0.047	0.075	0.04
Correlation	-0.361	-0.213	0.295	-0.075	-0.134	-0.268	-0.205	-0.496	0.111

4.4.2 Subsurface Water-ice table in the north Martian circumpolar area

The depth of the water-ice table on Mars has been studied by various workers (e.g. Mellon and Jakosky, 1995; Boynton et al., 2002; Titus et al. 2006; Bandfield, 2007). The methods include theoretical models, GRS (gamma ray spectrometer) data, TES (thermal emission spectrometer) and THEMIS images, and the impact of Martian obliquity oscillation on the condensation and diffusion of water-ice in the subsurface. Water-ice

was estimated to be stable at a depth of < 1-2 meters and to constitute 35 ± 15% of the layer by weight (Boynton et al., 2002) at high latitude areas based on the large concentrations of hydrogen detected by the GRS. The depth to the ice table at three PLS candidate sites in the north circumpolar area was estimated to be within 3-6.4 cm based on MGS/TES temperatures during Martian springtime when seasonal CO_2 disappears (Titus et al. 2006). This result is consistent with the estimate (4-6 cm) of Prettyman et al. (2004) at high southern latitudes from neutron counts of the neutron spectrometer. The content of water-ice in the subsurface was estimated to be about 50 % by weight by Titus et al. (2006). The observation of the seasonal temperature response of the Martian surface with THEMIS indicates significant variability of regional and local water-ice depths (Bandfield, 2007).

4.4.3 Water vapor and ice in the atmosphere of the north Martian circumpolar area

The water vapor and ice in the atmosphere at latitudes between 60º and 90 º N were mapped by Tamppari et al. (2006) based on their optical depths using the data from the MGS/TES (Mars Global Surveyor Thermal Emission Spectrometer) instruments. The study showed the spatial and seasonal change of water ice and vapor opacity during the Martian northern spring and summer (Ls = 0 -180) over 3 Martian years. The water vapor was about 50 precipitable (pr) μm, up to 200 pr μm at some locations (average pr in the Earth's atmosphere is about 2 cm), higher in the west circumpolar area than the east circumpolar area.

The absorption band at 1.87 μm is considered to be caused by atmospheric water vapour (Hobbs, 2000). The absorption depth of 1.87 μm is small, merely about 0.02 to 0.04 at the PLS, as shown in Table 4-3 and 4-4. This small absorption depth may imply that the content of water vapour in the atmosphere above the PLS is rare, which is

consistent with the result of the MGS/TES data. The lack of variation of the absorption depths at 1.87 μm indicates there is no significant change of water vapour content in the atmosphere above the PLS and its surrounding areas.

4.5 Conclusion

The region of a box of 7º latitude × 20º longitude centered at 68.35N, 233.0E has been chosen as the Phoenix landing site. This region is a plain with a relatively flat landform and featureless surface, which is likely safe enough for the Phoenix Lander to touch down on Mars. The proposed landing site is very close to unambiguous identified water-ice bodies with strong water signatures. The surface materials are likely loose regolith or soil deposits of basaltic andesite composition and are made up of mixtures of common rock-forming minerals and clay minerals. These materials are homogenous at the kilometer scale. The surface materials show evidence of water and no clear trend of variation of water content at the PLS with its surrounding areas. The water-ice table or icy soil (permafrost) probably lies within centimetres or tens of centimetres below the surface. The proximity of the landing site to sulfates and possible recent volcanic cones may allow detailed information about geologic processes in the circumpolar areas to be gained. The PLS is a ground truth site for us to better understand the surface processes and climate at high Martian latitudes, and consequently the geologic evolution of Mars.

References

Arvdison R.E., L. Barge, J. Barnes, W. Boynton, J. Friedson, M.P. Golombek, J. Guinn, D.M. Kass, R. Kirk, M. Malin, M. Mellon, T. Michaels, D. Paige, T.J. Parker, S. Rafkin, K. Seelos, M.D. Smith, P.H. Smith, L. Tamppari, and D. Tyler, 2006. Overview of Mars exploration program 2007 Phoenix mission landing site. LPSC XXXVII, 1328.pdf.

Bandfield, J.L., 2007. High-resolution subsurface water-ice distributions on Mars. *Nature* 447, 64–67.

Beyer, R.A., 2006. Meter-scale slope from photoclinometry for the potential Phoenix landing sites. LPSCXXXVII, 1926.pdf.

Bibring J-P., Y. Langevin, A. Gendrin, B. Gondet, F. Poulet, M. Berthé, A. Soufflot, R. Arvidson, N. Mangold, J. Mustard, P. Drossart, the OMEGA team, 2005. Mars surface diversity as revealed by the OMEGA/Mars Express observations. *Science* 307, 1576–1581.

Boynton, W.V., W. C. Feldman, S. W. Squyres, T. H. Prettyman, J. Brückner, L. G. Evans, R. C. Reedy, R. Starr, J. R. Arnold, D. M. Drake, et al. , 2002. Distribution of Hydrogen in the Near Surface of Mars: Evidence for subsurface ice deposits. *Science* 297, 81–85.

Gendrin, A., N. Mangold, J-P. Bibring, Y. Langevin, B. Gondet, F. Poulet, G. Bonello, C. Quantin, J. Mustard, R. Arvidson, S. LeMouélic, 2005. Sulfates in Martian layered terrains: The OMEGA/Mars express view. *Science* 307, 1587–1591.

Guinn, J., G. Bonfiglio, L. Craig, P. Desai, M. Garcia, R. Grover1, T.J. Parker, J. Prince, K. Seelos, R. Shotwell and E. Slimko, 2006. The engineering behind Mars exploration program 2007 Phoenix mission landing site selection. LPSC XXXVII, 2051.pdf.

Hobbs, P.V., 2000. Introduction to atmospheric chemistry. Cambridge University Press.

Kirk, R.L., M. Rosiek, D. Galuszka, B. Redding, T. Hare, B. Archinal and T.J. Parker, 2006. Topography of candidate Phoenix landing sites from MOC images. LPSC XXXVII, 2033.pdf.

Langevin, Y., F. Poulet, J-P. Bibring and B. Gondet, 2005. Sulfates in the North Polar Region of Mars detected by OMEGA/Mars Express. *Science* 307, 1584–1586.

Mellon, M.T. and B.M. Jakosky, 1995. The distribution and behavior of Martian ground ice during past and present epochs. *J. Geophys. Res.* 100, 11,781–11,799.

Neukum, G. and S.V. Gasselt, 2006.Recent volcanisms at the Martian north pole. *Geophysical Research Abstract* 8, 11103.

Portyankinna, G. 2007. Personal communication.

Prettyman, T.H., W.C. Feldman, M.T. Mellon, G.W. McKinney, W.V. Boynton, S. Karunatillake, D.J. Lawrence, S. Metzger, A.E. Maurice, J.R. Murphy, S.W. Squyres, R.D. Starr and R.L. Tokar, 2004. Composition and structure of the Martian surface at high southern latitudes from neutron spectroscopy. *J. Geophys. Res.* 10. 1029/2003JE2139.

Poulet, F., J. Mustard, R. Arvidson, J-P. Bibring, Y. Langevin, B. Gondet, R. Milliken and S. Pelkey, 2006. Mineralogy of the Phoenix landing sites from the OMEGA-MEX imaging spectrometer. LPSC XXXVII, 1706.pdf.

Smith, P.H. and the Phoenix science team, 2006. Science consideration driving the choice of the Phoenix mission landing site. LPSC XXXVII, 1910.pdf.

Smith, P.H., P.H Smith., L.K. Tamppari, R.E. Aridson, W.V. Boynton and Phoenix science team, 2007. Phoenix landing site selection update. LPSC XXXVIII, 1176.pdf.

Titus, T.N., T.H. Prettyman and A. Colaprete, 2006. Thermal characterization of the three proposed Phoenix landing sites. LPSCXXXVII, 2161.pdf

CHAPTER 5

CONCLUSIONS

This research provides further evidence for a likely scenario that the Martian surface environment was warm and wet in its early history, and was subjected to water activity in the recent geologic time through two case studies. The research also includes a characterization of the Phoenix landing site, where an in-situ investigation of water and water-ice will be conducted.

The hypothesis for the origin and redistribution of sulfates in the equatorial region of western Mars proposed a new model of sulfate deposit formation, "sulfate evaporites in Valles Marineris + elevation by Tharsis rise + relocation of sulfates + sedimentary deposits of sulfates in Meridiani Planum". The model integrates logically 1) the fate of sulfates in Valles Marineris and the source of sulfates in Meridiani Planum, 2) the formation of sulfates in the equatorial region of western Mars, the Tharsis rise and Valles Marineris. It relates the formation of the sulfates to physiographic processes (volcanic, tectonic and sedimentary) affecting the Martian surface and implies that there was a dynamic Martian surface in the early Martian history and that liquid water was sporadically active until at least the Hesperian epoch.

An investigation of water signatures at four gully-exposed sites on Mars by hyperspectral image analysis found that the depths of water related absorption bands are greater at the gully-exposed sites than in their surrounding areas. The clear trend of the stronger signature of water at the gully-exposed sites than their surrounding areas indicates more water (water-ice, isolated water molecules and hydroxyl) is contained in

the surface materials at the gully-exposed sites than their surrounding areas. The result supports the conclusion that the formation of gullies has involved processes associated with liquid water, and subsequently implies that the liquid water is active in recent geological time, perhaps even to the present day.

The characterization of the Phoenix landing site indicates that the Phoenix landing site in the northern circumpolar area is in a plain with a flat landform and a featureless surface, soils or regolith of weathered basaltic andesite on the surface, and a water-ice table or icy soil (permafrost) within centimetres or tens of centimetres under the subsurface. The scenario of a warm and wet early Mars (Noachian), sporadically local warm and wet environments from Hesperian to Amazonian and active liquid water in places in recent geologic time, supports the promise of finding evidence for life (extant or fossils) on Mars. The landing site of Phoenix is an ideal site for investigating water and water-ice in-situ on Mars.

APPENDIX

Appendix 1 The primary parameters of Martian facts*

Parameters	**Mars**		**Mars/Earth**
	Range	**average**	
Distance from Sun	206 to 249 million km	228 million km	1.52
Oribital period	686.96 day		1.88
Rotation period	24.62 hour		1.03
Obliquity to orbit	25.19°		1.07
Natural satellite	2 (Phobos and Deimos)		2
Diameter	6,752.2 to 6,792.4 km	6,786 km	0.55
Mass	6.4185×10^{23} kg		0.001
Density	3.9 g/cm^3		0.71
Surface temperature	−125 °C to 22 °C	−63 ° C	
Surface pressure	4.0 to 8.7 millibars	6.36 millibars	0.006
Major composition in the atmosphere	Carbon dioxide: 95.72%, Nitrogen: 2.7%, Argon: 1.6%, Oxygen: 0.2%, Carbon Monoxide 0.07%, Water vapor 0.03%		

*Data derived from http://nssdc.gsfc.nasa.gov/planetary/factsheet/marsfact.html, http://en.wikipedia.org/wiki/Mars_(planet) and http://www.solarviews.com/eng/mars.htm

Appendix 2 Missions to Mars (successful or on schedule)*

Launch Date	Name	Country	Scientific goals and achievements
11/28/1964	Mariner 4	US	A flyby flew past Mars on July 14, 1965 and returned 21 images.
02/24/1969	Mariner 6	US	A flyby returned 75 images.
03/27/1969	Mariner 7	US	A flyby returned 126 images.
1971	Mars Orbiter /Lander	USSR	Orbiter obtained approximately 8 months of data and lander landed safely, but only 20 seconds of data.
05/30/1971	Mariner 9	US	First artificial satellite of Mars and returned 7,329 images.
1973	Mars 5	USSR	Returned 60 images; only lasted 9 days.
08/20/1975	Viking 1 Orbiter /Lander	US	First successful landing on Mars. Viking 1 landing at Chryse functioning till 11/11/1982 and Viking 2 landing at Utopia Planitia Planitia functioning till 04/11/1980. Science instruments: Biology instrument, gas chromatograph/mass spectrometer, X-ray fluorescence spectrometer, etc. Returned 16,000 images and extensive atmospheric data and soil experiments.
09/03/1975	Viking 2 Orbiter /Lander		
11/07/1996	Mars Global Surveyor	US	Studied the entire Martian surface, atmosphere, and interior. Mars Orbital Camera took more images than all Mars Missions and observed gully formation, new boulder tracks, recently formed impact craters, and diminishing amounts of carbon dioxide ice within the south polar cap etc.
12/04/1996	Mars Pathfinder	US	Landing at Ares Vallis and functioning till 09/ 27/1997. Returned more than 16,500 images from the lander and 550 images from the rover, as well as more than 15 chemical analyses of rocks and soil and extensive data on winds and other weather factors.
04/07/2001	Mars Odyssey	US	High resolution images of Mars. Collected more than 130,000 images and continues to send information to Earth about Martian geology, climate, and mineralogy. Provided spectacular views of Martian topography. Enabled scientists to create maps of minerals and chemical elements and identify regions with buried water ice.
06/2003	Mars Express Orbiter /Beagle 2 Lander	ESA	Orbiter imaging Mars in detail and lander lost on arrival. Provided evidence of recent glacial activity, explosive volcanism, and methane gas. MARSIS (Mars Advanced Radar for Subsurface and Ionospheric Sounding) provided information about features beneath the Martian surface, including buried impact craters, layered deposits, and hints of deep underground water ice.

Cont. Missions to Mars (successful or on schedule)*

06/10/2003	Mars Exploration Rover-Spirit	US	Opportunity in Meridiani Planum while Spirit in Gusev Crater and trekked for miles across the Martian surface. The twin rovers sent more than 100,000 spectacular, high-resolution, full-color images of Martian terrain as well as detailed microscopic images of rocks and soil surfaces to Earth. Four spectrometers amassed information about the chemical and mineralogical makeup of Martian rocks and soil. Special rock abrasion tools examined rocks' interior beneath the dusty and weathered surfaces. Opportunity's study revealed evidence for past inter-dune playa lakes that evaporated to form sulfate-rich sands and sedimentary bedrock exposures. Spirit's study revealed basaltic setting a variety of rocks indicating that early Mars was characterized by impacts, explosive volcanism, and subsurface water.
07/07/2003	Mars Exploration Rover– Opportunity		
08/12/2005	Mars Reconn-aissance Orbiter	US	Carries the most powerful camera High such as Resolution Imaging Science Experiment revealing features as small as 1 m across, and Compact Reconnaissance Imaging Spectrometer for Mars providing spectral information of minerals at a resolution of 200 meters. Other instruments include Electra, Context Camera, Mars Climate Sounder, Mars Color Imager, Shallow Subsurface Radar, Gravity Investigation and Optical Navigation Camera.
08/04/2007	Phoenix Mars Lander	US	First mission targeting at the sub-polar region of Mars. carries a complex suite of instruments that include Microscopy, Electrochemistry and Conductivity Analyzer, Thermal and Evolved Gas Analyzer, Robotic Arm, etc. The mission will 1) study the history of the water in the ice or icy soil, 2) study the climate and weather of the northern sub-polar region, and 3) search for evidence of a habitable zone and investigate the biologic potential of the ice-soil boundary.
Fall/2009	Mars Science Laboratory	US	Will examine Martian rocks and soils in greater detail than ever before to determine the geologic processes that formed them; study the Martian atmosphere; and determine the distribution and circulation of water and carbon dioxide, whether frozen, liquid, or gaseous.

* Data derived from http://mpfwww.jpl.nasa.gov/missions/future/msl.html

Appendix 3

Cation Sources for the Sulfate Evaporites in Valles Marineris, Mars

Introduction

A huge amount of hydrated Ca and Mg sulfates was identified through the Visible and Infrared Mineralogical Mapping Spectrometer (OMEGA) images (Gendrin et al., 2005; Bibring et al., 2005). The sulfates were likely formed by evaporation of the standing bodies of acidic water (Warren, 1999). Where did the huge amount of cations come from? Here, I propose that the cations were derived from the alteration of the ancient Martian basaltic crust from a comparison of the chemical compositions of the bedrocks at Gusev Crater and the layered deposits in Meridiani Planum, assuming the layered deposits in Meridiani Planum are derived from weathering of the basaltic crust in the southern highlands.

The bedrock and chemical composition at Gusev Crater

The Spirit of Mars Exploration Rover (MER) investigated the soils and bedrocks at Gusev Crater. The bedrocks are volcanic (with phenocrysts, Herkenhoff et al. 2004) and are dominantly composed of plagioclase, olivine and pyroxene (McSween et al., 2004). Fresh rocks exposed by the rock abrasion tool (RAT) are thought to be primitive basaltic rocks, similar to primitive terrestrial basalts [6]. The rocks were subjected to extensive weathering early in Martian history. The abraded bedrocks should represent the unweathered basaltic crust of Mars.

The chemical compositions of the bedrocks were analyzed using the alpha particle x-ray spectrometer (APXS, Gellert et al., 2004). I averaged the chemical compositions of the five abraded rock samples giving them equal weights (Table A-1). The sum of Si + Al and the sum of Mg + Ca + Fe are 26.96 wt% and 25.86 wt% respectively. The ratio of ∑Si+Al to ∑Mg+Ca+Fe is 51/49, which is consistent with the composition of basaltic rocks on Earth.

Table A-1 The chemical composition of the bedrock abraded by RAT at Gusev Crater*

Oxide	Adirondack	Humphrey		Mazatzal		Average (wt %)	
		Sample1	Sample2	Sample1	Sample2	Oxide	Element
Na_2O	2.70	3.10	2.80	3.10	3.10	2.97	2.20
MgO	11.90	10.40	11.50	9.90	10.70	10.92	6.56
Al_2O_3	10.90	10.90	10.60	10.00	10.80	10.68	5.63
SiO_2	45.40	46.10	45.70	45.40	45.50	45.80	21.33
P_2O_5	0.54	0.60	0.59	0.86	0.67	0.65	0.28
SO_3	1.15	1.02	1.20	3.20	1.39	1.60	0.64
Cl	0.13	0.21	0.17	0.36	0.15	0.20	0.20
K_2O	0.06	0.12	0.08	0.27	0.15	0.14	0.11
CaO	7.42	7.84	7.53	7.22	7.68	7.57	5.39
TiO_2	0.45	0.54	0.53	0.65	0.56	0.55	0.33
Cr_2O_3	0.59	0.66	0.59	0.44	0.53	0.56	0.38
MnO	0.38	0.38	0.38	0.37	0.39	0.38	0.29
FeO	18.00	17.80	18.00	17.70	18.00	17.97	13.91
Total	99.62	99.67	99.67	99.47	99.66	100.0	57.25
∑Si+Al	56.30	57.00	56.30	55.40	56.30	56.48	26.96
∑Mg+Ca+Fe	37.30	36.00	37.00	34.80	36.30	36.46	25.86

* Data derived from Gellert et al. (2004).

The bedrock and chemical composition in Meridiani Planum

The MER Opportunity Rover investigated the soils and bedrocks in Meridiani Planum. The bedrock outcrops display clear sedimentary characteristics and are composed of fine-grained siliciclastic materials (~50%), sulfate minerals (~40%) and hematite (~10%) (Squyres et al., 2004a). Squyres et al. (2004a) suggested that the fine-grained siliciclastic materials were derived from the weathering of basaltic parent rocks.

It has been proposed that the sulfates in Meridiani Planum were transported from sulfate evaporites deposited in Valles Marineris (Fan et al., 2007).

The chemical compositions of the abraded rocks in Meridiani Planum were analyzed using APXS (Rieder et al., 2004). I averaged the compositions of four abraded rock samples (Table A-2) except for Bounce Rock because its composition is unique at the Meridiani site (Squyres et al., 2004b). The sum of Si+Al is 30.29 wt% and the sum of Mg+Ca+Fe is 21.27 wt%. A large proportion Mg+Ca+Fe is in sulfates and hematite.

Table A-2 The chemical composition of the bedrock abraded by RAT in Meridiani Planum*

Oxide	Mckittrick	Guadalupe	Flat rock	Pilbara	Average (wt %)	
					Oxide	Element
Na_2O	1.10	1.00	1.20	1.10	1.11	0.82
MgO	7.40	7.80	7.80	8.00	7.82	4.71
Al_2O_3	6.00	5.70	6.00	5.60	5.87	3.11
SiO_2	38.10	36.30	36.20	34.70	36.63	27.18
P_2O_5	1.00	0.99	1.03	0.98	1.01	0.44
SO_3	21.00	24.60	23.30	24.70	23.60	9.45
Cl	0.39	0.33	0.36	0.44	0.38	0.38
K_2O	0.56	0.54	0.59	0.50	0.55	0.46
CaO	4.49	5.02	5.28	4.9	4.96	3.55
TiO_2	0.85	0.67	0.77	0.78	0.77	0.46
Cr_2O_3	0.22	0.19	0.23	0.23	0.22	0.15
MnO	0.32	0.32	0.27	0.37	0.32	0.25
FeO	17.6	15.8	16.3	16.7	16.74	13.01
Total	99.03	99.26	99.33	99.00	100.00	63.98
∑Si+Al	44.1	42.00	42.20	40.30	42.51	30.29
∑Mg+Ca+Fe	29.49	28.62	29.38	29.60	29.52	21.27

* Data derived from Rieder et al. (2004).

The sulfates are likely kieserite ($MgSO_4 \cdot H_2O$), gypsum ($CaSO_4 \cdot 2H_2O$) and jarosite ($KFe_3(SO_4)2(OH)_6$). If the same amount of sulfur (0.64 wt %) in Gusev crater is

contained in the rocks other than sulfates in Meridiani Planum, there is about 8.8 wt% of sulfur derived from sulfates. This amount of sulfur could combine with Mg, Ca and Fe in amounts ranging from 6.7 wt% (if sulfates are totally kieserite), through 11.0 wt% (totally Ca sulfates) to 23.0 wt% (totally jarosite) in the sedimentary rock. Hematite can contribute 5.4 wt% of iron in the sedimentary rocks. So there is at least about 12.1% of the sum of Mg+Ca+Fe in the rocks derived from sulfates and hematite. Removing this portion of Mg+Ca+Fe, the sum of Si+Al and the sum of Mg+Al+Fe in the siliciclastic materials are 32.29% and 9.2 % respectively. Thus, the ratio of ∑Si+Al to ∑Mg+Ca+Fe in the siliciclastic materials is 77.8/22.2, which is close to the chemical composition of phyllosilicate such as montmorillonite.

Discussion

Two types of rocks were recognized in the Martian crust, basalt in the southern highlands and basaltic andesite in the northern lowlands by the Mars Global Surveyor Thermal Emission Spectrometer (Hamilton et al., 2001). The outcrops with high concentrations of olivine and pyroxene were identified in the southern ancient terrains or crater floors (Mustard et al., 2005), while alteration products and phyllosilicates were identified in broad areas of the northern lowlands by the OMEGA images (Bibring et al., 2006). Incorporating the sedimentary characteristics of the bedrock outcrops, the siliciclastic materials in Meridiani Planum are most likely dominated by the clay minerals (mixed with a portion of basaltic fragments). This is consistent with the value of ∑Si+Al /∑Mg+Ca+Fe of the portion of siliciclastic materials removing sulfates and hematite.

These clay minerals were probably derived from weathering of the basaltic crust in the neighboring areas of the southern highlands, which had similar chemical compositions to the bedrocks analyzed in Gusev Crater. Based on the above discussion,

the ratio of ∑Si+Al to ∑Mg+Ca+Fe changed from 51.0/49.0 to 77.8/22.2 when the basaltic crust was altered to the phyllosilicate minerals. The calculation indicates that more than 50 wt% of ∑Mg+Ca+Fe in the basaltic rocks was released by the process. These released cations were likely dominated by magnesium and calcium (sodium and potassium are not considered here), because they have much higher solubility than iron. The released Mg and Ca were dissolved in acidic water and accumulated in standing bodies of water in the depression areas along the ancient dichotomy boundary of Mars. They precipitated to form sulfate evaporites in the area of Valles Marineris in Noachian before the uplift of the Tharsis rise combining with sulfur derived from elsewhere (Fan et al., 2007).

References:

Bibring, J-P., Y. Langevin, A. Gendrin, B. Gondet, F. Poulet, M. Berthé, A. Soufflot, R. Arvidson, N. Mangold, and J. Mustard, et al. (2005), Mars surface diversity as revealed by the OMEGA/Mars Express observations, *Science,* 307, 1576–1581.

Bibring, J-P., Y. Langevin, J.F. Mustard, F. Poulet, R. Arvidson, A. Gendrin, B. Gondet, N. Mangold, P. Pinet and F. Forget, 2006. Global mineralogical and aqueous Mars history derived from OMEGA/Mars Express data. *Science* 312, 400–404.

Fan, C., D. Schulze-Makuch, J.A. Wolff and A.G. Frairen, in press. A New Hypothesis for the origin and redistribution of sulfates in the equatorial region of western Mars. *Geophys. Res. Lett.*

Gellert, R., R. Rieder, R.C. Anderson, J. Brückner, B.C. Clark, G. Dreibus, T. Economou, G. Klingelhöfer, G.W. Lugmair and D.W. Ming, 2004. Chemistry of rocks and soils

in Gusev Crater from the Alpha Particle X-ray Spectrometer. *Science* 305. 829–832.

Gendrin, A., N. Mangold, J-P. Bibring, Y. Langevin, B. Gondet, F. Poulet, G. Bonello, C. Quantin, J. Mustard, R. Arvidson, and S. LeMouélic (2005), Sulfates in Martian layered terrains: The OMEGA/Mars Express view, *Science,* 307, 1587–1591.

Hamilton, V.E., M.B. Wyatt, H.Y. McSween Jr. and P.R. Christensen, 2001. Analysis of terrestrial and Martian volcanic compositions using thermal emission spectroscopy: 2. Application to Martian surface spectra from the Mars Global Surveyor Thermal Emission Spectrometer. *J. Geophysics. Res.,* 106, 14,733–14,746.

Herkenhoff, K.E., S.W. Squyres, R. Arvidson, D.S. Bass, J.F. Bell, III, P. Bertelsen, N.A. Cabrol, L. Gaddis, A.G. Hayes, S.F. Hviid, et al. (2004), Textures of the soils and rocks at Gusev Crater from Spirit's microscopic imager, *Science,* 305, 824–826.

McSween, H.Y., R.E. Arvidson, J.F. Bell, III, D. Blaney, N.A. Cabrol, P.R. Christensen, B.C. Clark, J.A. Crisp, L.S. Crumpler, D.J. Des Marais, et al., 2004. Basaltic rocks analyzed by the Spirit Rover in Gusev Crater. *Science* 305, 842–845.

Mustard, J.F. F. Poulet, A. Gendrin, J.-P. Bibring, Y. Langevin, B. Gondet, N. Mangold, G. Bellucci and F. Altieri, 2005. Olivine and pyroxene diversity in the crust of Mars. *Science* 307, 1594–1597.

Rieder, R., R. Gellert, R.C. Anderson, J. Brückner, B.C. Clark, G. Dreibus, T. Economou, G. Klingelhöfer, G.W. Lugmair and D.W. Ming, 2004. Chemistry of rocks and soils at Meridiani Planum from the Alpha Particle X-ray Spectrometer. *Science* 306, 1746–1749.

Squyres, S.W. J.P. Grotzinger, R.E. Arvidson, J.F. Bell, III, W. Calvin, P.R. Christensen, B. C. Clark, J. A. Crisp, W. H. Farrand, K. E. Herkenhoff, et al., 2004a. In situ evidence for an ancient aqueous environment at Meridiani Planum, Mars. *Science* 306, 1709–1714.

Squyres, S.W., R.E. Arvidson, J.F. Bell, III, J. Brückner, N.A. Cabrol, W. Calvin, M.H. Carr, P.R. Christensen, B.C. Clark and L. Crumpler, 2004b. The Opportunity Rover's Athena science investigation at Meridiani Planum, Mars. *Science* 306, 1698–1703.

Warren, J. (1999). *Evaporites: Their Evolution and Economics* (Blackwell Science, Oxford, UK.

Appendix 4 The solubility of Mg sulfate, Ca-sulfate, halide and jarosite

The solubility of $MgSO_4$ (2.8 mol/l or 337 g/l) is about 169 times greater than $CaSO_4$ (0.015 mol/l or 2.0 g/l) at 25^{o}C. NaCl is the most soluble salt (6.1 mol/l or 359 g/l, whereas the solubility of jarosite is very low (about 10^{-11} mol/l or $5*10^{-9}$ g/l) at 25^{o}C.